INFORMATION TO USERS

This manuscript has been reproduced from the microfilm master. UMI films the text directly from the original or copy submitted. Thus, some thesis and dissertation copies are in typewriter face, while others may be from any type of computer printer.

The quality of this reproduction is dependent upon the quality of the copy submitted. Broken or indistinct print, colored or poor quality illustrations and photographs, print bleedthrough, substandard margins, and improper alignment can adversely affect reproduction.

In the unlikely event that the author did not send UMI a complete manuscript and there are missing pages, these will be noted. Also, if unauthorized copyright material had to be removed, a note will indicate the deletion.

Oversize materials (e.g., maps, drawings, charts) are reproduced by sectioning the original, beginning at the upper left-hand corner and continuing from left to right in equal sections with small overlaps.

Photographs included in the original manuscript have been reproduced xerographically in this copy. Higher quality 6" x 9" black and white photographic prints are available for any photographs or illustrations appearing in this copy for an additional charge. Contact UMI directly to order.

Bell & Howell Information and Learning
300 North Zeeb Road, Ann Arbor, MI 48106-1346 USA
800-521-0600

A photochemical sink for dissolved organic carbon in the ocean

by
Sophia Johannessen

Submitted in partial fulfillment of the requirements
for the degree of Doctor of Philosophy

Dalhousie University
Halifax, Nova Scotia
May, 2000

DALHOUSIE UNIVERSITY

FACULTY OF GRADUATE STUDIES

The undersigned hereby certify that they have read and recommend to the Faculty of Graduate Studies for acceptance a thesis entitled "A Photochemical Sink for Dissolved Organic Carbon in the Ocean"

by Sophia Johannessen

in partial fulfillment of the requirements for the degree of Doctor of Philosophy.

Dated: May 5, 2000

External Examiner

Research Supervisor

Examining Committee

DALHOUSIE UNIVERSITY

Date: **May, 2000**

Author: **Sophia Johannessen**

Title: **A photochemical sink for dissolved organic carbon in the ocean**

Department: **Oceanography**

Degree: **Ph.D.** Convocation: **October** Year: **2000**

Permission is herewith granted to Dalhousie University to circulate and to have copied for non-commercial purposes, at its discretion, the above title upon request of individuals or institutions.

[redacted]

Signature of the Author

Table of Contents

List of Figures and Tables

Figures

Tables

Abstract

The photochemical oxidation of coloured or chromophoric dissolved organic matter in the ocean plays an important role in the carbon cycle. The production of dissolved inorganic carbon, DIC, represents the most rapid direct photochemical loss of dissolved organic carbon, DOC. The goal of this thesis is to make a quantitative estimate of the photochemical source of DIC in the ocean.

To calculate the rate of DIC photoproduction, efficiency (quantum yield) spectra, relationships between *in situ* and remotely-sensed optical properties and a model of solar spectral irradiance were required. This thesis presents the first quantum yield spectra for DIC in sea water. The magnitude of quantum yield increases with distance from shore.

Relationships between remotely-sensed reflectance and *in situ* attenuation of ultraviolet radiation were determined. They apply over a wide range of water types in the Bering Sea, the Mid-Atlantic Bight, and Bedford Basin, Nova Scotia from May to August. Absorption by coloured dissolved organic matter is responsible for almost all the attenuation of ultraviolet radiation in the study areas.

The monthly rate of DIC photoproduction was estimated pixel by pixel for January, April, July and October, 1998 in the Mid-Atlantic Bight from SeaWiFS ocean colour images. It increases with distance from shore. The same approach can be applied to any photoproduct with a known quantum yield. Photoproduction rates of CO, H_2O_2 and CS_2 were estimated from SeaWiFS images and published quantum yield spectra. The ratio of DIC photoproduction to the production of CO, H_2O_2 and CS_2 increases from the inshore to the open ocean zone.

Global photochemical production rates of DIC, CO, H_2O_2 and CS_2 were also calculated. The global production rates of CO and CS_2 compare well with published values. The global annual DIC photoproduction rate is approximately 10^{15} moles DIC $year^{-1}$. This rate is higher than the annual input of terrestrial DOC to the ocean, which probably reflects the importance of the photochemical transformation of DOC formed *in situ* from the degradation of phytoplankton. The rate of DIC photoproduction is also comparable to the annual rate of DIC use in new production.

List of Symbols and Abbreviations

$a(\lambda)$	Total spectral absorptivity (m^{-1})
$A_{CDOM}(\lambda)$	Spectral absorbance by CDOM (AU)
$a_{CDOM}(\lambda)$	Spectral absorptivity by CDOM (m^{-1})
$b(\lambda)$	Total spectral scattering coefficient (m^{-1})
C	Constant in absorptivity correction equation (m^{-1})
CDOM	Coloured or chromophoric dissolved organic matter
D	Julian day (January 1 = 1)
DIC	Dissolved inorganic carbon
DOC	Dissolved organic carbon
e	Eccentricity of the Earth's orbit around the sun (dimensionless)
$E_0(\lambda)$	Spectral scalar irradiance (W $m^{-2}nm^{-1}$ or moles photons $m^{-2}s^{-1}nm^{-1}$)
$E_{abs}(\lambda)$	Spectral irradiance absorbed by CDOM (W $m^{-2}nm^{-1}$ or moles photons $m^{-2}s^{-1}nm^{-1}$)
$E_i(\lambda)$	Spectral incident irradiance in a spectrophotometer (W $m^{-2}nm^{-1}$ or moles photons $m^{-2}s^{-1}nm^{-1}$)
$E_d(\lambda)$	Spectral incident (downwelling) irradiance (W $m^{-2}nm^{-1}$ or moles photons $m^{-2}s^{-1}nm^{-1}$)
$E_d(\lambda,0+)$	Spectral incident (downwelling) irradiance just above the surface of the ocean (W $m^{-2}nm^{-1}$ or moles photons $m^{-2}s^{-1}nm^{-1}$)
$E_d(\lambda,0-)$	Spectral incident (downwelling) irradiance just below the surface of the ocean (W $m^{-2}nm^{-1}$ or moles photons $m^{-2}s^{-1}nm^{-1}$)
$E_d(\lambda,z)$	Spectral incident (downwelling) irradiance at depth z (W $m^{-2}nm^{-1}$ or moles photons $m^{-2}s^{-1}nm^{-1}$)
$F_0(\lambda)$	Mean extra-terrestrial spectral solar irradiance corrected for earth-sun distance and orbital eccentricity ($Wm^{-2}nm^{-1}$)
$\phi(\lambda)$	Apparent spectral quantum yield (moles DIC produced/ mole photons absorbed)
$H_0(\lambda)$	Mean extra-terrestrial spectral solar irradiance (W $m^{-2}nm^{-1}$)
$K_d(\lambda)$	Spectral attenuation coefficient for downwelling irradiance (m^{-1})
λ	Wavelength (nm)
$L_u(\lambda,0-)$	Spectral upwelling radiance just below the surface of the ocean (W $m^{-2}nm^{-1}sr^{-1}$ or moles photons $m^{-2}s^{-1}nm^{-1}sr^{-1}$)
$L_w(\lambda,0+)$	Spectral upwelling (water-leaving) radiance just above the surface of the ocean (W $m^{-2}nm^{-1}sr^{-1}$ or moles photons $m^{-2}s^{-1}nm^{-1}sr^{-1}$)
m_1	Regression constant in quantum yield fitting equation
m_2	Regression constant in quantum yield fitting equation
$\bar{\mu}_d(\lambda)$	Spectral average cosine of downwelling irradiance (dimensionless)
$nL_w(\lambda)$	Spectral normalized water-leaving radiance (W $m^{-2}nm^{-1}sr^{-1}$ or moles photons $m^{-2}s^{-1}nm^{-1}sr^{-1}$)
$dDIC/dt$	Production rate of DIC (moles DIC $m^{-2}time^{-1}$)
$d[DIC]/dt$	Production rate of DIC (moles DIC $m^{-3}time^{-1}$)

$R(\lambda)$	Spectral radiance reflectance (sr^{-1})
S	Absorptivity slope from fitting equation (nm^{-1})
SeaWiFS	Sea-viewing Wide Field-of-view Sensor
UV	Ultraviolet radiation (280 - 400 nm)
UVA	Radiation from 320 – 400 nm
UVB	Radiation from 280 – 320 nm
z	Pathlength of spectrophotometer cell or depth in the ocean (m)

Acknowledgements

Firstly, I would like to thank my supervisor, Dr. Bill Miller, for inspiration and enthusiasm, and for supervising me exactly as much as I needed. When I have my own students, I want to be just like you.

I have been very lucky with my committee, too. Drs. John Cullen, Bob Moore and Bernie Boudreau set high standards and then helped me to meet them. I appreciate the time you have all spent in explaining the many things that puzzled me.

Dr. Richard Zepp did me the great honour of flying up from Georgia to be the External Examiner at my thesis defense. Your comments improved the thesis greatly and have given me much to think about.

Several other professors who were not on my committee also took an interest in my work and helped me considerably. Dr. Keith Thompson designed the statistical method I used to calculate the error in my global DIC production calculation. He also provided the even more useful advice that "if statistics and intuition don't agree, the statistics are probably wrong." Dr. Owen Hertzman gave me a great deal of advice on the effects of clouds on irradiance, as well as on more general topics. Dr. Eric Mills taught a fascinating course on the history of marine science, which has given me a deeper appreciation of Oceanography and of the importance of the contribution of each individual. I will try to remember never to treat history as if the end were predestined from the beginning.

I could not have accessed or used any satellite data without the excellent course taught by Dr. Marlon Lewis and Mike Macdonald. I thank you both especially for continuing to help me after the course was over. Karen Baith at the SeaDAS help desk provided very patient and useful advice about the manipulation of the satellite data.

I thank Richard Davis, Penny Kuhn, Gary Maillet, Cyril Dempsey and Angela Kennedy for their assistance in the field and lab, and with the Horrible Problem of Computers. I probably would have been here much longer without the benefit of your ungrudgingly shared experience. Dianne, Tammy, Pamela, and Tammie made all the administrative details go smoothly and helped to make the department a friendly place to work.

Jurgen Mueller, Alex Feargrieve and Simon Trussler made several pieces of vital lab equipment for us, after making much-appreciated improvements to the original designs. Sherry Niven and Kumiko Azetsu-Scott made it possible for me to take samples in Bedford Basin from the *Ibis*, and helped me with my sampling plan.

I appreciate very much the financial support that I and the project received from ONR and NSERC. I would also like to thank the officers and crews of the *R/V Cape Henlopen*, the *R/V Wecoma* and the *R/V Seward Johnson* for dealing graciously with all my peculiar requests, both scientific and culinary.

My friends here in Halifax have been more than just friends, but also fellow-sufferers, colleagues, and mentors. I would especially like to thank Aurea, J.P., Yannick, and Becky. Aurea (or Didi) took me under her wing when I arrived. We have been friends

through some really strange years. I hope we will work and play together again in the future. I have to thank Becky for *almost* always "playing nice", but I'd like to add that I already miss our countless cups of tea and gossip sessions. I hope you will make it over to the West Coast someday soon. Yannick, who is probably hoping that I will mention how cute he is, has inspired me with his hard work, sense of humour, and that infectious laugh. Thank you also for the lessons in optics and soccer. J.P. - I appreciate your answering all my phytoplankton questions, but more than that your cheerful friendship. I may never think as Big as you do, but I'll certainly give it a try. And thank you for giving me the soccer MVP trophy for my birthday. I'm as proud of it as I would have been if I had actually won it... All my other friends at Dal, new and old, have helped me when I needed it and given me lots to laugh about. I'll miss you.

I'm going back to B.C. now, to be with my family. My parents and my brother, James, deserve much of the credit for my being here at all. Your constant belief that I could do anything I wanted to got me to Halifax and now all the way through the Ph.D.. I'm proud of you, too. Samantha, Stephanie, Meredith, Karina (Kaisa, you fit here with my family better than anywhere else) and Duncan's family, your support has meant more than I can say.

Finally, I thank Duncan, *sine qua non*. And our little baby, not yet born, who has helped me to keep science in perspective.

Chapter 1. Introduction

1.1 Introduction

Sunlight hits the surface of the ocean, and the ocean smoulders. The fuel is coloured or chromophoric, dissolved organic matter, CDOM. The products are numerous. Like those of a fire, they include carbon dioxide, although many other species, biologically and chemically reactive, are also produced. Some products provide nutrients for phytoplankton and bacteria, and react with many organic and inorganic molecules in sea water. As the new species are formed, chromophores are destroyed. Consequently, CDOM fades with exposure to radiation. Photochemical fading has been observed in the laboratory (Miller, 1994), in lakes (for example Morris and Hargreaves, 1997; Moore, 1999), and probably also in the ocean (Vodacek *et al.*, 1997). This process is important, because as CDOM absorbs fewer photons of ultraviolet, UV, radiation in the surface layer, UV radiation penetrates further into the water column, inhibiting phytoplankton activity (Smith *et al.*, 1992; Cullen and Neale, 1994) and increasing damage to bacteria (for example, Kaiser and Herndl, 1997). As discussed below, the photo-oxidation of CDOM also plays a role in the marine carbon cycle.

Each year, about 2.5×10^{13} - 4.2×10^{13} moles of terrestrial organic carbon are transported to the ocean by rivers, half as particulate organic carbon and half as dissolved organic carbon, DOC (Sarmiento and Sundquist, 1992). Near shore heterotrophy consumes about 7×10^{12} - 10×10^{12} moles of this carbon each year, and about 8×10^{12} moles of carbon are buried in coastal sediments. The fate of about 0.7×10^{13} - 2.7×10^{13} moles of terrestrial

organic carbon remains unclear, and this carbon has been assumed to be transported to the open ocean. However, the larger part of DOC found in the deep ocean does not appear to have a terrestrial origin; Meyers-Schulte and Hedges (1986) reported that about 0.5% of DOM in the ocean was terrestrial in origin, as determined using lignin as a tracer. Malcolm (1990) also found that DOM in the open ocean was different from that found in inshore waters, according to isotopic analyses and ^{13}C NMR spectroscopy. Hedges *et al.* (1992) supported Malcolm's findings with further ^{13}C NMR results, and added that DOM found in the open ocean was relatively enriched in nitrogen. The average age of marine DOM is also greater (3400 years, according to Williams *et al.*, 1969) than would be expected for the rate of fluvial addition, using a residence time calculation that assumes a steady state concentration of oceanic DOM (Deuser, 1988). Clearly, the sources and sinks are not well characterized.

Spontaneous precipitation and offshore microbial degradation have both been suggested as sinks for the terrestrial DOC that is not consumed by near-shore heterotrophy or burial, but neither is supported by observation. Blough *et al.* (1993) reported that in the Orinoco River estuary, which transports about 1% of the global terrestrial organic carbon input to the ocean, there was no significant loss of riverine DOC to spontaneous precipitation; however, they did report that the optical properties of the CDOM changed, possibly due to bacterial degradation, changes in pH or ionic strength, selective precipitation of parts of the CDOM, or photobleaching. The mechanism by which terrestrial DOM is modified remains unclear, although Norrman *et al.* (1995) presented a carbon isotope study on water from Woods Hole Harbor that suggested that much of it was untouched by bacteria.

The bacteria preferred the DOM newly produced by phytoplankton, which had a high $\delta^{13}C$ similar to that of DOM found in the open ocean. Most DOM found in the ocean at depths greater than 500 m is biologically refractory on a time scale of a few thousand years (Williams *et al.*, 1969). Hedges (1987) concluded that there must be an "as yet undiscovered process by which the sea eventually recycles this huge reservoir of recalcitrant organic molecules back to inorganic carbon."

Kieber *et al.* (1989) first suggested that the photochemical oxidation of CDOM might provide an important marine sink for organic carbon. (See "*Carbon cycle*" section that follows.) The most rapidly produced inorganic product of the photochemical oxidation of CDOM is DIC, probably as CO_2 (Miller and Zepp, 1995). The formation of DIC represents a direct loss of organic carbon from the ocean, so its production is a useful proxy for the rate of photochemical loss of DOC. **The goal of this thesis is to make a quantitative estimate of the photochemical source of dissolved inorganic carbon in the ocean.**

To reach that goal, the following objectives were set:

1) To determine the first quantum yield spectra for the photochemical production of DIC from CDOM in the ocean.

2) To relate *in situ* UV attenuation and UV absorption by CDOM to remotely-sensed ocean colour.

3) To determine the proportion of UV attenuation due to absorbance by CDOM.

4) To combine the quantum yield spectra with remotely-sensed ocean colour and a solar irradiance model to calculate depth-resolved and total water column production rates for DIC photoproduction.

The remainder of Chapter 1 provides a historical context for this work within organic marine photochemistry. This history is not intended to be an exhaustive review of the subject, but to describe, with examples, the major trends in organic marine photochemistry over the last three decades. A selective history of the development of ocean optics can be found in Appendix 1. Each of Chapters 2-4 is self-contained, with its own background, methods, results, and discussion sections. Chapter 2 describes the determination of quantum yield spectra for the photochemical production of DIC. Chapter 3 explains the relationships determined between *in situ* and remotely-sensed optical properties. Chapter 4 combines the results of the preceeding two chapters with satellite images to calculate regional and global DIC production rates. Chapter 5 compares the production rate of DIC with those of several other products. Chapter 6 contains the main conclusions of the thesis.

1.2 History of Marine Organic Photochemistry

Organic marine photochemistry is a relatively new discipline. In 1977 Zafiriou wrote that the subject was "in its infancy" and lacked a significant body of literature to review, so instead he previewed areas for future research. General photochemistry was already highly developed both theoretically and experimentally by that time, with much work

done on absorption and emission spectra in the 1800s, and with revolutionary advances in quantum chemistry in the early 1900s. (Longworth (1982) provides an extensive history of the subject.) But there were many difficulties unique to the ocean that had yet to be overcome. Zafiriou mentioned, for example, that in the ocean the chromophores were largely unknown and that photochemical reactions in the ocean were complicated by the high ionic strength of sea water, leading to a variety of primary, secondary, and photosensitized reactions. In addition, neither a light field nor an absorbance spectrum of precursor molecules could be generalized to apply to the whole ocean.

Zafiriou also described a series of questions within the scope of organic, marine photochemistry. He suggested that photochemical reactions might affect both the metallic and organic ligands in organometallic complexes; remove micronutrients from the water column; supply the unknown oceanic sink for refractory dissolved organic carbon (DOC); and explain why, despite the regular addition of coloured organic material to the surface ocean, photons were not all eventually trapped at the surface. He also mentioned speculation by earlier authors that photochemical reactions in the early ocean might have been responsible for the origin of life, and later for mass extinctions of phytoplankton. He felt that these topics would be tractable both with respect to the photochemical reactions of anthropogenic compounds with known composition and reactivity and, in a general way, for reactions with naturally occurring organic molecules as precursors. Zafiriou was either exceptionally foresighted or very influential (or both), because almost all the topics he mentioned in 1977 have since been, and in some cases still are, studied in detail.

Photochemistry of environmental contaminants

The publication of Carson's book Silent Spring in 1962 introduced non-scientists to the idea that the chemical by-products of industrialization were destroying wildlife. By the mid-1970s, there was a public outcry against the chemical pollution of air and water. Probably as a result of the high general awareness of the problem, most of the work in marine organic photochemistry during the 1970s related to the fate of anthropogenic contaminants. Wedgewood (1952) and Hoather (1953) had shown that UV absorbance measurements could be used to trace organic contaminants in water, as a less expensive and simpler method than measuring total organic carbon. A series of publications followed, which demonstrated the use of various wavelengths of UV radiation for this measurement (for example, Dobbs *et al.*, 1972).

Knowing that some contaminants absorbed UV radiation strongly, later researchers investigated the possibility of their photochemical breakdown. Zepp and Cline (1977) applied an approach previously used for studies of photochemical smog transformations to study the direct photolysis of the herbicide Trifluralin and the insecticide Carbamate. They measured absorbance spectra and quantum yield values at 366 nm, and assumed that the quantum yield was independent of wavelength. In this way they calculated half lives for the pollutants in solution, considering depth, latitude and time of day in their calculations. However, the quantum yield measurements had to be made on highly concentrated samples, unlike those found in the environment. Zepp (1978) later solved this problem. He published a method of determining the quantum yield of pollutant photolysis in very dilute solution. Bunce and Chittim (1979) felt that Zepp's and Cline's

(1977) approach was too time-consuming, and described a simple alternative for determining the relative reactivity of a pollutant. Since many components of the half-life determination equation presented by Zepp and Cline varied in time and space – the solar irradiance and the UV absorbance of the water body in question, for example – Bunce and Chittim defined a photoreactivity index that used a simple ratio of the photolysis rate of the pollutant multiplied by its spectral absorbance to that of a standard multiplied by its spectral absorbance. They suggested that the irradiation be done with a standard solvent and in a standard irradiance field. Then, the photoreactivity index would describe the likely persistence of the pollutant relative to that of the standard. The idea did not seem to gain wide acceptance, possibly because it was not really very difficult to obtain absolute measurements of quantum yield of contaminant photolysis in the laboratory.

Miller and Zepp (1978) refined pollutant photo-oxidation rate estimates by calculating the effect of suspended sediments on photolysis rates, since pollutants were often discharged into turbid rivers. They found that turbidity increased volumetric photolysis rates by increasing the pathlength of incident photons and allowing more radiation to be absorbed by the dissolved pollutant.

During the 1980s, the focus of organic marine photochemistry shifted from the direct photoxidation of environmental pollutants to reactions involving naturally occurring dissolved organic matter. At first this area of research was still related to the fate of pollutants. Zepp and Schlotzhauer (1981) and Zepp *et al.* (1981) discussed the effect of naturally-occurring coloured or chromophoric dissolved organic matter (CDOM;

although Zepp *et al.* referred to the natural organics as "humic substances") on organic contaminants. They measured CDOM absorbance spectra in samples taken from soils, natural waters and commercially available isolates, and compared the potential of CDOM from these sources as a photosensitizer. They found that a secondary photochemical reaction, the oxidation of a substance by CDOM which had itself been photooxidized, could break down the pollutant 2,5-dimethylfuran.

While most photochemical researchers studied the breakdown of pollutants, Amador *et al.* (1989) studied another effect of CDOM photochemistry. Using glycine as a model organic compound that was transparent to UV and visible radiation and which was released after photooxidation of larger molecules, they showed that the photochemical oxidation of CDOM could release smaller organic molecules. They commented that this could result in the re-release into the environment of pollutants that had initially been scavenged by CDOM. Clearly, the effect of solar irradiance on contaminants is not simple.

Biological importance of organic marine photochemistry

Interest in the biological effects of photochemistry began in the 1960s and has grown during the subsequent three decades. The first studies on the subject related to the potential destruction of inorganic nutrients by photo-oxidation (for example, Hamilton, 1963). As organic marine photochemical research focussed increasingly on the products of CDOM photo-oxidation, however, researchers also discovered a number of

biologically labile substrates that were formed during the photochemical breakdown of CDOM.

Finden *et al.* (1984) reported that CDOM helped to make more iron available to phytoplankton. Iron III was reduced directly to soluble, biologically available iron II, but the reduction rate decreased with time. The addition of CDOM made the iron more susceptible to reduction, and appeared to make the iron II more available to phytoplankton than when it was formed through reduction of iron III in the absence of CDOM. The mechanism probably involved the complexation of iron III with CDOM, just as iron III - EDTA complexes are often used in algal culture experiments (Finden *et al.*, 1984). Wells *et al.* (1987), Miller and Kester (1994) and Miller *et al.* (1995) tested the Finden *et al.* result by making direct measurements of photochemically produced reduced iron and of the effect of the increased concentration of that iron on a marine diatom culture. They added a mechanistic interpretation of the iron reduction in which iron was oxidized by oxygen and hydrogen peroxide and both oxidized and reduced by photochemically produced superoxide.

Not only phytoplankton but also bacteria are affected by photochemical reactions. Amador *et al.* (1989) used radiolabelled glycine as a model organic molecule to show that the photodegradation of biologically refractory CDOM produced smaller, biologically available molecules that were usable by bacteria. They suggested that in the ocean, photooxidation and microbial degradation acted together to break down the large CDOM molecules. Kieber *et al.* (1989) confirmed that the photooxidation of CDOM

could produce molecules available to bacteria. They found that the rate of uptake of pyruvate by bacteria was directly proportional to its photochemical production rate. Wetzel *et al.* (1995) further supported this result, finding significant increases in the concentration of small fatty acids and in associated bacterial growth after CDOM photolysis. Only a small portion of the DOC was destroyed, while the products were sufficient to support a large increase in bacterial growth rate in those cultures innoculated with the irradiated CDOM. Bushaw *et al.* (1996) reported that biologically available, nitrogen-rich compounds such as ammonium were produced photochemically from CDOM. Such a source of biologically available nitrogen could affect both bacteria and phytoplankton in nitrogen-limited environments where there was a high terrestrial input and thus a high concentration of CDOM. More biologically available photoproducts continue to be identified, and in a 1997 review, Moran and Zepp listed 15 of them. Since then, Bertilsson and Tranvik (1998) have added some carboxylic acids (oxalic, malonic, formic, and acetic) to the list, although their work was done in a lake, not in the ocean.

The combination of photochemical and bacterial degradation of CDOM has received much attention in recent years. Since the suggestion of the idea by Kieber *et al.* (1989), work has continued on the direct comparison of the effectiveness of the two components. Amon and Benner (1996) found that photochemical oxidation of CDOM did not add significantly to the rate of microbial degradation of DOM. However, their irradiations were done in glass bottles that excluded most of the UVB and much of the UVA radiation, so it is possible that they did not make significant concentrations of biologically available, low molecular weight compounds. They did notice, however, that

DOC was lost during the irradiations. Miller and Moran (1997), using UV-transparent quartz irradiation vessels, found that bacterial growth was stimulated by the irradiation of CDOM prior to innoculation with the bacteria. In fact, bacterial productivity increased too much to have been the result only of the previously identified low molecular weight compounds, so the authors postulated the production of another, as yet unidentified, biologically labile photoproduct. For the irradiance field used, the loss of DOC by photochemically stimulated microbial degradation was roughly equal to that lost through the production of inorganic carbon gases. The interaction between photochemical transformations and bacterial assimilation is of continuing interest (for example, Geller *et al.*, 1985; Lindell *et al.*, 1995; Thomas and Lara, 1995; Naganuma *et al.*, 1996; Nelson *et al.*, 1998), and in August 1998, a session of the 8th International Symposium on Microbial Ecology in Halifax, Nova Scotia was devoted to the subject.

Reactive photoproducts

A number of chemically reactive species are produced photochemically, including reactive oxygen species (Kotzias *et al.*, 1986, 1987; review by Cooper *et al.*, 1989; review by Blough and Zepp, 1995), inorganic carbon gases, methyl halides, and alkenes. Hydroxyl radical is extremely reactive in sea water; it reacts particularly strongly with organic molecules, heavy metals, and major seawater constituents, such as bromide (Zafiriou, 1974). If a photochemical source were large enough, it could play a significant role in the chemistry of sea water. Zafiriou (1974) reported the photochemical production of hydroxyl radical from nitrate, an inorganic source, and its subsequent reaction with organic matter and other radicals. Haag and Hoigné (1985) reported the

same reaction, and added that since the hydroxyl produced reacted so efficiently with DOC in fresh water and with bromide in the ocean, its reaction rate with trace organics, such as pollutants, must be very slow. While the photochemical production of hydroxyl radical from nitrate can be important in upwelling regions, CDOM seems to be the main source in most of the ocean. Mopper and Zhou (1990) and Zhou and Mopper (1990) compared hydroxyl radical production in a variety of environments and concluded that the photochemical degradation of CDOM was probably the main source of hydroxyl radical in the sea.

One of the most intensely studied chemically reactive photoproducts is hydrogen peroxide. Hydrogen peroxide is formed as a reaction intermediate in the production of many free radicals, and it reacts strongly with organic matter (Sikorski and Zika, 1993a, 1993b). A production mechanism has been suggested (Moore *et al.*, 1993), but it has been difficult to determine precisely because of the largely unknown structure of CDOM. Since Van Baalen and Marler (1966) first suggested that H_2O_2 had a photochemical source in sea water, its production and distribution have also been studied (for example Sikorski and Zika, 1993a; Sikorski and Zika, 1993b; and Miller and Kester, 1994). Its concentration is so strongly dependent on its photochemical production rate that hydrogen peroxide can be used as a tracer for mixing (for example, Zika *et al.*, 1985; Miller and Kester, 1994; Scully *et al.*, 1998).

Another chemically reactive photoproduct is carbonyl sulphide. Carbonyl sulphide, COS, is the longest lived naturally-occurring sulphur species in the atmosphere (Andreae

and Ferek, 1992). Its longevity allows it to be carried up to the stratosphere, where it can form sulphate aerosols which may become cloud condensation nuclei or destroy ozone (Andreae and Ferek, 1992). The ocean is thought to be the largest source of COS to the atmosphere, and Ferek and Andreae (1983) discovered that COS was formed photochemically from CDOM in the ocean. Because of the atmospheric importance of COS, a large number of studies of its production followed. Andreae and Ferek (1992) measured a diel cycle in COS concentration, which they modelled as the result of photochemical production and removal by hydrolysis. Zepp and Andreae (1994) studied the wavelength dependence of COS production using sunlight and solar simulator irradiations, and determined that UV was the most effective region of the spectrum for its production. They also noted the importance of photosensitizers and speculated that the highest production rates might be found in coastal water. Weiss *et al.* (1995) studied the UV wavelength dependence of COS production in some detail, using monochromatic irradiations, and found that the wavelength of maximum production varied with location; in tropical waters the most effective wavelength was 313 nm, while 336 nm was more effective in the southern Pacific, near Antarctica. The volumetric production rate was higher in coastal than in offshore waters, as Zepp and Andreae (1994) had suggested. Uher and Andreae (1997) continued this work, and found that COS production was very strongly correlated with CDOM absorbance. They suggested that remote sensing of CDOM absorbance could be used to predict COS production. Besides the direct photochemical production of COS which is then released to the atmosphere, there is an indirect photochemical source in the ocean. Carbon disulphide, CS_2, is oxidized in the

atmosphere by hydroxyl radical to form COS. Xie *et al.* (1998) demonstrated that photochemical oxidation of CDOM was a significant source of CS_2 in the ocean.

Photochemical reactions of CDOM also produce a number of other reactive species, including methyl iodide (Moore and Zafiriou, 1994), alkenes (Ratte *et al.*, 1998), and superoxide ion (Baxter and Carey, 1983). Zafiriou and Dister (1991) presented a method for determining the total concentration of free radicals produced photochemically in oceanic waters. They concluded that the production was high enough to have a geochemical effect, but that it was unknown what that effect would be.

Carbon cycle

By 1994 anthropogenic emissions had increased the concentration of carbon dioxide in the atmosphere by 27% since the Industrial Revolution (Sarmiento and Bender, 1994). That increase is particularly dramatic when compared with the relatively stable atmospheric concentration over the preceding 800 years. It has led to widespread concern about the "greenhouse effect" and other potential global climate changes. Since dissolved organic matter in the surface ocean is a significant active reservoir of organic carbon (Amon and Benner, 1994), photochemical researchers over the past decade have become particularly interested in studying the role of photochemical reactions in the global carbon cycle.

Deuser (1988) pointed out that carbon cycle models did not balance, that roughly half of the terrestrial organic carbon that entered the ocean each year had no known sink. Kieber

et al. (1989) suggested the photochemical breakdown of the refractory, high molecular weight organic carbon compounds into smaller, biologically available molecules as a potentially significant sink for DOC. They provided evidence of increased biological uptake of pyruvate after its production during the irradiation of high molecular weight material. For a discussion of the combined photochemical - biological sink, see the earlier section "*biological effects of photochemistry*". A number of subsequent authors have supported the idea of a significant photochemical sink for DOC in the ocean (for example, Kieber and Mopper, 1987; Kieber *et al.*, 1990; Mopper *et al.*, 1991; Valentine and Zepp, 1993; Miller, 1994; Moran and Zepp, 1997; Vodacek *et al.*, 1997).

Miller (1994) wrote a review of recent work in aquatic, organic photochemistry, which demonstrated that by the early 1990s the idea that photochemical breakdown could be an important sink for organic carbon was well established. It was clear, however, that the calculations made at that time concerning the size of the sink required many simplifying assumptions about the radiation field in the ocean, and about the proportion of DOC that was photochemically available. Also, at that time, the direct photoproduction of DIC, now known to be the most rapidly produced inorganic carbon photoproduct, had not been measured. Carbon monoxide was the largest measurable carbon photoproduct (Erickson, 1989; Valentine and Zepp, 1993). Valentine and Zepp (1993) reported that CO photoproduction could represent a loss of 0.1-0.5% organic C day^{-1} at 40°N in shallow, natural waters.

The photochemical production of DIC, probably as CO_2, has been measured by a number of researchers (for example, Chen *et al.*, 1978; Miles and Brezonik, 1981; Allard *et al.*, 1994; Salonen and Vähätalo, 1994; Miller and Zepp, 1995; Granéli *et al.*, 1996; Moore, 1999). Miller and Zepp (1995) reported that DIC was produced at about ten to twenty times the rate of CO production, although the spectral efficiency of the reaction remained unknown. Granéli *et al.* (1996) reported the direct photoproduction of DIC in five lakes in Sweden and found that photoproduction at a series of depths was most strongly correlated with the penetration of UVA radiation (320-400 nm). Salonen and Vähätalo (1994) determined a quantum yield spectrum for DIC in a Scandinavian lake, also using tubes suspended at several depths. Moore (1999) irradiated samples of Nova Scotia lake water in a solar simulator to calculate the quantum yield for DIC in a well-defined irradiance field. She measured a 50-60% colour loss across the spectrum associated with a calculated total summer (June 16 - September 29, 1997) photochemical production of 0.029 moles DIC m^{-3}. Assuming no input of DOC during this time, Moore calculated a seasonal loss of 2.7% of the standing DOC concentration in the lake.

The role of photochemistry in the carbon cycle continues to be an area of active research, and may result, as Zafiriou predicted, in the closure of the non-anthropogenic part of global carbon cycle models. **This thesis fits into the carbon cycle branch of organic marine photochemistry and combines it with ocean optics and remote sensing to make a reasonable, quantitative estimate of the photochemical source of dissolved inorganic carbon in the ocean.**

Chapter 2. Quantum Yield of DIC Photoproduction

2.1 Introduction

Quantum yield

The photochemical oxidation of coloured or chromophoric dissolved organic matter, CDOM, is known to produce a number of biologically and chemically reactive substances, as described in Chapter 1. To calculate the rate of formation of these products in natural waters, it is essential to know the efficiency of the reaction that produces them. Since the energy of solar radiation varies with wavelength, the quantum efficiency of many photochemical reactions is wavelength-dependent. As a result, it is useful to study the spectral efficiency or "spectral quantum yield" of a reaction.

Spectral quantum yield has been determined for a number of photochemical products, including hydrogen peroxide (Moore *et al.*, 1993), formaldehyde (Kieber *et al.*, 1989), and carbon monoxide (Valentine and Zepp, 1993; Kettle, 1994). Valentine and Zepp (1993) reported that the high quantum yield of carbon monoxide probably made its production a significant sink for biologically refractory DOM in sea water. Miller and Zepp (1995) found that DIC was produced from CDOM at about twenty times the rate of carbon monoxide production. Several authors have since measured quantum yield points or spectra in fresh water, as described in the "*Carbon cycle*" section of Chapter 1, but currently there are no published quantum yield spectra for DIC in sea water.

The spectral quantum yield, $\phi(\lambda)$, of a reaction is defined as (Balzani and Carassiti, 1970):

$$\phi(\lambda) = \frac{\text{number of molecules undergoing a process}}{\text{number of photons absorbed by the reactant}} \quad (2.1)$$

(All symbols and abbreviations used in this thesis are listed in the table on page ix.) For the production of DIC from CDOM, equation (2.1) becomes:

$$\phi(\lambda) = \frac{\text{moles of DIC produced from CDOM}}{\text{moles of photons absorbed by CDOM}} \quad (2.2)$$

Because neither the molar absorptivity of CDOM nor the reaction mechanism for the photochemical production of DIC is known with confidence, equation (2.2) represents an "apparent" spectral quantum yield.

This chapter presents the first DIC quantum yield spectra calculated for sea water. They were determined using samples from the Gulf Stream, the Mid-Atlantic Bight, and Bedford Basin and the North West Arm, Nova Scotia. The variability of DIC quantum yield with location and depth is also described, and an explanation for that variability is suggested.

CDOM Absorptivity

The first law of photochemistry, the Grotthus-Draper Law, states that only light that is absorbed can effect a chemical change (Balzani and Carassiti, 1970). In the ocean

CDOM absorbs the radiation that drives the photoproduction of DIC. CDOM is coloured, biologically refractory, and of high molecular weight (100 000 to 300 000 amu; Poutanen and Morris, 1983). It is also known as "Gelbstoff", "gilvin", "dissolved humic substance" and "non-living dissolved organic matter". Since Kalle's (1966) work on the absorbance of UV radiation by CDOM, much research has concentrated on the characterization of this material – its origin, composition, distribution, spectral absorbance, complexation, and sinks. It has both terrestrial and marine sources, which seem to result in different chemical compositions, although the structure of CDOM is as yet unknown. Ertel *et al.* (1984) described the composition of terrestrially-derived CDOM; it includes proteins, carbohydrates and lignin, and has a large phenolic component which is derived from the lignin. Marine-derived CDOM has fewer aromatic structures and contains no lignin. Marine- and terrestrially-derived CDOM have been shown to be different by ^{13}C-NMR (Hedges *et al.*, 1992), chemical composition analysis (Mopper, 1977), and fluorescence spectroscopy (Coble, 1996.) Several authors have demonstrated the *in situ* formation of marine CDOM from the degradation products of phytoplankton (Nissenbaum and Kaplan, 1972; Harvey *et al.*, 1983; Poutanen and Morris, 1983), while terrestrial CDOM is thought to come from the decomposition of terrestrial plants. However, some of the CDOM found in the open ocean may be reworked terrestrially-derived material.

Despite compositional differences in CDOM among source locations, its absorbance spectrum is always a fairly smooth, exponential decay with increasing wavelength (for example, Bricaud *et al.*, 1981; Zepp and Schlotzhauer, 1981; Carder *et al.*, 1989; Blough

et al., 1993; Green and Blough, 1994; Vodacek *et al.*, 1996). The smoothness of the spectrum is probably caused by the size and complexity of the material, which contains many different chromophores.

Absorbance, $A(\lambda)$, is defined as the attenuation of radiation over a defined path length (modified from the Beer-Lambert Law presented in Balzani and Carassiti, 1970):

$$A(\lambda) = \log_{10}(E_i(\lambda,0) / E_i(\lambda,z)) \qquad (2.3)$$

where, in a spectrophotometer, $E_i(\lambda,0)$ is the irradiance ($Wm^{-2}nm^{-1}$ or moles photons $m^{-2}s^{-1}nm^{-1}$) that enters the medium, $E_i(\lambda,z)$ is the irradiance ($Wm^{-2}nm^{-1}$ or moles photons $m^{-2}s^{-1}nm^{-1}$) that leaves it, λ is wavelength (nm), and z is pathlength (m). Since pathlength varies among spectrophotometers, absorptivity is commonly used instead of absorbance. Absorptivity, $a(\lambda)$ (m^{-1}), is related to absorbance by:

$$a(\lambda) = 2.303\, A(\lambda) / z \qquad (2.4)$$

The factor 2.303 converts from base 10 logarithm to natural logarithm.

In general, the magnitude of CDOM absorptivity at all wavelengths decreases offshore (Bricaud *et al.*, 1981) by as much as an order of magnitude. While some authors have reported that the slope of the log-linearized CDOM absorbance spectrum (hereafter referred to as the "slope of the absorbance spectrum" or "absorbance slope" for

consistency with general usage) is fairly constant everywhere, with an average slope of about -0.015 nm^{-1} (Bricaud *et al.*, 1981; Zepp and Schlotzhauer, 1981; Carder *et al.*, 1989), more recent work has shown great variability (Blough *et al.*, 1993; Højerslev, 1998). In this study, absorbance slopes were measured with a range of -0.007 to -0.05 nm^{-1} in the Mid-Atlantic Bight alone. The slope depends strongly on the spectral range over which it is calculated.

2.2 Methods

The photochemical production rate of DIC, *d[DIC]/dt* (moles DIC $m^{-3}s^{-1}$), in an optically thin solution can be expressed as:

$$d[DIC]/dt = \int E_0(\lambda)\, a_{CDOM}(\lambda)\, \phi(\lambda)\, d\lambda \qquad (2.5)$$

where $E_0(\lambda)$ is the scalar irradiance (moles photons $m^{-2}s^{-1}nm^{-1}$), and $a_{CDOM}(\lambda)$ is CDOM absorptivity (m^{-1}). The spectral quantum yield can be calculated from measurements of spectral irradiance, absorptivity and DIC production rate during an irradiation experiment as described below. (In the solar simulator, we measure downwelling irradiance, not scalar irradiance, but since the cells are arranged on a black, velvet cloth inside the irradiation box, and the incident radiation is approximately collimated, the measurement is probably reasonable.)

Water sample collection and storage

Samples were taken from the Mid-Atlantic Bight and from Bedford Basin and the North West Arm, Nova Scotia (figure 2.1; sample names and locations in table 2.1). One litre of sea water was collected from within a metre of the surface and 1 litre from below the mixed layer at each station, using a CTD rosette, except in Bedford Basin, where water was only collected from the surface, using a Niskin bottle on a hydrowire, and in the North West Arm, where water was collected from the surface in a 4 l polycarbonate bottle. Each sample was filtered immediately on board the ship through a 0.2 μm Schleicher and Schuell Nylon 66 filter to remove particles and bacteria, except for the Bedford Basin and North West Arm samples, which were filtered on return to the laboratory within a day of collection. The Bedford Basin and North West Arm samples and those taken during the August 1997 cruise in the Mid-Atlantic Bight were pressure-filtered using a peristaltic pump with an in-line filter; the others were vaccuum-filtered. After filtration, samples were stored for less than a year at 4°C in amber glass bottles to minimize biological activity and photochemical breakdown of CDOM.

DIC stripping and irradiations

The determination of quantum yield spectra for the photochemical production of DIC in seawater presents several difficulties. The high concentration of DIC in sea water (about 2000 μM, Libes, 1992) would mask completely the low concentrations of DIC produced photochemically over a 4 - 12 hour irradiation — typically 1-8 μM in this study — if the DIC initially present were left in the sample. Accordingly, all the pre-existing DIC was stripped from the samples before irradiating them. Each stored sample was refiltered

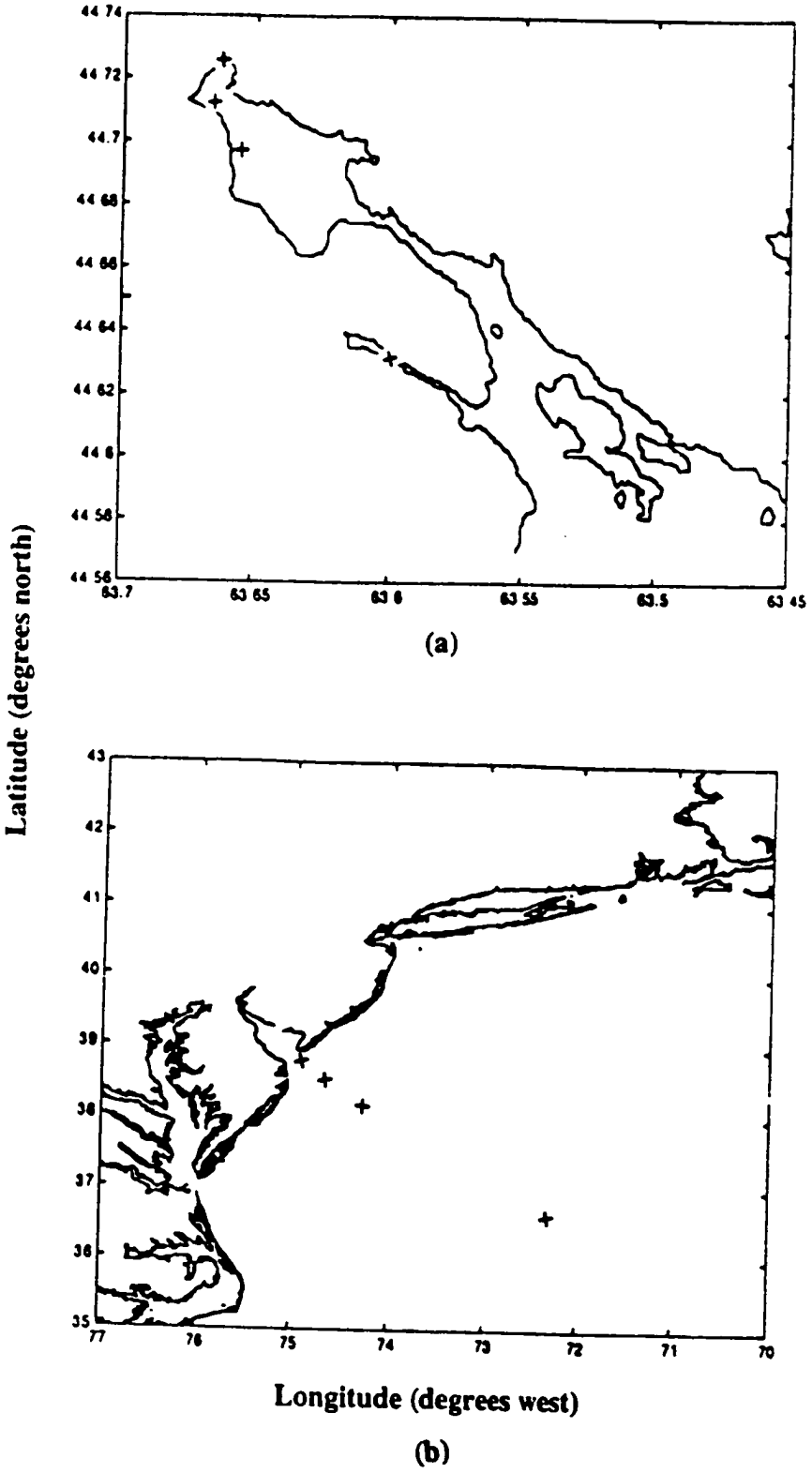

Figure 2.1. Sample locations for quantum yield determinations: (a) Halifax Harbour, Nova Scotia; (b) Mid-Atlantic Bight.

Sample name	Latitude (°N)	Longitude (°W)
M9705-03s	38.67	74.88
M9705-03d	38.67	74.88
M9705-05s	30.52	74.68
M9705-05d	30.52	74.68
M9705-16s	36.21	72.00
M9708-08s	37.27	74.36
M9708-08d	37.27	74.36
M9708-16As	36.21	72.00
M9708-16Ad	36.21	72.00
F9805-01	44.73	63.66
F9805-03	44.71	63.67
F9805-04	44.70	63.66
NW Arm 9906 (unfaded)	44.62	63.56
NW Arm 9906 (faded)	44.62	63.56

Table 2.1. Sample names and locations. Samples beginning with "M" come from the Mid-Atlantic Bight; those beginning with "F" come from Bedford Basin, Nova Scotia; and "NW Arm" refers to the North West Arm, Nova Scotia. The four digits following the location code refer to the year and month of collection, for example "9708" means August 1997. The number following the hyphen is the station number, and "s" and "d" mean surface and deep, i.e. below the mixed layer, respectively. "Faded" means previously exposed to prolonged irradiation in the solar simulator, as explained in the text.

sequentially through two 47 mm Schleicher and Schuell Nylon 66 membrane filters (pore size 0.2 μm) into a glass Erlenmeyer flask and then into a glass sparging vessel. The sparging system was assembled as shown in figure 2.2 and the sample acidified to a pH between 3 and 4 with concentrated HCl to convert all the carbonate and bicarbonate into CO_2. Carbon dioxide-free air was then bubbled through the sample for about an hour, until no measurable DIC remained.

The stripped sea water was buffered back approximately to the original pH with powdered Fisher ACS sodium borate ($Na_2B_4O_7 \cdot 10\ H_2O$). The addition of the acid and buffer to a sample was found to increase its absorptivity by about 5% in the UVB, leaving the longer-wavelength portion of the spectrum essentially unchanged. Control experiments showed that neither of these additives produced measurable DIC photochemically. It was not feasible to strip the DIC from sea water samples without acidification; two days of bubbling with CO_2-free air without acidification resulted in no measurable decrease in the DIC concentration.

Another complication of initial attempts at these experiments (data not shown) resulted from the production of DIC by bacterial respiration during the irradiations. Bacterial respiration could not be subtracted from the total production in each cell using the dark value in these early experiments, because bacteria did not grow equally well in all cells: UV radiation damages bacteria (Kaiser and Herndl, 1997), so they were more metabolically active in the dark and long wavelength cut-off cells. The experiments contaminated in this way were not used to calculate the fourteen quantum yield spectra

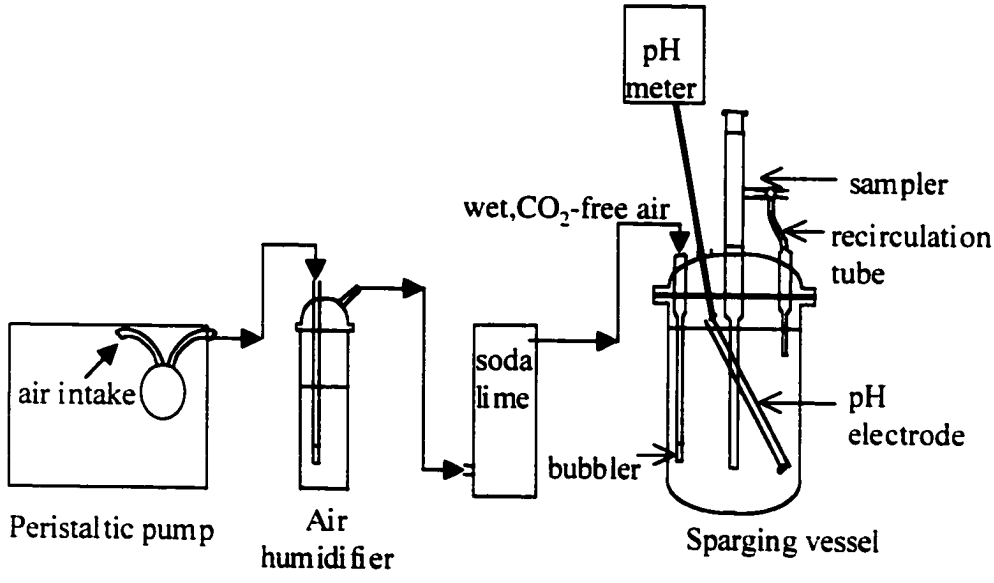

Figure 2.2. Sparging system: CO_2-free air is bubbled through acidified sample to remove all DIC initially present.

presented in this thesis. To minimize such contamination in the experiments whose results are shown here, the quartz irradiation cells and their silicon fittings were sterilized for at least three hours under a Phillips TUV 30W / G30 T8 long-life ultraviolet UVC source in a laminar flow clean hood before each experiment. The fittings were attached to the irradiation cells inside the laminar flow hood. The DIC-free sea water was injected into the irradiation cells through their sterilized silicon septa, directly from the sparger's sample port, using a new, sterile 21.5 gauge needle for each experiment. Gloves were always worn when the glassware was being handled, and all the glassware and tubing for the sparging system were soaked overnight in 10% HCl before each use. With these precautions, the dark control value of DIC production was typically the same as that measured under the 480 cut-off filter (filters described in the following section) and lower than that measured under the next shortest wavelength cut-off filter (380 nm).

To determine spectral quantum yield, samples were irradiated in a Heraeus Suntest CPS solar simulator with a 1000 W xenon lamp as described by Xie *et al.* (1998). Fourteen quartz irradiation cells were arranged in an aluminum and brass frame under Schott long-pass cut-off filters as shown in figure 2.3. Each cell was wrapped in black electrical tape, leaving only the ends open, to prevent the lateral leakage of radiation among cells. Two dark cells were included to correct for non-photochemical production of DIC during irradiation, although production under the 480 nm cut-off filter was eventually used instead of the dark, because that value was often indistinguishable from the dark production. Cells were always oriented as near to vertical as possible to avoid pathlength variations. The method was not very sensitive to such variations however; a cell with a

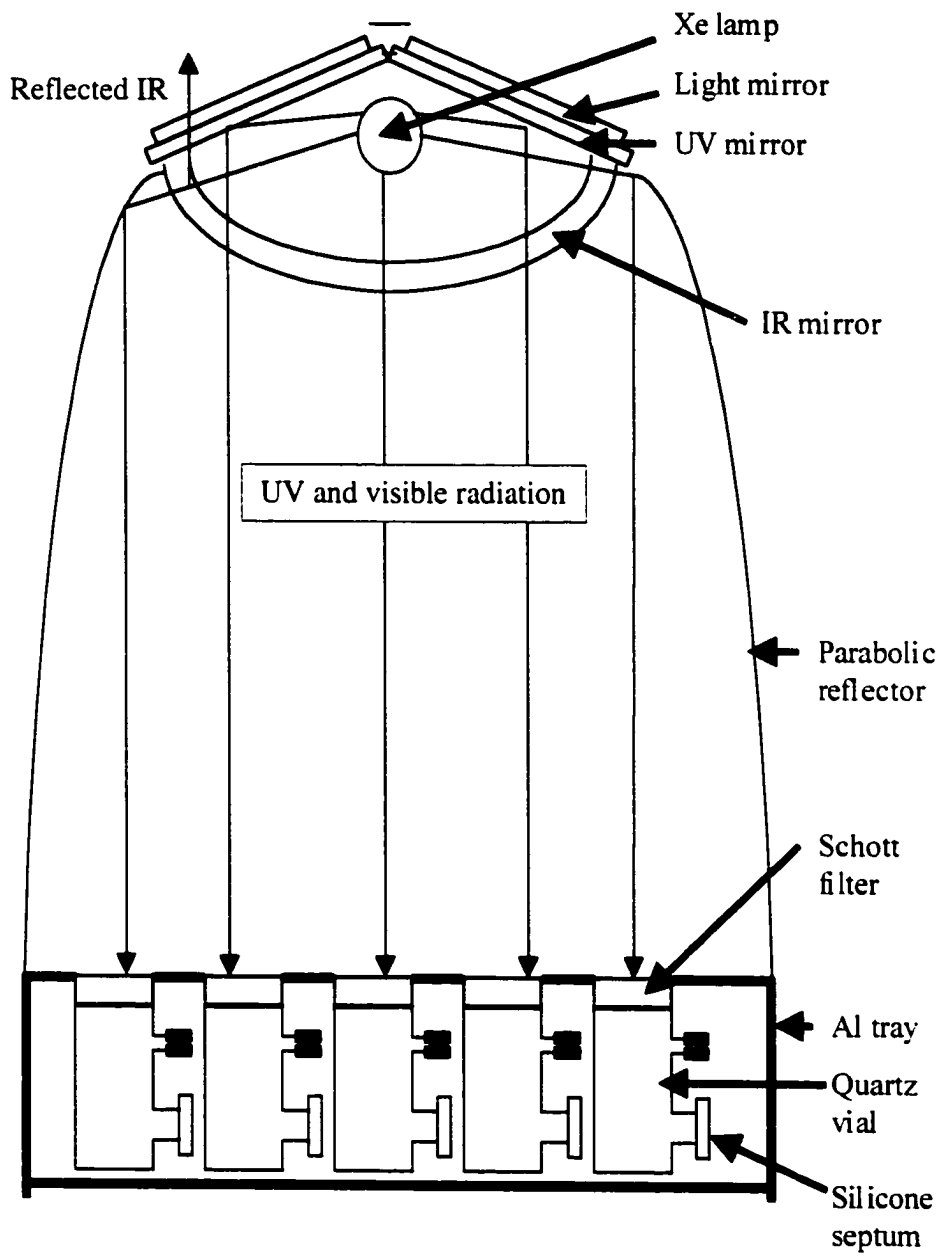

Figure 2.3. Schematic diagram of solar simulator with irradiation cells. (Modified from Moore, 1999.)

thirty degree tilt from vertical showed only ten percent less DIC production than observed in previous irradiations. During all other irradiations, cells were oriented within five degrees of vertical. Each filter transmitted about 90% of the incident radiation at long wavelengths; the transmission decreased sharply to zero at shorter wavelengths, with 50 % transmission at one of the following "cut-off" wavelengths: 280, 295, 320, 335, 380, and 480 nm. Six pairs of matched filters were used for replicate irradiations. It was not always possible to obtain data from replicate cells because of limited sample volumes and because some samples developed bubbles during irradiation, making them unusable. Where replicates were used, the two production values were within five percent of one another, despite the slight non-uniformity of the light field in the solar simulator. Irradiation times varied from 4 to 7 hours. Spectral downwelling irradiance was measured under each filter with an Optronics OL754 spectroradiometer fitted with a fibreoptic cable. Successive measurements with the spectroradiometer showed less than 1% variation in the irradiance measured at any wavelength. Figure 2.4 shows the spectral irradiance measured under each filter.

To test the effect of irradiation history on quantum yield, 1 litre of water from the North West Arm was prefaded by irradiating it for 111 hours at the full output intensity of the solar simulator in an open borosilicate vessel covered with UV-transparent polyethylene film (Cling Wrap®). The maximum intensity of the solar simulator was 3.3 times that of the irradiance shown in figure 2.4. Two quantum yield experiments were then conducted as usual, one on the prefaded water and the other on a portion of the same sample which

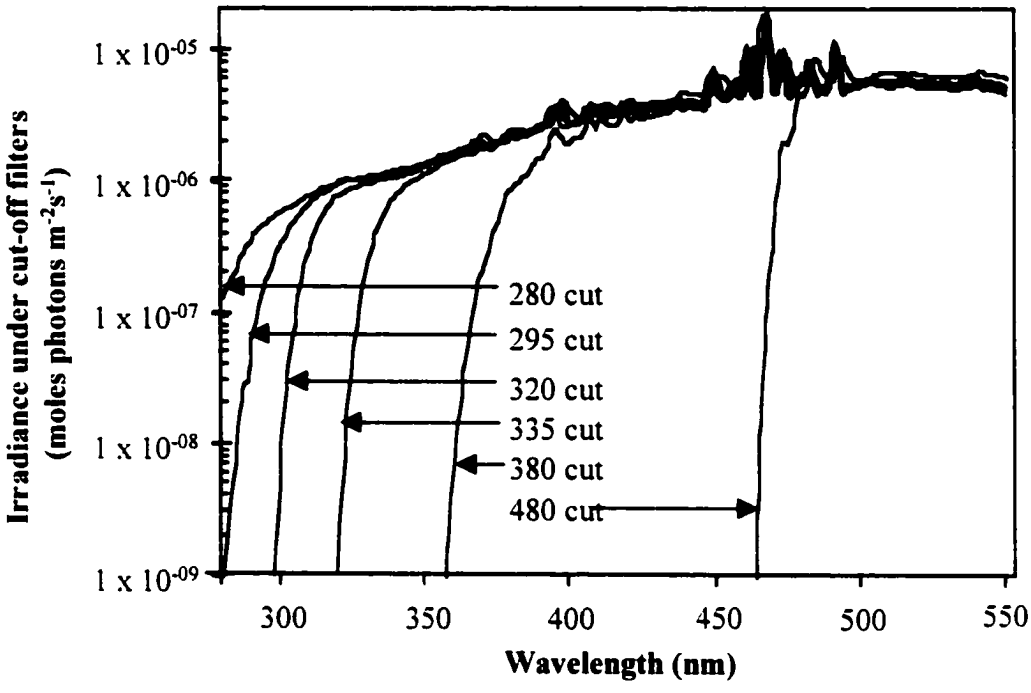

Figure 2.4. Dowwelling irradiance measured under cut-off filters in solar simulator set to minimum output.

had not been previously faded but which had been stored at 4°C in an amber glass bottle while the first portion was faded.

DIC measurements

After irradiation, several millilitres of water from each irradiation cell were extracted with a 21.5 gauge needle into a 10 ml gas-tight syringe though the silicon septum. Three to seven replicate 200 µl sub-samples were injected with a repeating pipet into the acid trap and sparger of the CO_2 analyzer system shown in figure 2.5. The phosphoric acid (pH=2.0) in the acid trap converted all the inorganic carbon species into CO_2 which was then stripped from the sample and carried into the system in a stream of UHP nitrogen gas. The sample CO_2 passed sequentially through Drierite (anhydrous $CaSO_4$, Hammond Drierite Company) and magnesium perchlorate ($Mg(ClO_4)_2$, Aldrich ACS) columns to remove water vapour before entering a Li-Cor 6262 CO_2 / H_2O infrared detector. The CO_2 analyzer was calibrated daily with a series of standards (0, 5, 10 and 20 µM DIC) made each day from a stock 5mM sodium carbonate solution that was made freshly about once a month from dried sodium carbonate (Na_2CO_3, BDH AnalaR). All the calibration curves had $r^2 > 0.98$ except one which had $r^2 = 0.97$. The standard deviation of the mean of 50 replicate injections of distilled water was 0.16 µM. The limit of detection, defined as 3 times the standard deviation for the distilled water measurement, was 0.5 µM. This is definitely a conservative estimate of precision, since the distilled water injections were done over several months and their standard deviation included the day to day variability of the machine, while a new standard curve was made every day.

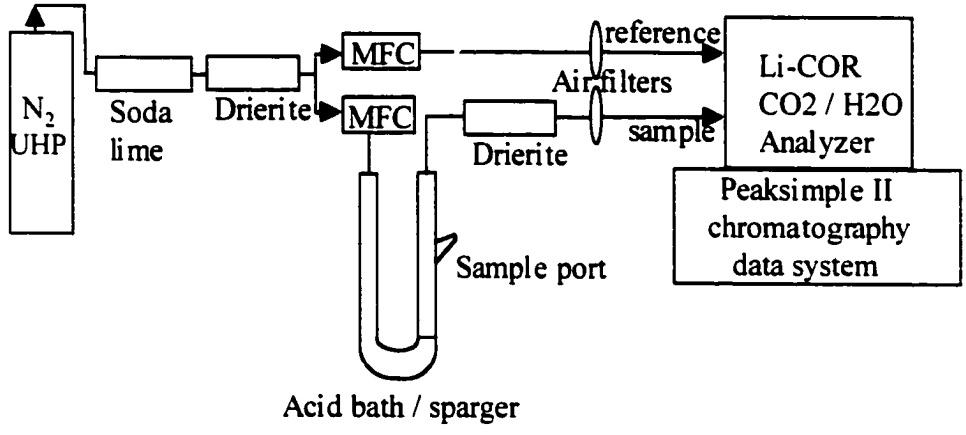

Figure 2.5. CO_2 analysis system. Sample is injected into acid bath in sparger to convert DIC to CO_2. CO_2 is carried on N_2 stream through infra-red detector in Li-COR CO_2 / H_2O Analyzer. The signal from the Li-COR is analyzed by SRI Instruments Peaksimple II chromatography software. "UHP" nitrogen is ultra-high purity grade. "MFC" stands for mass flow controller.

Absorbance measurements

The spectral absorbance of each filtered, DIC-stripped sample was measured with reagents added prior to irradiation, so that it represented as closely as possible the colour of the solution that was irradiated. Spectral absorbance was measured against a Nanopure, UV-irradiated distilled water blank in a cylindrical, 10 cm quartz cell with a Varian CARY3 dual-beam scanning spectrophotometer. (Absorbance measurements for the optical relationships determined in Chapter 3 were made using a Hewlett Packard HP8453 diode array spectrophotometer. The two spectrophotometers gave nearly identical results after the spectra were corrected as described below.) The sea water samples and distilled water for the blank were temperature-equilibrated in a shallow water bath at room temperature for an hour prior to absorbance measurement. Absorbance, $A_{CDOM}(\lambda)$ (AU), was measured from 280 nm to 800 nm, and the values were converted to absorptivity, $a_{CDOM}(\lambda)$ (m^{-1}), using equation (2.4).

Scattering by fine particles, blank drift (in diode array spectrophotometers), and a difference between the index of refraction of the seawater sample and of the distilled water blank can all affect the measured spectral absorbance. Instead of correcting for each problem individually, an equation of the form:

$$a_{CDOM}(\lambda) = Ce^{-S\lambda} + a_0 \qquad (2.6)$$

was fitted to each absorbance spectrum over the range 280-550 nm, where C (m^{-1}),

S (nm^{-1}) and a_0 (m^{-1}) are fitting parameters and λ is wavelength (nm). The offset, a_0, was then subtracted from the whole spectrum. The fit was not used for any purpose other than to provide an offset value. Figure 2.6 shows the absorptivity spectra for the darkest and clearest samples. All the absorptivity spectra and the calculated fits are shown in Appendix 2.

Calculation of quantum yield spectra

Spectral quantum yield for each irradiation experiment was calculated by two methods: calculation by difference, and a curve fit based on the method described by Rundel (1983). The difference method consisted of dividing the difference between the number of moles of DIC produced under filters with adjacent wavelength cut-offs by the difference between the irradiance measured under the two filters, as described by Xie *et al.* (1998). For example:

$$\phi(287.5\text{nm}) = \frac{d[DIC]/dt\,(280cut) - d[DIC]/dt\,(295cut)}{E_0(280cut)a_{CDOM} - E_0(295cut)a_{CDOM}} \qquad (2.7)$$

The resulting quantum yield point was plotted at the wavelength halfway between the two successive cut-off wavelengths. In this way, five quantum yield points were calculated for each experiment, using six different cut-off filters. (Plotting the quantum yield point at the central wavelength between two cut-off wavelengths is not ideal where the quantum yield changes rapidly with wavelength; the point should actually be plotted closer to the shorter cut-off wavelength, as explained by Rundel (1983) and Cullen and Neale (1997)). This method was complicated by the non-uniformity of the light field

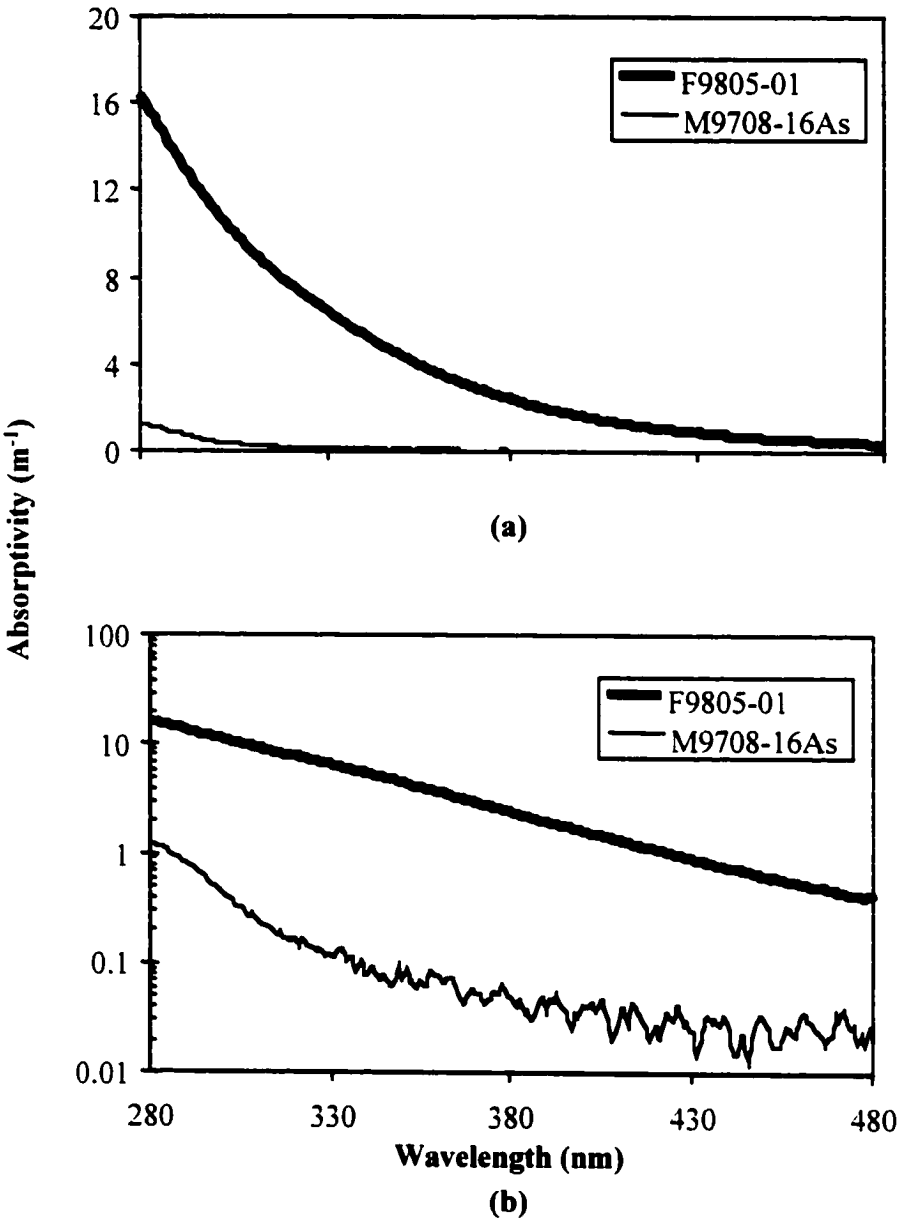

Figure 2.6. Absorptivity spectra for water from the darkest (F9805-01) and clearest (M9708-16As) stations used in this study. (a) linear scale (b) log scale

inside the solar simulator. Irradiance and production values had to be corrected to represent the values that would have been measured had the intensity of incident radiation been the same above the each filter at every location in the box. Each irradiance spectrum and production value was normalized with respect to the irradiance measured under the filter in hole #1 of the irradiation box by summing the irradiance measured under each filter from 450 to 550 nm and calculating the ratio of that sum for each filter to that measured in hole #1. (It was important to compare the spectra measured under each cut-off filter in the position in which the filter was used during irradiation, rather than to compare the irradiance at each location under the same filter, to account for differences in the reflective properties and thicknesses of the different filters.) The sum of irradiance measured under each filter from 280 nm to 550 nm was divided by the ratio calculated as above before adjacent irradiance measurements were subtracted. The production value in each cell was divided by the same ratio. Obviously, the normalization described above introduced errors into the quantum yield estimate, but the difference calculation could not be made without it.

The curve-fit (Rundel) method did not require any such normalization. Instead, this method assumed a spectral shape for the quantum yield. The measured DIC production values and the product of spectral irradiance and CDOM absorptivity in each cell (after subtraction of the production value from the cell under the 480 nm cut-off filter, which was used as a dark) were entered into a Matlab® program. The program then calculated best fit parameters m_1 and m_2 for the equation:

$$\phi(\lambda) = e^{-(m1+m2(\lambda-290))} \qquad (2.8)$$

(A double exponential fit did not improve the fit to the data and seemed an unnecessary complication.) The program changed m_1 and m_2 iteratively from initially input values to find the best match between the measured production values and those predicted by equation (2.5). The agreement between predicted and measured DIC production values was very good, with r^2 values ranging from 0.92 to 0.99 (n=6-9). Figure 2.7 shows the match between measured and calculated values of DIC production for the best and worst fits obtained. It demonstrates that even the worst fit described the observed production rates reasonably well. Eleven of the fourteen calculated quantum yield spectra predicted DIC production with $r^2 > 0.96$. Error bars in figure 2.7 show the 95% confidence intervals for measured DIC production, determined from the variability in fifty replicate distilled water DIC measurements made throughout the five-month period of the experiments.

The curve-fit method has several advantages over the difference method. It does not require so much data manipulation and uses all the spectral information available. Because it does not rely on differences between adjacent production values, it is more resistant to single outlying values. It also avoids the problem of plotting quantum yield values at the central wavelength of each irradiance band, as described for the difference method. However, the difference method, while somewhat clumsy, is thoroughly transparent at each step. It requires a detailed understanding of the unit changes and calculations performed at each step. It also provides an order-of-magnitude check for the

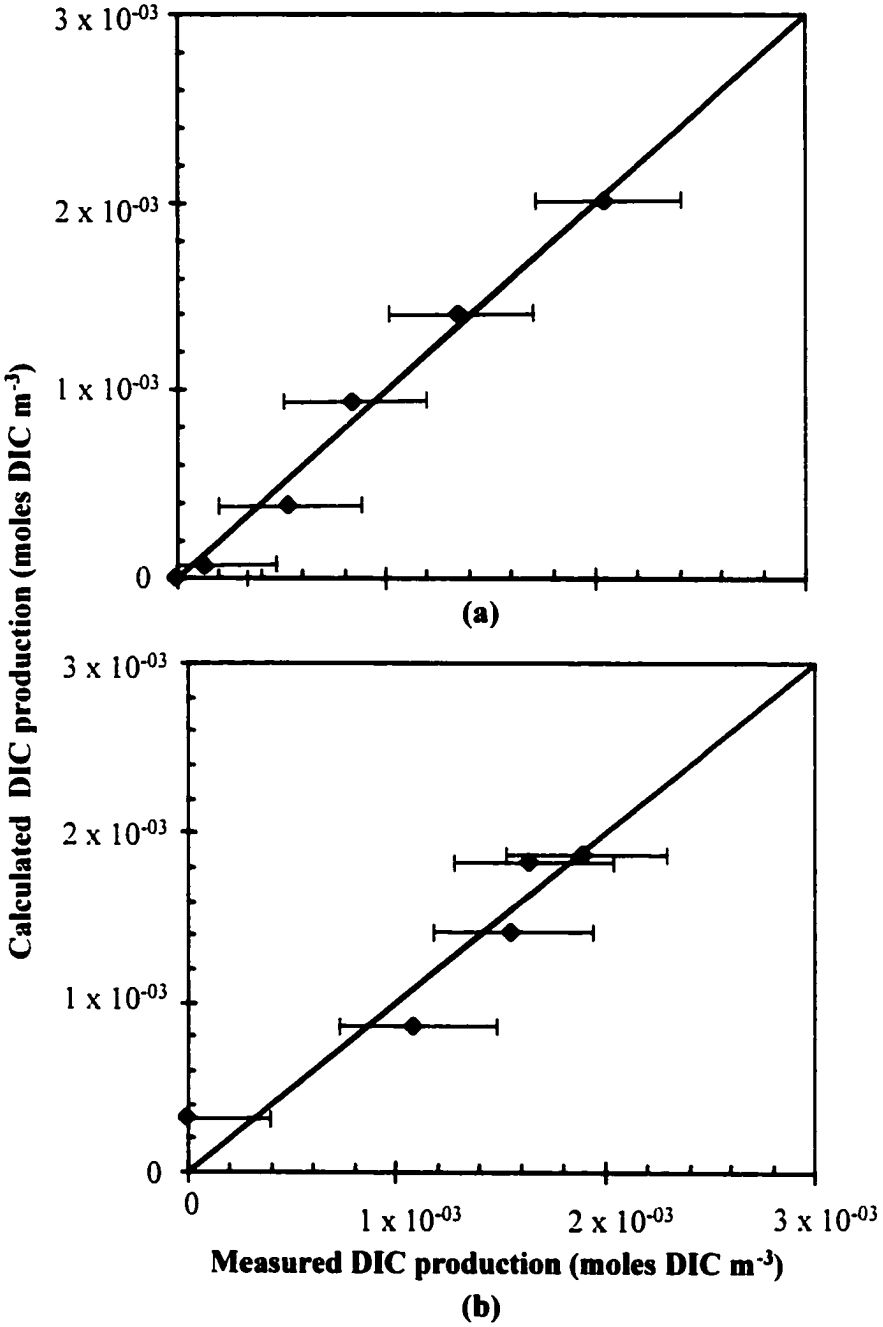

Figure 2.7. Calculated (using Rundel statistical fit) *vs.* measured DIC photoproduction in irradiation cells for samples with the best and worst fits: (a) sample F9805-04 ($r^2 = 0.99$); (b) sample m9701-03d ($r^2 = 0.92$). One-to-one lines show where the calculated values would fall if they reproduced exactly the measured values. Error bars show the 95% confidence intervals for the measured DIC production values, calculated from the variability in 50 replicate distilled water DIC measurements made over a five-month period.

curve-fit method, which can give completely erroneous answers without any indication of a problem. Calculating every spectrum both ways increases confidence in the estimate of quantum yield. Figure 2.8 shows the quantum yield spectrum for the surface sample from station 5 calculated using both methods. For all other spectra only the results of the curve-fit method are shown.

2.3 Results

Apparent quantum yield spectra were determined for fourteen samples from the Gulf Stream, the Mid-Atlantic Bight, and the Northwest Arm and Bedford Basin, Nova Scotia. The spectra varied, both in shape and in magnitude. See table 2.2 for a summary of the equations that describe the quantum yield spectra. Although none of the quantum yield spectra could pass through zero at 480 nm, because they were fit to single exponential equations, the resulting production calculated for the cell underneath the 480 cut-off was below the limit of detection in every experiment. Therefore, a non-zero quantum yield at 480 nm is not inconsistent with experimental results. However, this result shows that more experiments are required with additional cut-off filters at wavelengths between 400 and 480 nm to define better the shape of the quantum yield spectra in that region of the irradiance spectrum. Improved measurement sensitivity would also help to determine whether or not there was any photochemical production of DIC by radiation at wavelengths longer than 480 nm.

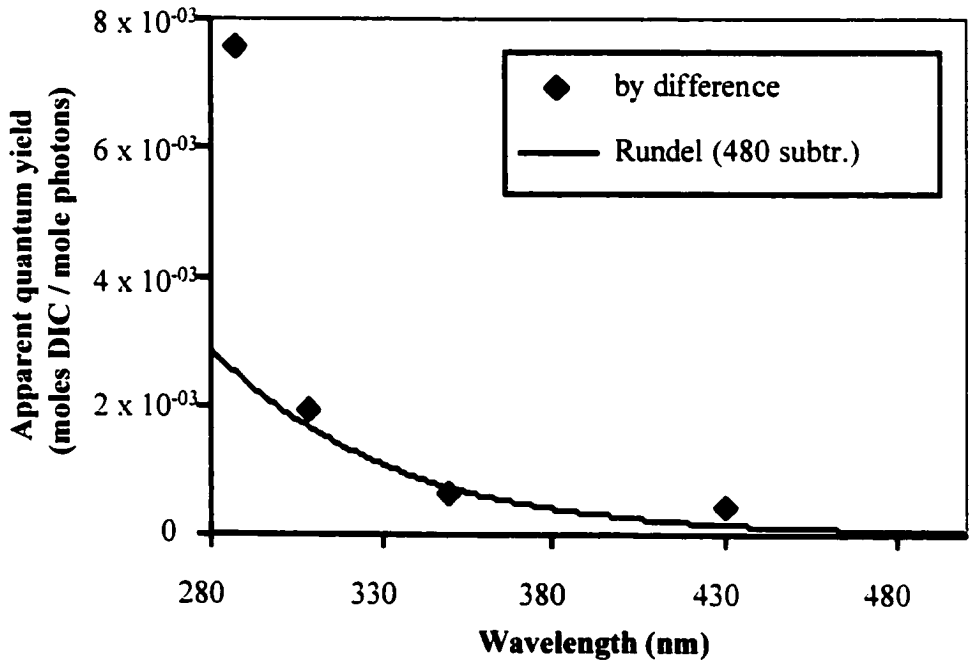

Figure 2.8. Apparent quantum yield spectra for sample m9705-05, calculated using both the Rundel and difference methods.

Sample name	m_1	m_2
Inshore / terrrestrially influenced samples		
NW Arm 9906 (unfaded)	7.5	0.0096
M9708-08s	6.0	0.041
F9805-01	6.7	0.026
F9805-03	5.9	0.051
F9805-04	7.0	0.032
Inshore pooled spectrum	**6.66**	**0.0285**
Coastal samples		
M9708-08d	6.2	0.013
M9705-05s	6.1	0.020
M9705-05d	7.1	0.0083
NW Arm 9906 (faded)	5.7	0.017
Coastal pooled spectrum	**6.36**	**0.0140**
Open ocean samples		
M9705-16s	5	0.012
M9708-16As	5.3	0.013
M9708-16Ad	5.7	0.0073
Open ocean pooled spectrum	**5.53**	**0.00914**
Stn 3 (should be inshore)		
M9705-03s	3.6	0.058
M9705-03d	5.9	0.0068

Table 2.2. Apparent quantum yield fit parameters for the equation: $\phi = e^{-(m1+m2(\lambda-290))}$. Pooled spectra calculated as best fit to all production and irradiance data for each zone.

Neither the slope of an individual log-linearized quantum yield spectrum ($-m_2$; hereafter referred to as the "slope of the quantum yield spectrum" or the "quantum yield slope") nor its magnitude at 290 nm (e^{-m1}) was well predicted by the slope of the corresponding CDOM absorptivity spectrum or by the magnitude of CDOM absorptivity at 290 or 350 nm ($r^2 < 0.4$; data not shown). However, sample location was a strong predictor of quantum yield shape and magnitude, as described below.

The sample locations fell into three broad categories: (1) inshore, including the turbid Bedford Basin, North West Arm, and surface samples just outside the Delaware Bay that were strongly terrestrially influenced; (2) coastal, on the continental shelf in the Mid-Atlantic Bight; and (3) open ocean, Gulf Stream samples of blue water. These zones could be defined roughly by salinity: inshore (salinity less than 31), coastal (salinity between 31 and 35), and open ocean (salinity greater than 35 on the Practical Salinity Scale).

A pooled quantum yield spectrum was calculated for each zone by applying a single exponential fit to all the DIC production, absorbance, and irradiance data for that zone at once (figure 2.9). The equations of the pooled quantum yield spectra are recorded in table 2.2, and figure 2.10 shows their 80% confidence intervals. The confidence intervals for the three pooled spectra overlap. This is not surprising, however, considering the gradational boundaries between the environments represented. The width of the confidence intervals reflects the variability among the samples taken within each zone. The inshore and coastal zone spectra were more variable (r^2 of pooled spectra 0.83

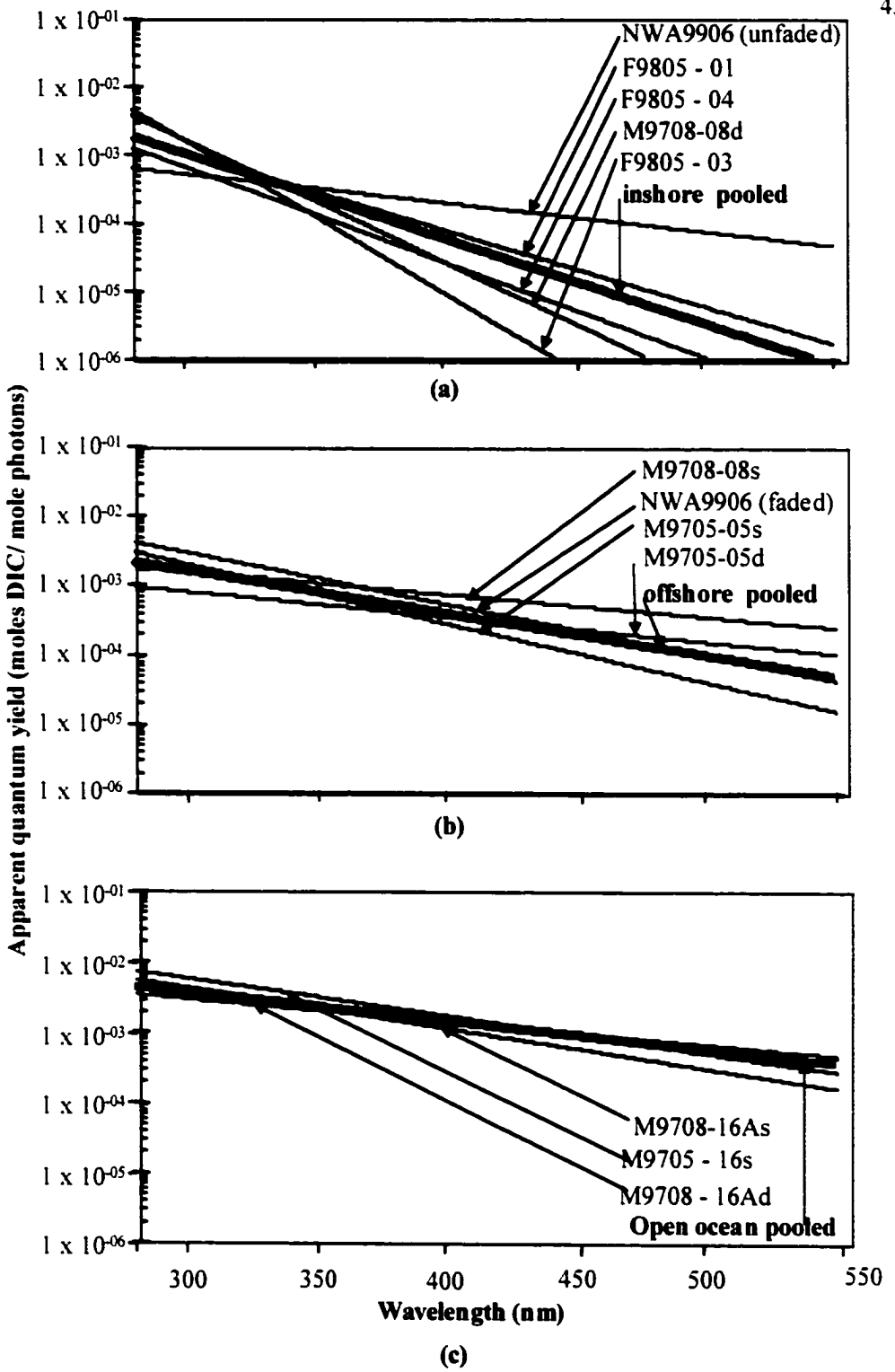

Figure 2.9. Apparent quantum yield spectra for the photochemical production of DIC, arranged by zone, with zone pooled spectra shown. (a) inshore; (b) coastal; (c) open ocean.

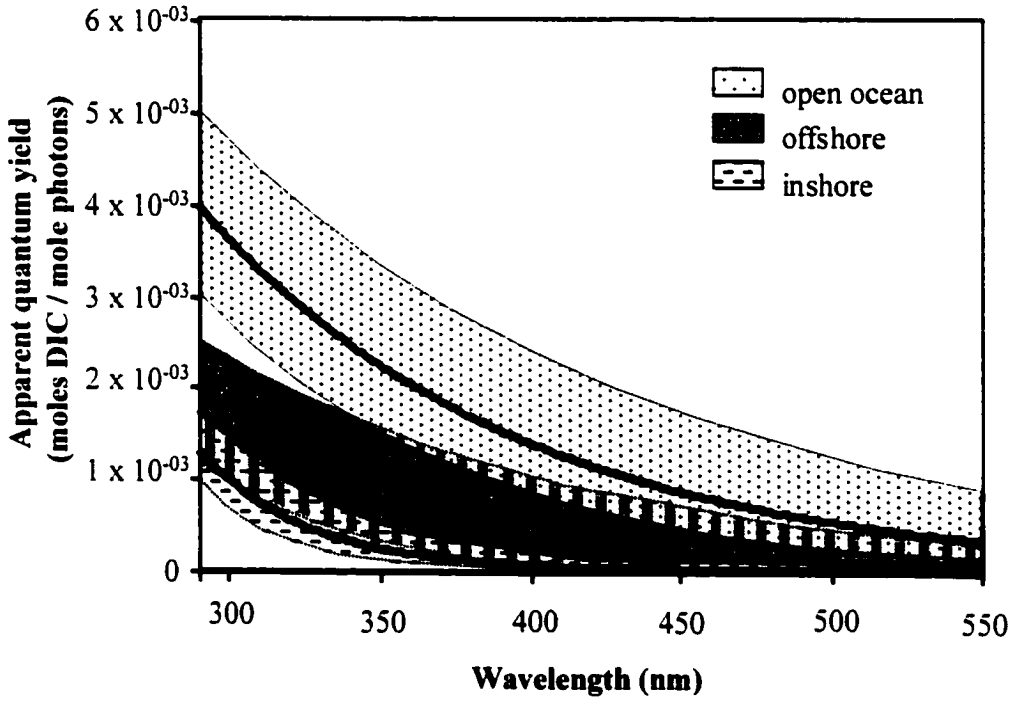

Figure 2.10. Zone average quantum yield spectra plotted with 80% confidence intervals.

(n=25) and 0.82 (n=20), respectively) than were those in the open ocean zone ($r^2 = 0.93$, n=15). The pooled spectra show trends of increasing magnitude and decreasing slope from inshore to offshore. Both trends lead to a greater efficiency of DIC production offshore.

To demonstrate the combined effects of the trends in slope and magnitude, equation (2.2) was used to calculate a volume production rate for each quantum yield spectrum and for the pooled spectra, using identical absorptivity and irradiance spectra (irradiance measured in the solar simulator under 280 nm cut-off filter as shown in figure 2.4) for each calculation (figure 2.11). This isolated the role of quantum yield in production rate calculations. It is clear from this figure that the inshore water is the least efficient at producing DIC, while the open ocean water is the most efficient. For a given colour and irradiance spectrum the largest estimated production rate is twenty-one times that of the smallest. A single quantum yield spectrum clearly cannot be used to predict DIC production rate everywhere in the ocean. The other noteworthy feature of figure 2.11 is the close approximation of the production rates calculated from the individual quantum yield spectra in each zone to that calculated using the corresponding pooled spectrum. Production rates calculated from the pooled spectrum for each zone predict the calculated production rates in water from individual stations in that zone to within 40%. The quantum yield spectrum for the unfaded water from the North West Arm fitted into the inshore category, while, to judge from the calculated production rates, the prefaded sample was more like the shelf samples.

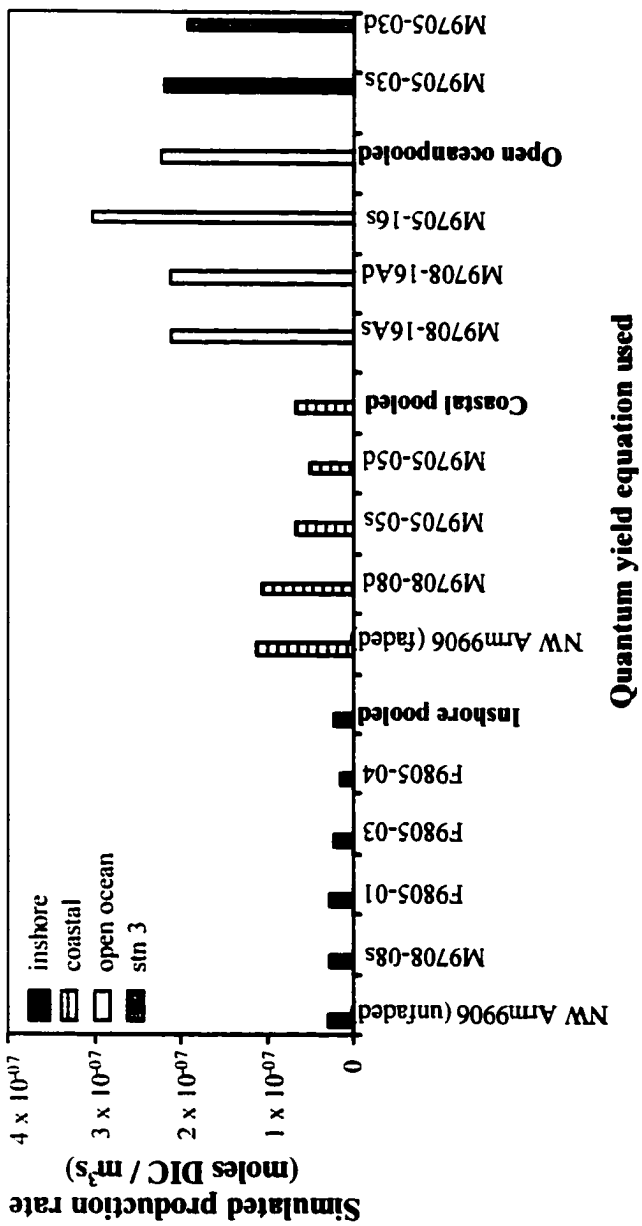

Figure 2.11. Simulated DIC production rate estimates made by multiplying each of the fourteen quantum yield spectra by identical absorptivity and downwelling irradiance spectra. These production numbers should NOT be applied to the real ocean; they are included only to demonstrate the effect of the variability among quantum yield spectra on calculated production rates.

A finer scale trend apparent from the data was that the surface sample at any given station always had a steeper quantum yield slope than did the sample taken from below the surface mixed layer at that station (figure 2.12, for example). Corresponding pairs of surface and deep spectra crossed one another, though not at a consistent wavelength, so that the quantum yield values of the deep samples were higher than those of their surface counterparts in the visible region of the spectrum. The surface sample was always more efficient in the UVB than was the deep sample. It is not unreasonable that the water taken from two depths should show distinct photochemical characteristics, since optical profiles taken at all the stations where deep and surface samples were taken showed a change in the attenuation of UVA and blue radiation at the bottom of the mixed layer. (See Chapter 3).

Response curves were calculated for the three zone pooled quantum yield spectra, defined as the product of $\phi(\lambda)$ and $E_d(\lambda)$ (after Moore, 1999). The response curves represent spectral, water column production rates; they show which region of the spectrum is the most effective over the whole water column at producing DIC. For this calculation the total monthly, clear sky, spectral scalar irradiance just beneath the ocean's surface at 40°N in July (figure 2.13) was used, calculated according to Gregg and Carder (1990) (modified by Arrigo, 1994). To determine the total monthly irradiance, irradiance spectra were calculated at fifteen minute intervals for every day in July 1998 and summed. The response spectra are shown in figure 2.14. Because of the variation in quantum yield slope, the response spectra for different zones have different shapes. The peak response for the inshore zone is at 320 nm, while for the coastal and open ocean

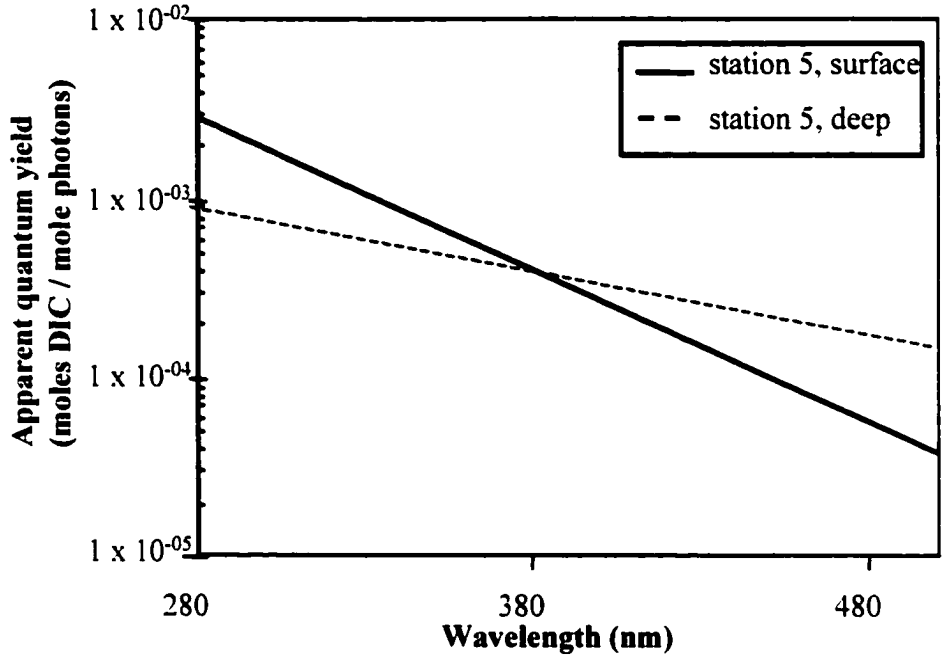

Figure 2.12. Apparent quantum yield for station m9705-05, surface and deep samples. The quantum yield determined for the surface sample was steeper than that for the sample from below the mixed layer at every station.

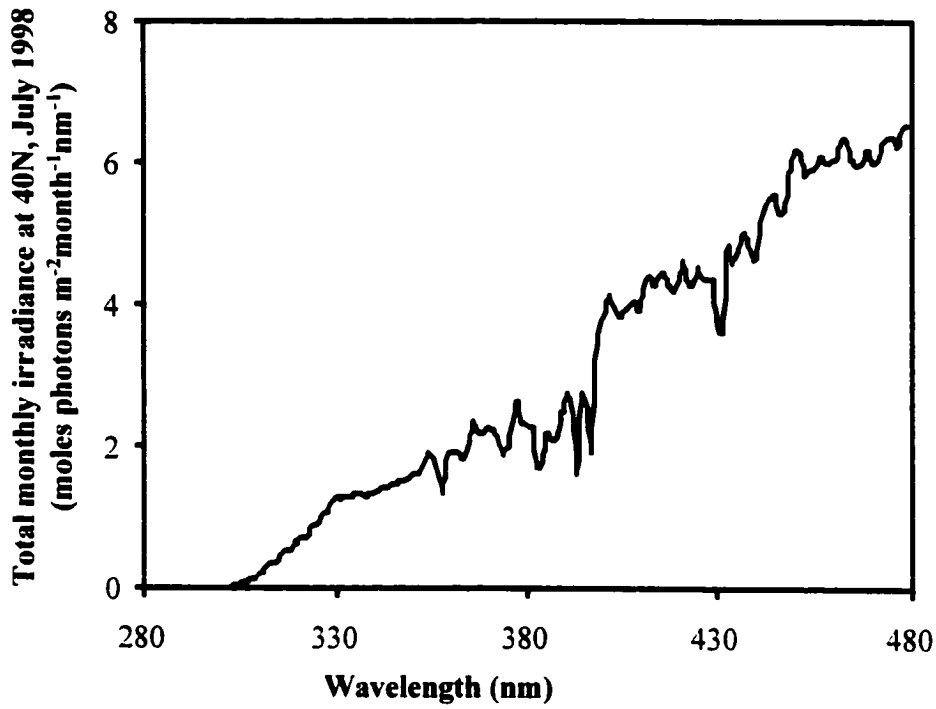

Figure 2.13. Total monthly, clear-sky, scalar irradiance at 40°N, calculated as described in text, from Gregg and Carder, 1990, modified by Arrigo (1994).

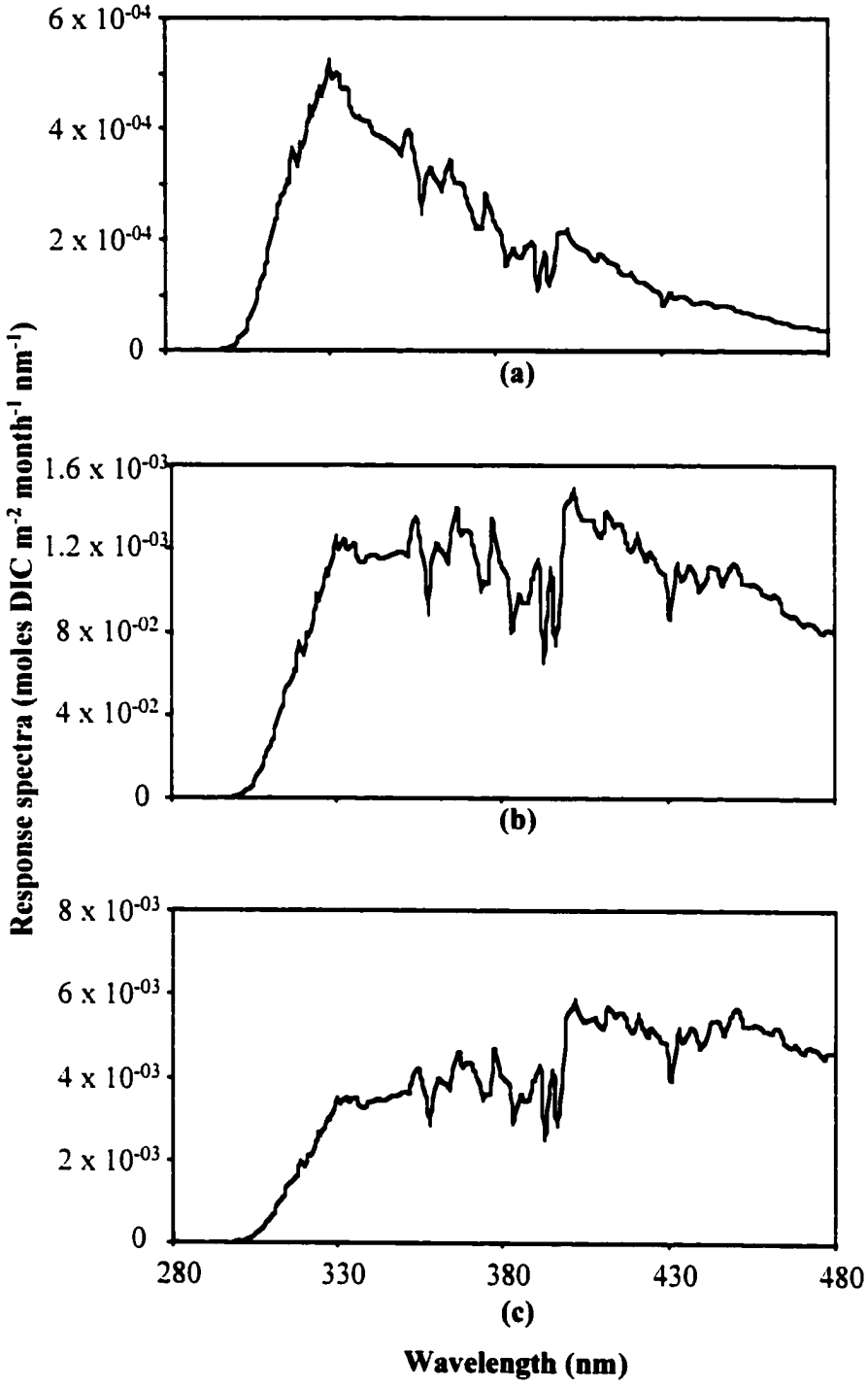

Figure 2.14. Response spectra ($\phi(\lambda)$ x $E_d(\lambda)$) using scalar irradiance spectrum from figure 2.13 and (a) inshore, (b) coastal, and (c) open ocean zone pooled quantum yield spectra.

zones, which have shallower quantum yield slopes, it is shifted to 400 nm. Spectral, near-surface production rates are shown in figure 2.15. They were calculated as the product of the zone pooled quantum yield spectra, the monthly spectral scalar irradiance at 40°N, and absorptivity spectra taken from stations within each zone. The decreasing slope of the quantum yield spectrum with distance from shore combined with the steepening of the absorptivity slope resulted in a peak near-surface DIC production rate at 330 nm for all three zones.

2.4 Discussion

The photochemical production of DIC in all areas of the ocean cannot be calculated accurately using a single quantum yield spectrum. However, it does seem possible to estimate DIC production using a combination of three pooled spectra, one for inshore water (salinity less than 31), one for coastal water (salinity between 31 and 35), and one for open ocean water (salinity greater than 35). Using the pooled quantum yield spectra with appropriate absorptivity and irradiance spectra, it may be possible to calculate DIC production to within 40% of the correct value at any station and probably more accurately as an average over a wider area, since the zone pooled spectra represent averages, not individual stations. More quantum yield determinations would be helpful in assessing the broad applicability of the pooled spectra presented here.

The oligotrophic water was more efficient at producing DIC photochemically than was either the shelf or the inshore water. Of course, the actual surface production rate

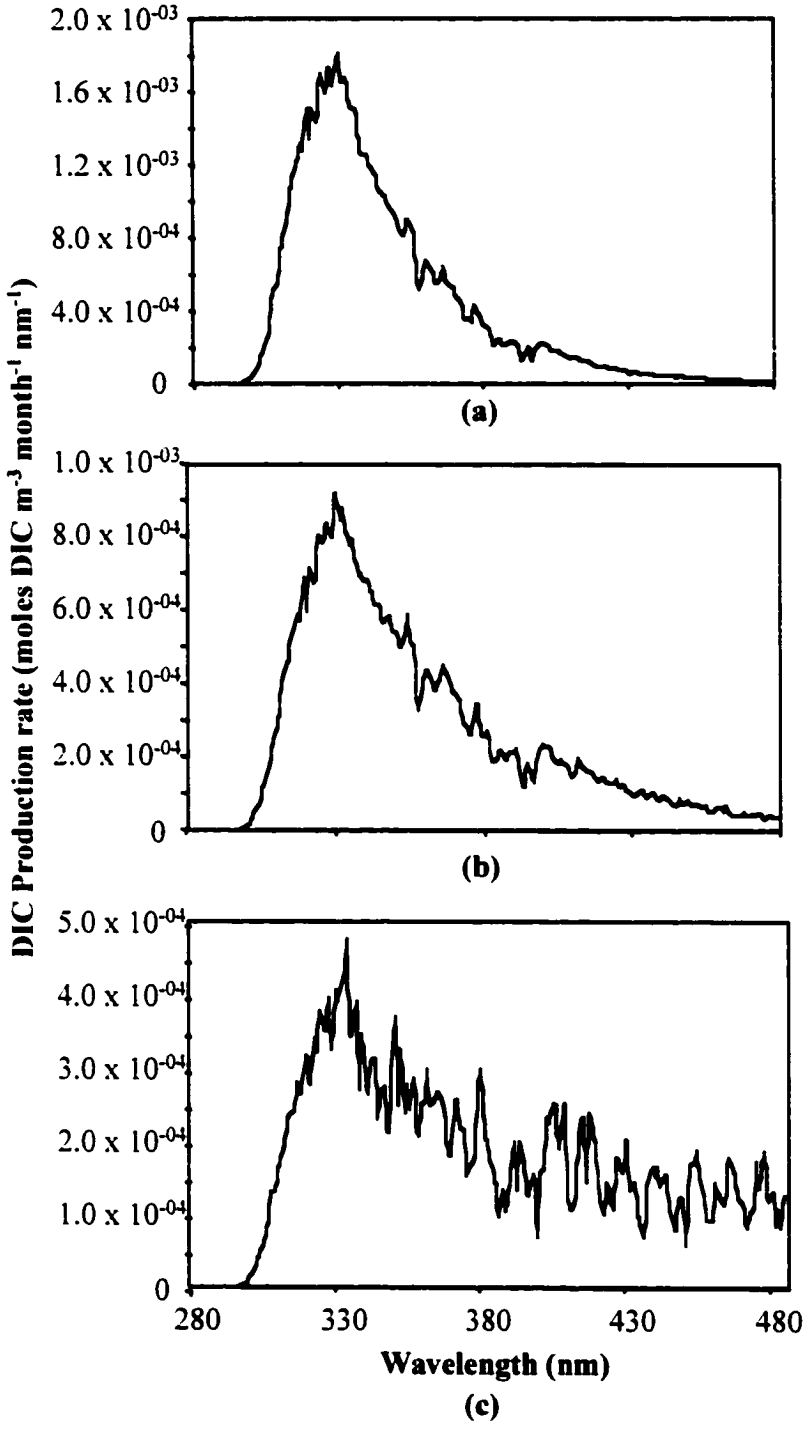

Figure 2.15. Spectral dependence of monthly DIC production rate (scalar irradiance x zone pooled quantum yield x representative absorptivity spectrum)
(a) inshore; (b) coastal; (c) open ocean.

depends on the colour of the water, and inshore water absorbs UV more strongly than does open ocean water. Consequently, the relative importance of the three zones for carbon photochemistry in the surface waters of the ocean is not as skewed toward the blue water as it appears from figure 2.11. However, if one considers photochemical production over the whole water column rather than surface production, then oligotrophic water does produce more DIC photochemically than does inshore water. Since CDOM is thought to be the main absorber of UV radiation in all areas of the ocean (for example, Bricaud *et al.*, 1981), UV penetrates more deeply in water with a lower concentration of CDOM. Ultimately, for the same incident irradiance, about the same amount of UV radiation is absorbed by CDOM over the whole water column, regardless of water type. In that case, for a given irradiance field, only the quantum yield and not the colour of the water will control total water column DIC photoproduction.

The inshore to offshore trend toward greater production efficiency suggests an insight into the DIC photoproduction mechanism. Considering terrestrially-derived CDOM, one might expect that the less degraded material found close to the source would produce DIC more efficiently than the reworked molecules found offshore after prolonged exposure to sunlight, but the opposite is true. The following explanation might resolve the apparent paradox. Photodecarboxylation is the likely mechanism by which DIC is formed from CDOM (Chen *et al.*, 1978). Molecules containing aromatic structures can undergo photodecarboxylation, but it is the attached carboxylic acid functional groups and not the ring structures themselves which produce CO_2 (Budac and Wan, 1992). Inshore, terrestrially-dominated CDOM contains more of the highly-coloured, aromatic

ring structures than does CDOM collected in the open ocean (Meyers-Schulte and Hedges, 1986), while CDOM from both sources contains carboxyl groups. It is possible then, that the largely aromatic components of terestrially-derived CDOM which are responsible for the majority of absorption are not those responsible for DIC photoproduction. As the aromatic structures are eliminated by photochemical fading or as marine-derived CDOM begins to dominate absorbance, the proportion of DIC-producing to non-DIC-producing chromophores within CDOM increases. In this way, the efficiency of the DIC-producing chromophores might remain constant, while the efficiency of the whole molecule for DIC production increased. The loss of non-DIC-forming chromphores by fading is supported by the increased quantum yield determined in North West Arm water following prolonged irradiation in the solar simulator. It is possible that other photochemical products might show different or even opposite trends in efficiency with location and irradiation history, depending on which components of CDOM produce them and on their relative roles in light absorption within the molecule. This should be examined in future studies.

2.5 Summary

This chapter presents the first quantum yield spectra for the production of dissolved inorganic carbon in sea water. Despite wide geographic variability in the spectral quantum yield of dissolved inorganic carbon, it can be represented by three pooled spectra for zones defined by salinity. The selective loss by photobleaching or microbial degradation of highly-absorbing chromophores which do not produce dissolved inorganic

carbon may explain the trend toward increased efficiency of dissolved inorganic carbon photoproduction offshore.

Chapter 3. Optics

3.1 Introduction

Coloured or chromophoric dissolved organic matter, CDOM, in the ocean is a strong absorber of UV and visible radiation (for example, Clarke and James, 1939; Burt, 1958; Kalle, 1966; Bricaud *et al.*, 1981; Druffel *et al.*, 1992) and the precursor for many photochemical reactions, including the photochemical production of dissolved inorganic carbon, DIC. (See Chapter 2.) Both the magnitude and the shape of the CDOM absorbance spectrum vary with time and location (for example, Siegel and Michaels, 1996; Højerslev, 1998), so a single spectrum cannot be assumed for the whole ocean. For depth-resolved production, it is important to know both the absolute spectral absorptivity of UV by CDOM, $a_{CDOM}(\lambda)$, and the rate of total attenuation of photochemically active irradiance with depth, $K_d(\lambda)$. For calculations of total water column production, the proportion of photons absorbed by CDOM must be known (Cullen *et al.*, 1997).

Austin and Petzold (1981) showed that the downwelling attenuation coefficient, $K_d(\lambda)$, for visible radiation could be estimated as a function of the ratio of the upwelling radiance, $L_u(\lambda)$, at two wavelengths, for example as measured by the Coastal Zone Color Scanner satellite. The wavelength ratio approach has also been applied to the prediction of chlorophyll concentration in surface waters (Gordon *et al.*, 1983; review by Aiken *et al.*, 1992). Images of global ocean chlorophyll concentrations are now produced routinely from satellite data taken by the Sea-viewing Wide Field-of-view Sensor (SeaWiFS; SeaWiFS Project, 1999).

A number of investigators have determined algorithms that they suggest could be used to relate remotely-sensed properties to *in situ* absorption or scattering by CDOM or to the concentration of DOC (for example, Fenton *et al.*, 1994; Vodacek *et al.*, 1995; Ferrari *et al.*, 1996). Hochman *et al.* (1994) and Hoge *et al.* (1995) used the water-leaving radiance at 443 nm calculated from CZCS data together with an assumed CDOM absorbance spectral slope to determine *in situ* CDOM absorption.

The SeaWiFS sensor, launched in 1996 on the SEASTAR satellite, has an additional detector for upwelling radiance at 412 nm. Part of the purpose of this sensor was to facilitate remote estimates of DOM (Nelson, 1997). Several satellite images of CDOM absorbance have been produced, using a variety of algorithms and presented at conferences (for example, Kahru and Mitchell, 2000; Siegel *et al.*, 2000). To produce images of CDOM absorbance and of photochemical production rates that did not require the assumption of a single spectral absorbance slope, Cullen *et al.* (1997) suggested an approach in several steps which would make use of the 412 nm sensor: (1) relate satellite measurements of water-leaving radiance to *in situ* radiance reflectance, $R(\lambda)$, defined as the ratio of upwelling radiance to downwelling irradiance; (2) find empirical relationships between the ratio of reflectance at two visible wavelengths (412 nm and 555 nm) and K_d at several UV wavelengths; (3) calculate total UV absorbance from $K_d(UV)$; (4) determine the magnitude of absorbance by particles, particularly phytoplankton; and (5) subtract absorbance due to particles and water from the total to calculate the CDOM absorbance. Photochemical production is then calculated using the CDOM absorbance, a solar irradiance model, and a quantum yield spectrum for the reaction.

SeaWiFS does not have UV detectors; atmospheric interference makes direct satellite measurements of UV upwelling radiance from the ocean extremely difficult. However, it seems reasonable to apply the Austin and Petzold (1981) reflectance ratio approach to $K_d(UV)$, since the components of sea water which absorb UV radiation also absorb visible radiation. For this study, the Cullen *et al.* (1997) approach was modified to determine a direct, empirical relationship between $K_d(UV)$ and $a_{CDOM}(UV)$ at corresponding wavelengths without first subtracting the contributions of other absorbing components (Johannessen *et al.*, 1999).

This chapter presents relationships among *in situ* visible reflectance, $K_d(UV)$, and $a_{CDOM}(UV)$. It also includes relationships between visible reflectance calculated from SeaWiFS ocean colour data and *in situ* $K_d(UV)$ and $a_{CDOM}(UV)$, and compares measured with predicted values of $K_d(UV)$. The optical relationships developed here should prove useful in areas of research beyond those addressed in this thesis. For example, changes in CDOM absorbance due to photobleaching (for example, Vodacek *et al.*, 1996) can change the depth of penetration of UV radiation, which is of interest to biologists, because UV radiation is known to inhibit phytoplankton productivity (for example, Cullen and Neale, 1994; Smith and Cullen, 1995) and to damage bacteria (for example, Jeffrey *et al.*, 1996; Kaiser and Herndl, 1997; Huot, 1999). CDOM can also interfere with estimates of chlorophyll concentration made from remotely-sensed data (for example, Mortimer, 1988; Carder *et al.*, 1989; Doerffer and Fischer, 1994; Hochman *et al.*, 1994; Siegel and Michaels, 1996; Yentsch and Phinney, 1996; Nelson *et al.*, 1998; Bontempi, 1999; Siegel, 1999), because it can absorb strongly at short, visible

wavelengths. A more extensive discussion of the development of ocean optics can be found in Appendix 1.

3.2 Methods

Sample locations

Two cruises were undertaken in the Mid-Atlantic Bight in the summers of 1996 and 1997 and one in the Bering Sea in June 1997. Samples and data collected during two more Mid-Atlantic Bight cruises taken in the summers of 1997 and 1998 were also available. Sample locations are shown in figure 3.1. During the July 1997 cruise aboard the *R/V Seward Johnson*, optical casts were made at five stations along cross-shelf transects. Optical casts were made aboard the *R/V Cape Henlopen* in May and August 1997 and in July 1998 at 11, 24 and 37 stations, respectively. In the Bering Sea aboard the *R/V Wecoma*, optical casts were made at 13 stations along a cross-shelf transect.

Water collection and storage

At each station water was collected from the surface, and at many stations samples were also collected from below the mixed layer using a CTD rosette. Water samples were filtered immediately to remove particles and bacteria; during the first Mid-Atlantic Bight cruise in 1997, samples were filtered on board through Whatman GF/F (nominal pore size 0.7μm) filters and then refiltered through 0.2μm Schleicher and Schuell Nylon 66 membrane filters on return to the lab. Water taken during the other cruises was

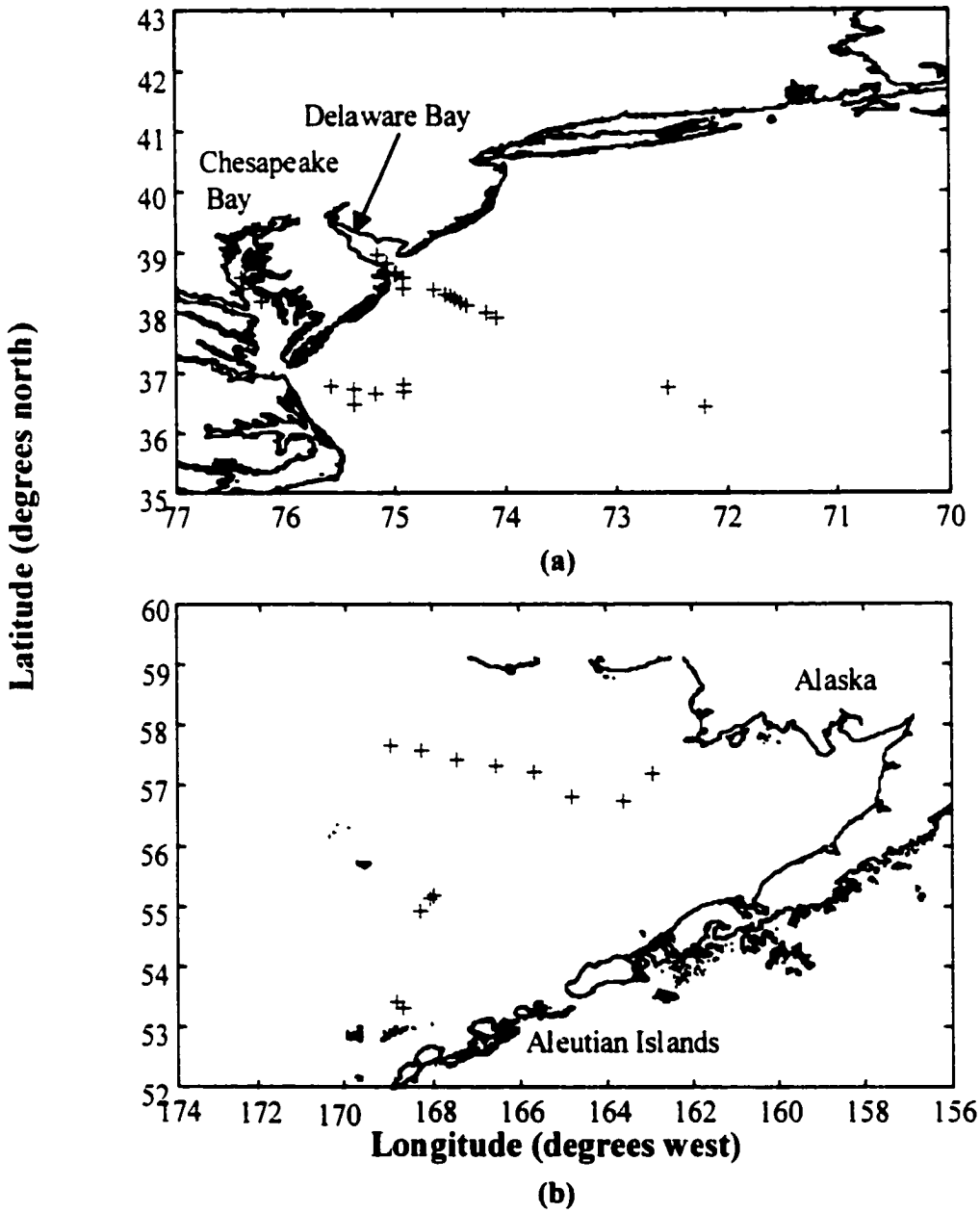

Figure 3.1 Sample locations for optical measurements. (a) Mid-Atlantic Bight August 1996, May and August 1997, July 1998; (b) Bering Sea June 1997

immediately filtered through 0.2 µm Schleicher and Schuell Nylon 66 filters. During the August 1997 cruise, samples were pressure-filtered through the 0.2 µm filters using a peristaltic pump with an in-line filter; samples from the other cruises were vaccuum-filtered. Water samples were stored for less than a year at 4°C in amber glass bottles to minimize biological activity and photochemical breakdown of CDOM.

Absorbance Measurements

Spectral absorbance was measured in a 10 cm quartz flow cell in a Hewlett Packard HP 8453 diode array spectrophotometer from 190 to 1100 nm at 1 nm resolution. and the values were converted to absorptivity, $a_{CDOM}(\lambda)$ (m^{-1}), as described in Chapter 2 (equation 2.4). A correction was made for scattering, baseline drift, and refractive index differences as described in Chapter 2 (equation 2.6).

Optical Measurements

Two instruments were deployed at each optical station (figure 3.2). A Satlantic SeaWiFS Profiling Multichannel Radiometer measured downwelling irradiance at depth in thirteen channels (2 nm bandwidth for UV, 10 nm for visible channels; acquisition rate 6 Hz) centred on the following wavelengths: 305, 323, 338, 380, 412, 443, 490, 510, 532, 555, 670, 683, and 700 nm. The visible channels coincided with those of the radiance sensors on the SeaWiFS satellite (Satlantic, 1999; SeaWiFS, 1999), although the SeaWiFS bandwidth was wider (20 nm for 412-555 nm; 40 nm for 670-700 nm). The downwelling attenuation coefficient was calculated over the first optical depth (from the surface to the depth at which the downwelling irradiance fell to 1/e of its surface value) using the

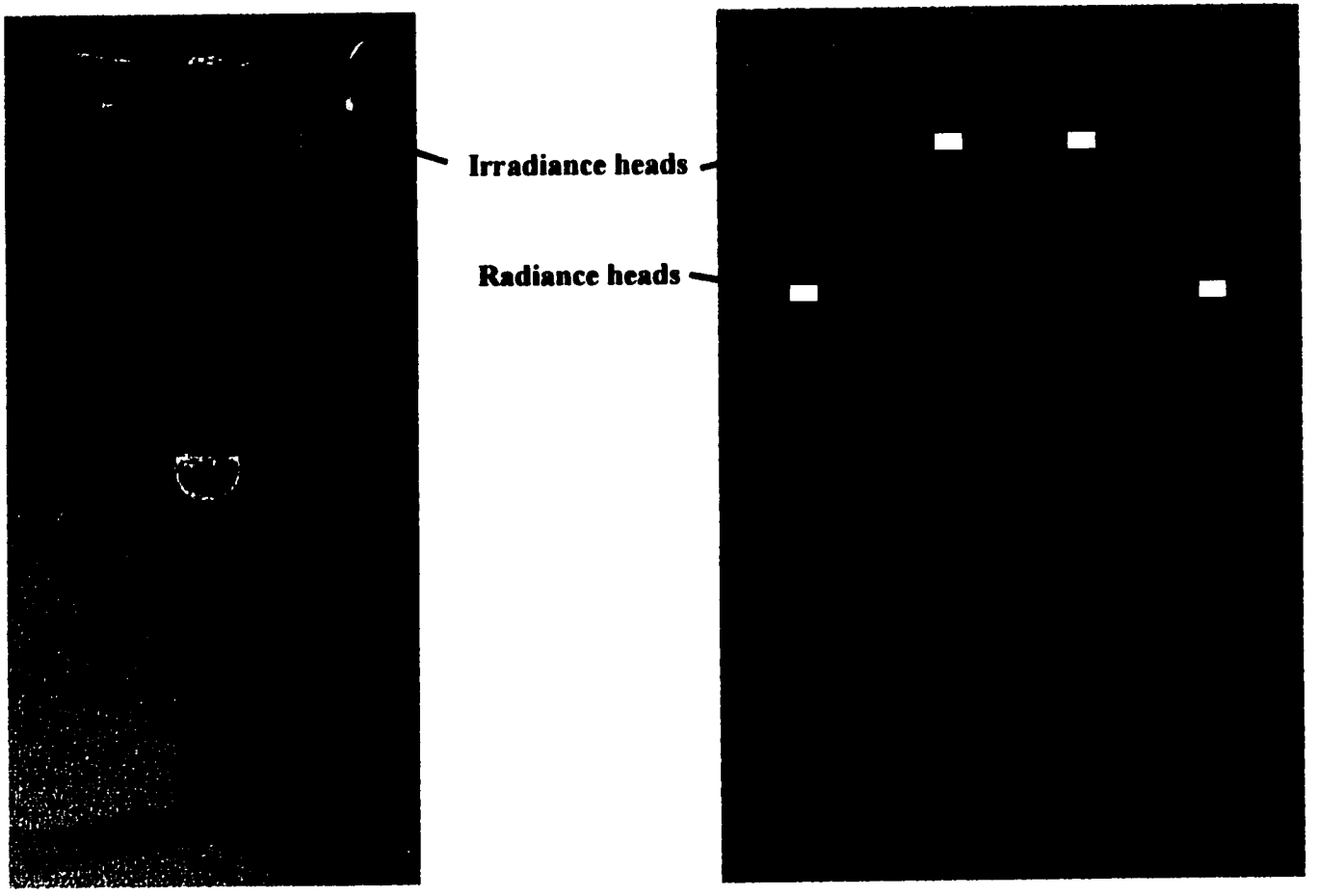

Figure 3.2. (a) Satlantic SeaWiFS Profiling Multichannel Radiometer (from Satlantic, 2000)
(b) Satlantic Ocean Colour Radiometer, OCR-200

profiler data with the Matlab® routine "ksurf " written by R. Davis. The routine made use of the relationship:

$$K_d(\lambda,\ z + 1/2\Delta z) = ln(E_d(\lambda,z) / E_d(\lambda,z+\Delta z)) / \Delta z \qquad (3.1)$$

(Kirk, 1983) where $E_d(\lambda,z)$ ($Wm^{-2}nm^{-1}$) is downwelling irradiance measured at the first depth, $E_d(\lambda,z+\Delta z)$ ($Wm^{-2}nm^{-1}$) is the downwelling irradiance at the subsequent depth, and Δz is the change in depth, z (m), between two consecutive measurements. Figure 3.3 shows a typical irradiance profile. The standard deviation of K_d measurements at UV wavelengths and 412 nm, based on replicate profiles (n=2-3), ranged from 2% for open ocean stations to 6% for inshore stations. The profiles were dark-corrected using the stated dark calibration values given by Satlantic Inc.. The bend in the 380 nm profile at the bottom of the mixed layer was typical of all August profiles. Measurable irradiance at 323 nm and 338 nm usually did not reach the bottom of the mixed layer, so there is no way to tell whether or not their rate of attenuation would have changed at that depth.

A Satlantic Ocean Colour Radiometer (OCR) simultaneously measured incident downwelling irradiance just above the ocean's surface in the same thirteen wavebands as the profiler and also at 590 nm (acquisition rate 6 Hz). It provided a surface reference for the profiler's irradiance measurements to correct for changes in incident irradiance during the profile. The OCR also measured upwelling radiance within a few cm of the water's

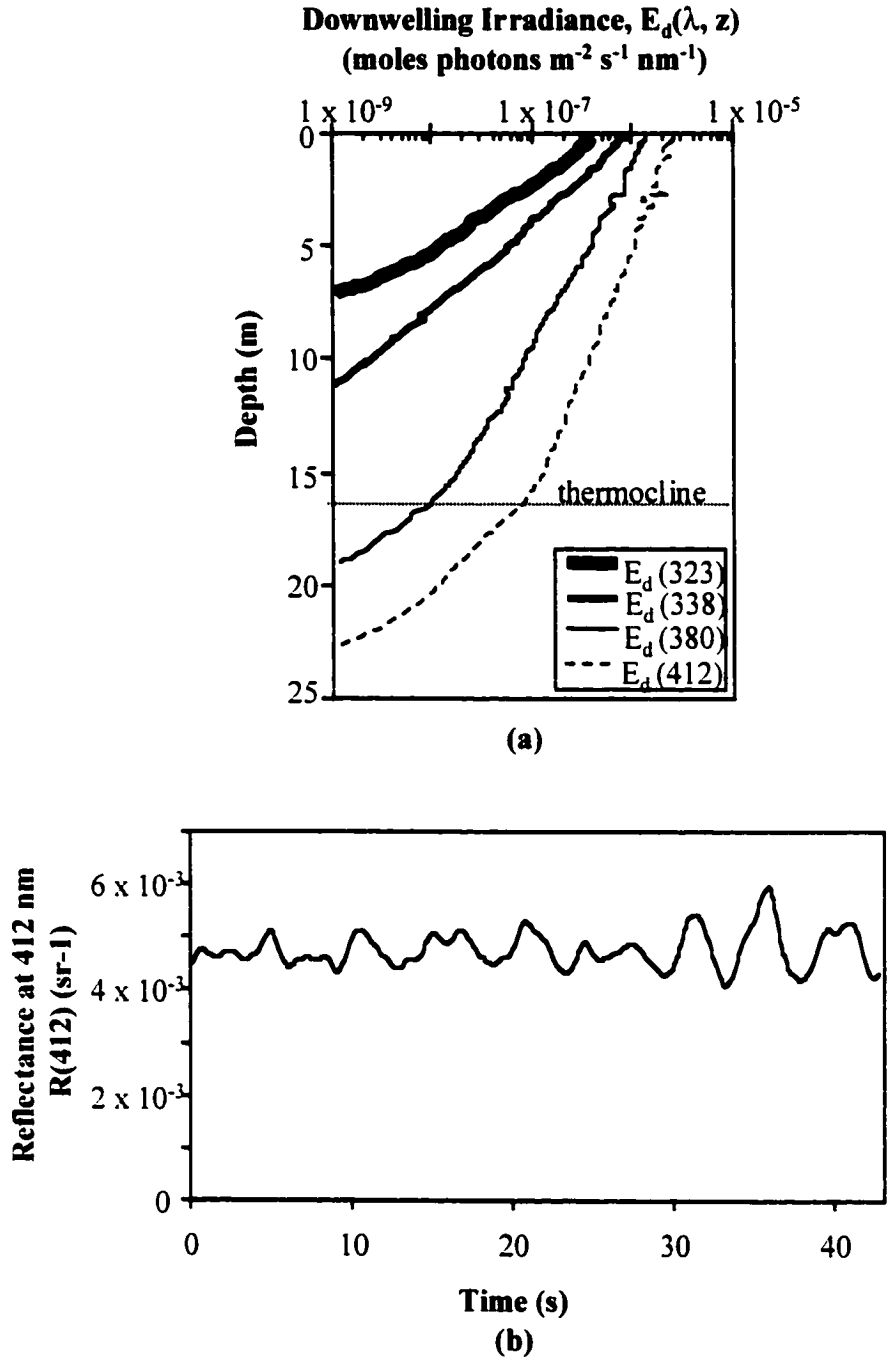

Figure 3.3. Station M9708-07: (a) irradiance profile (b) reflectance at 412 nm during profile

surface (no correction made for attenuation with depth) in the same fourteen channels. Reflectance, $R(\lambda)$ (sr^{-1}), was calculated as the ratio of the average upwelling radiance, $L_u(\lambda, 0-)$ ($Wm^{-2}nm^{-1}sr^{-1}$), to the average downwelling irradiance, $E_d(\lambda, 0+)$ ($Wm^{-2}nm^{-1}$), just above the surface during the profile (Kirk, 1983).

$$R(\lambda) = L_u(\lambda, 0-) / E_d(\lambda, 0+) \qquad (3.2)$$

The standard deviation of the time-averaged reflectance at each station ranged from 5 to 17 % for both 412 and 555 nm, with less variability in clearer water. A typical plot of reflectance *vs.* time during a profile is shown in figure 3.3. Figure 3.4 shows typical plots of the wavelength-dependence of reflectance and K_d at an open ocean station (blue water) and at a coastal station (green water).

3.3 Results

Relationship between in situ $K_d(\lambda)$ and in situ reflectance

The downwelling attenuation coefficient at 323, 338 and 380 nm was plotted against several ratios of visible reflectance to find the strongest correlation. The ratio of reflectance at 412 nm to reflectance at 555 nm predicted K_d at 323, 338, and 380 nm most robustly (figure 3.5). (Although by convention the y-axis is reserved for the dependent variable, the purpose of the plot was to find an equation that could be used to predict K_d from reflectance.) For clarity, error bars are omitted from figure 3.5. Reflectance at 412 nm alone predicted $K_d(UV)$ fairly well for those stations outside of the very turbid

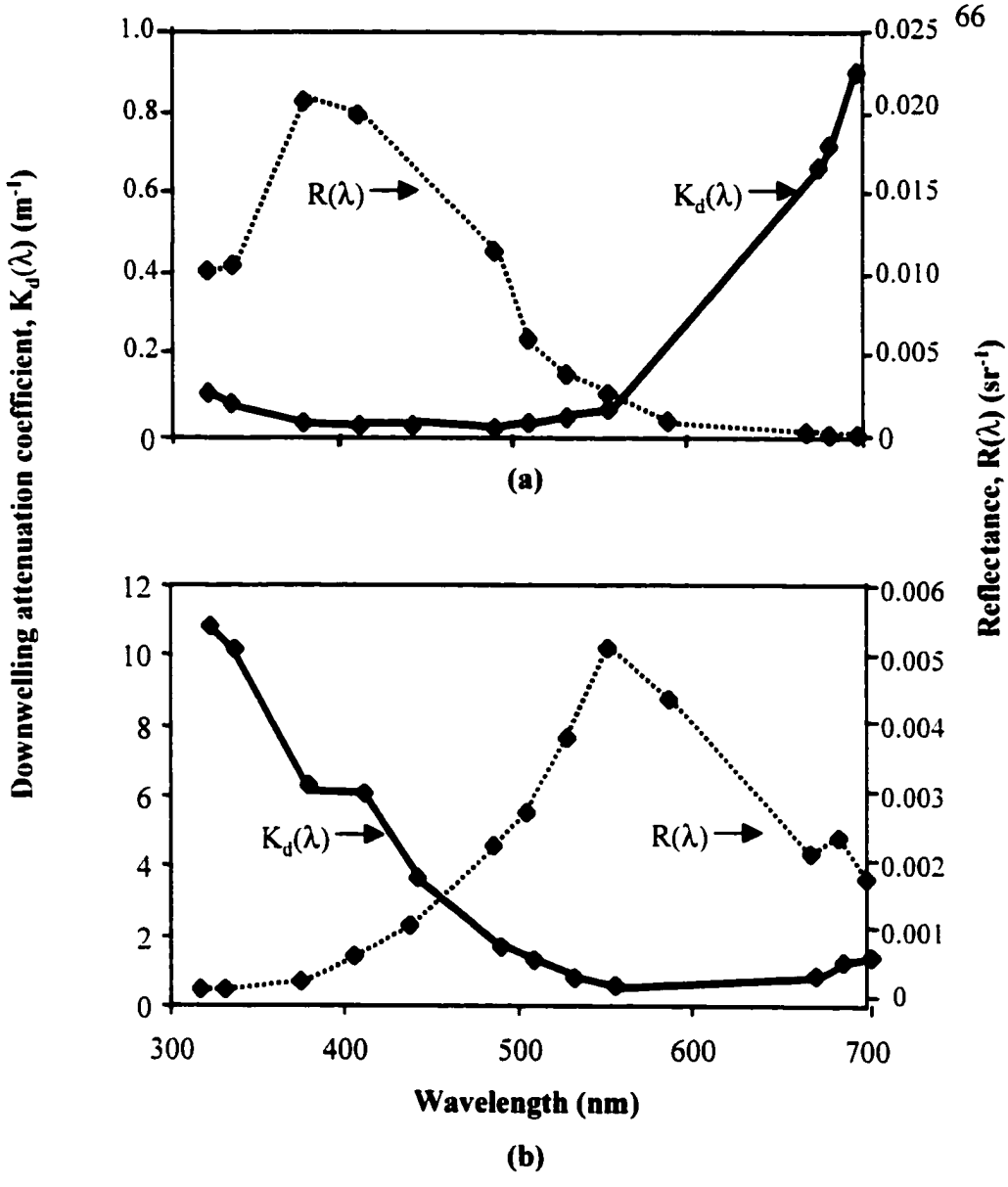

Figure 3.4. Downwelling attenuation coefficient and reflectance vs. wavelength for (a) and open ocean station (M9708-15), and (b) an inshore station (F9805-03).

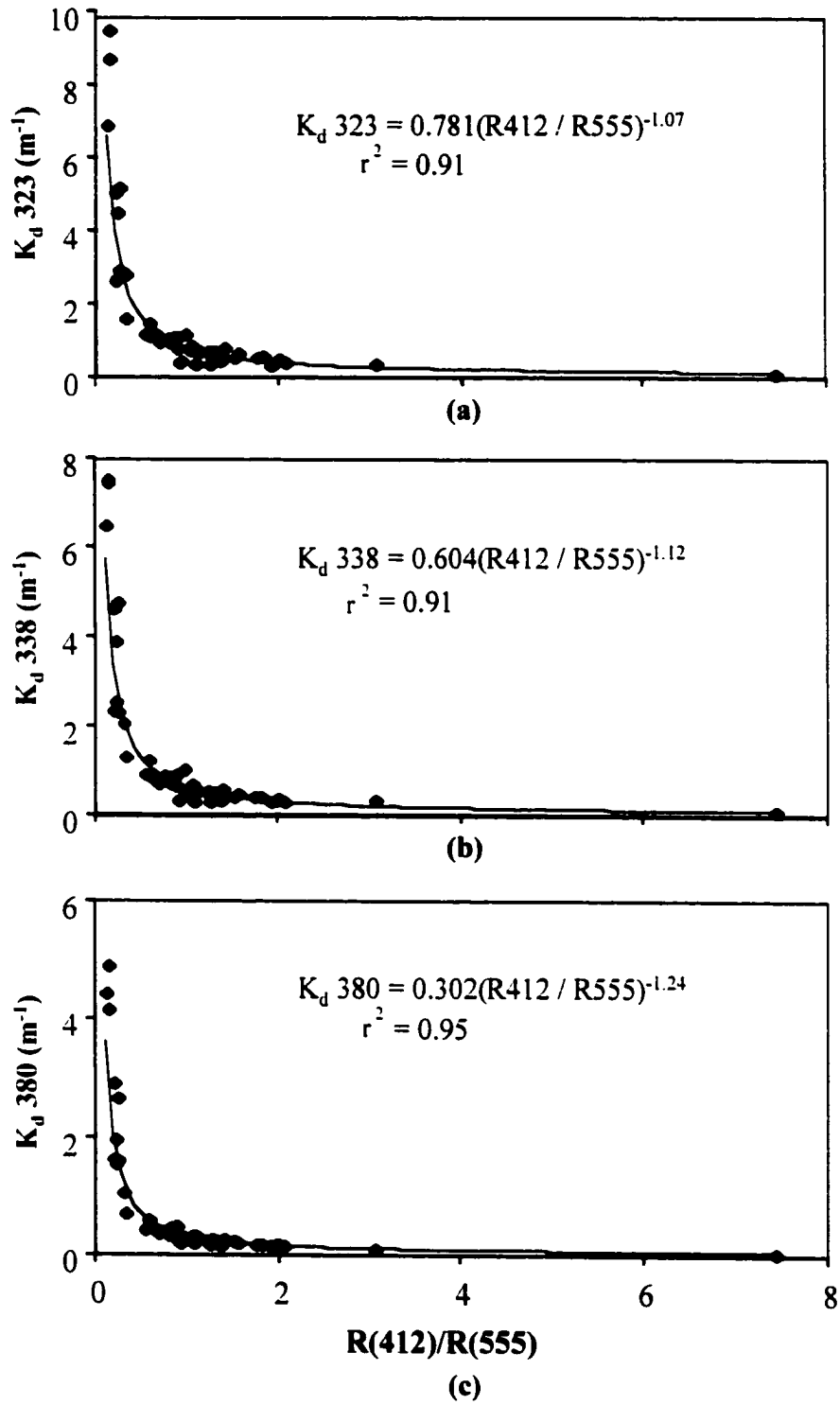

Figure 3.5. Relationship between reflectance ratio R(412)/R(555) and (a) $K_d(323)$; (b) $K_d(338)$; (c) $K_d(380)$; n=53.

Delaware and Chesapeake Bays (data not shown). However, the *R(412) / R(555)* ratio allowed the inclusion of all stations in a single relationship. Regressions on these data yielded the following empirical relationships (n=53):

$$K_d(323nm) = 0.781\ R(412nm) / R(555nm)^{-1.07} \qquad r^2 = 0.91 \qquad (3.3)$$

$$K_d(338nm) = 0.604\ R(412nm) / R(555nm)^{-1.12} \qquad r^2 = 0.91 \qquad (3.4)$$

$$K_d(380nm) = 0.302\ R(412nm) / R(555nm)^{-1.24} \qquad r^2 = 0.95 \qquad (3.5)$$

To obtain a continuous spectrum for UV attenuation, a single exponential regression line was fitted through the three K_d points (at 323, 338 and 380 nm) either measured or generated from the reflectance data. (See figure 3.6 for an example of the exponential fit to K_d.)

Calculation of CDOM absorptivity from K_d

CDOM is the main component responsible for UV attenuation in the ocean. To determine the proportion of $K_d(UV)$ due to CDOM, and to investigate how that proportion varied with location, measured a_{CDOM} was plotted against measured K_d at corresponding wavelengths for all stations (figure 3.7). K_d predicts a_{CDOM} well at 323 and 338 nm, and reasonably well at 380 nm; the correlation breaks down at longer wavelengths where other components, particularly phytoplankton pigments, absorb more strongly. K_d and a_{CDOM} seem to be related linearly. The following regression equations were determined for water taken from a wide variety of environments - from coastal to off-shelf, blue

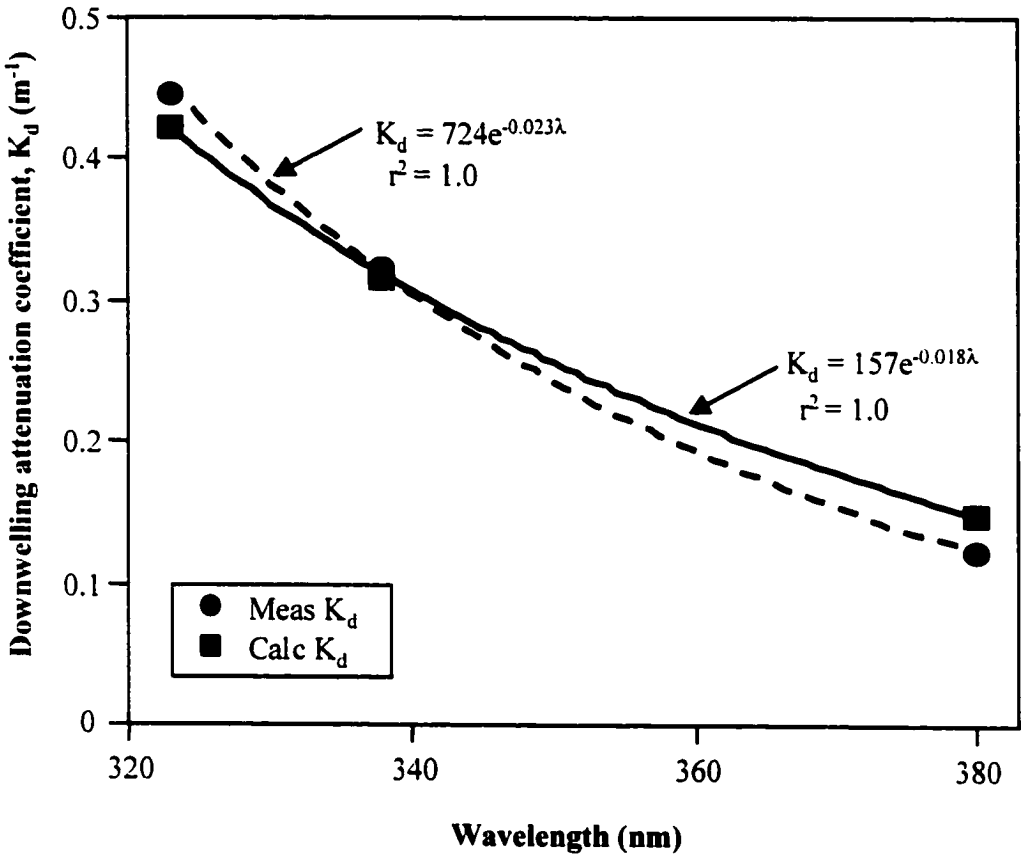

Figure 3.6. Downwelling attenuation coefficient measured at an open ocean station in the Mid-Atlantic Bight (M9807-14) in July 1998 and calculated at the nearest pixel from the SeaWiFS monthly-binned image for July 1998. Single exponential fits were determined for discrete K_d points to calculate K_d at 1 nm intervals.

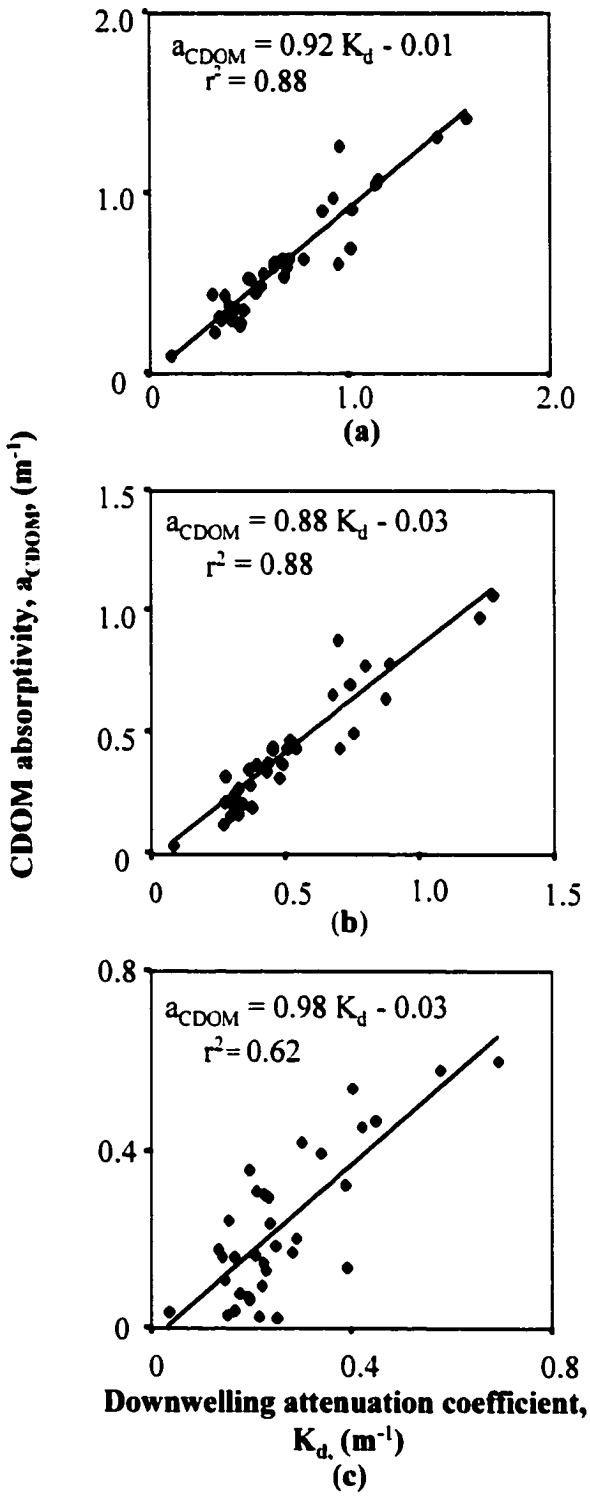

Figure 3.7. CDOM absorptivity vs. Kd at three UV wavelengths: (a) 323 nm, (b) 338 nm, (c) 380 nm; n=33.

waters in the Bering Sea and from the coast to the Gulf Stream in the Mid-Atlantic Bight (n=33):

$$a_{CDOM}(323) = 0.92\ K_d(323) - 0.01; \qquad r^2 = 0.88 \qquad (3.6)$$

$$a_{CDOM}(338) = 0.88\ K_d(338) - 0.03; \qquad r^2 = 0.88 \qquad (3.7)$$

$$a_{CDOM}(380) = 0.97\ K_d(380) - 0.02; \qquad r^2 = 0.66 \qquad (3.8)$$

Since the intercept values given above are within the uncertainty of the absorbance measurement, these equations suggest that at each UV wavelength, CDOM absorptivity contributes a constant proportion of attenuation. The six samples from inside the turbid Delaware and Chesapeake Bays did not fit the above relationships at all well. While the number of bay samples was too low to give convincing statistics, the plots of a_{CDOM} *vs.* K_d for these samples were strikingly linear. The equations of the best fit regression lines to the bay data are (n=6):

$$a_{CDOM}(323) = 0.31\ K_d(323) + 0.05; \qquad r^2 = 0.97 \qquad (3.9)$$

$$a_{CDOM}(338) = 0.26\ K_d(338) + 0.66; \qquad r^2 = 0.94 \qquad (3.10)$$

$$a_{CDOM}(380) = 0.22\ K_d(380) + 0.34; \qquad r^2 = 0.72 \qquad (3.11)$$

The lower proportion of K_d attributable to CDOM inside the bays probably results from absorption of UV by organic or organically-coated particles and from increased particle back-scattering.

Calculation of K_d and CDOM absorptivity from satellite data

The empirical relationships described above were applied to three SeaWiFS archive data scenes to evaluate their use as predictors of K_d. Data were level 3, monthly-binned images with 9 x 9 km resolution from May, July and August 1998. The satellite was not yet operational during the 1996 and 1997 cruises, but the July 1998 image includes the period of the last cruise.

Images of normalized water-leaving radiance at 412 and 555 nm from the Distributed Active Archive Center (DAAC, 1999; for example, see figure 3.8), were used to calculate a reflectance ratio ($L_u(412):E_d(412) / L_u(555):E_d(555)$) at each pixel as described below. (The wavelength dependence of each variable is left implicit to simplify the equations). Normalized water-leaving radiance, nL_w (W $m^{-2}nm^{-1}sr^{-1}$), is calculated according to:

$$nL_w = L_w(0+)\,(F_o / E_d(0+)) \qquad (3.12)$$

(modified from Fraser *et al.*, 1997) where $L_w(0+)$ is water-leaving radiance measured just above the surface of the water (W $m^{-2}nm^{-1}sr^{-1}$), F_o is mean extraterrestrial solar irradiance corrected for earth-sun distance and orbital eccentricity (W $m^{-2}nm^{-1}$); and $E_d(0+)$ is downwelling irradiance measured just above the surface of the ocean (W $m^{-2}nm^{-1}$). Since the OCR reference measures upwelling radiance just below the surface of the ocean, $L_u(0-)$ (W $m^{-2}nm^{-1}sr^{-1}$), $L_w(0+)$ was calculated from $L_u(0-)$, according to Gordon and Clark (1981):

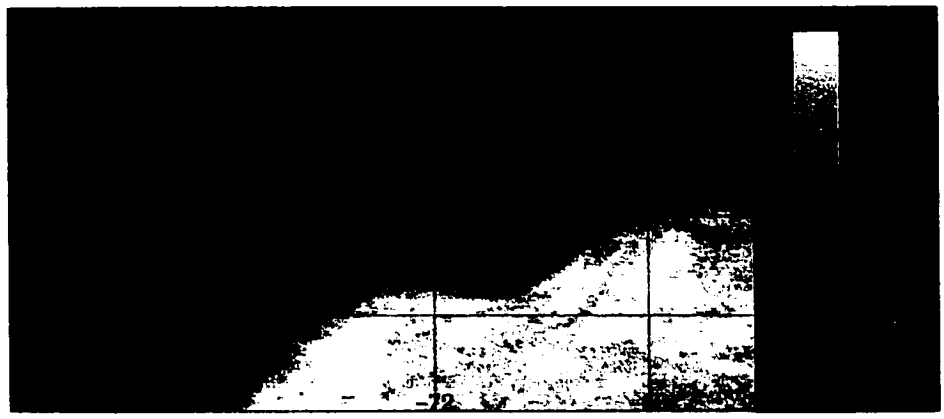

(a)

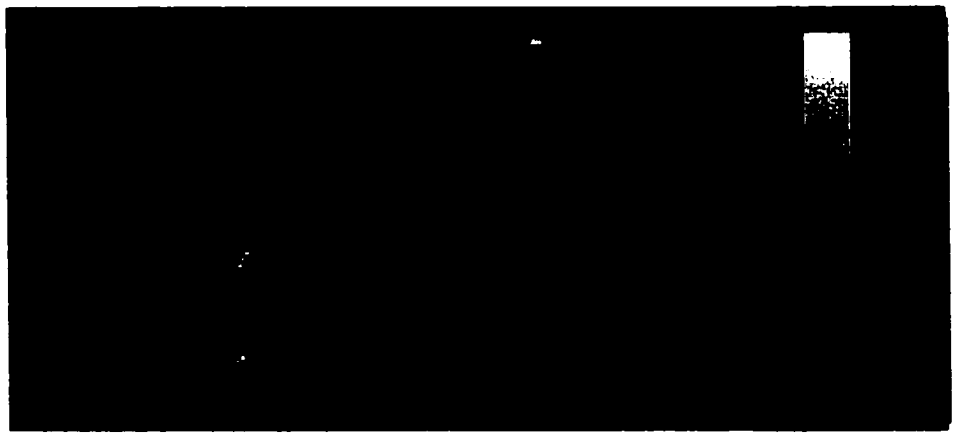

(b)

Figure 3.8. Normalized water-leaving radiance in the Mid-Atlantic Bight for July 1998 (mW $cm^{-2}\mu m^{-1}sr^{-1}$): (a) 412 nm; (b) 555 nm.

$$L_w(0+) = \sim 0.57\, L_u(0-) \qquad (3.13)$$

Substituting for $L_w(0+)$ in equation (3.12), the ratio of water-leaving radiance at 412 nm to that at 555 nm was related to the ratio of the measurable, *in situ* reflectance at those wavelengths:

$$\frac{nL_w(412)}{nL_w(555)} = \frac{0.57\, F_o(412)\, L_u(412, 0-) / E_d(412, 0+)}{0.57\, F_o(555)\, L_u(555, 0-) / E_d(555, 0+)} \qquad (3.14)$$

$F_o(412)$ and $F_o(555)$ were calculated according to Gordon *et al.*, 1983:

$$F_o(\lambda) = H_o(\lambda)\,(1+e\cos(2\pi(D-3)/365))^2 \qquad (3.15)$$

where $H_o(\lambda)$ is the mean extraterrestrial solar irradiance ($Wm^{-2}nm^{-1}$), and e is the eccentricity of the earth's orbit (0.0167; Gordon *et al.*, 1983). Values for $H_0(412)$ and $H_0(555)$ were taken from Gregg and Carder (1990),

$$H_o(412) = 1.812\ Wm^{-2}nm^{-1} \qquad (3.16)$$

$$H_o(555) = 1.896\ Wm^{-2}nm^{-1} \qquad (3.17)$$

Using the empirical relationships described in earlier sections of this paper and the reflectance ratio $R(412) / R(555)$ calculated from the SeaWiFS normalized water-leaving radiance values at each pixel, K_d and a_{CDOM} were calculated throughout the UV.

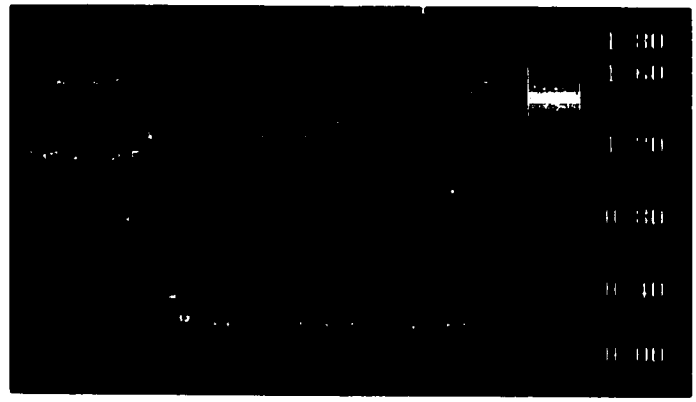

(a)

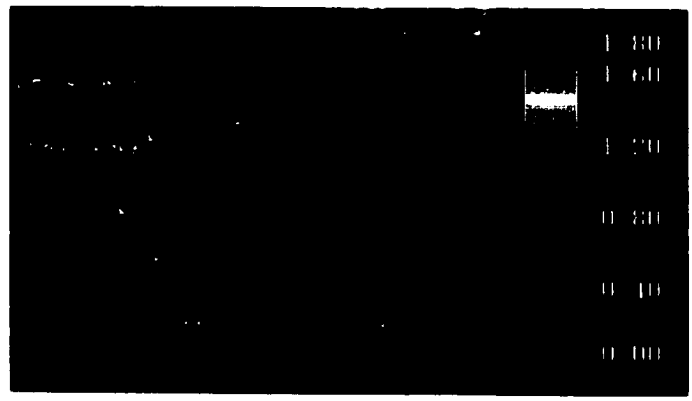

(b)

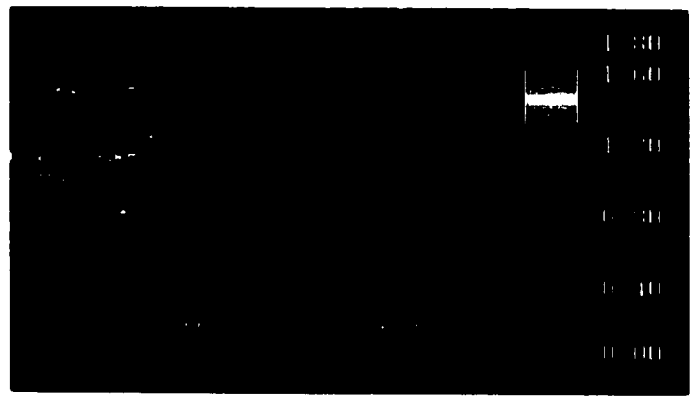

(c)

Figure 3.9. Downwelling attenuation coefficient (m^{-1}) at 323 nm in the North Atlantic Ocean, calculated from SeaWiFS normalized water-leaving radiance data, binned to 9 km x 9 km, monthly resolution. (a) May 1998; (b) July 1998; (c) August 1998.

Figure 3.9 shows maps of calculated K_d at 323 nm for May, July and August 1998 in the Mid-Atlantic Bight. The 412 nm normalized water-leaving radiance data generated from SeaWiFS images are unreliable in areas with a high concentration of particles in the water (Marlon Lewis, personal communication), because the algorithm used to calculate *nLw(412)* includes the assumption that all the radiation at 670 nm incident on the surface of the water is absorbed (Fraser *et al.*, 1997). The assumption is not valid in areas of high particle concentration. This problem is often manifested in negative nearshore *nLw(412)* values. Therefore, for this study, an arbitrary cut-off value of 2.0×10^{-3} Wm^{-2} $nm^{-1}sr^{-1}$ was chosen, and all pixels with *nLw(412)* or *nLw(555)* below that value were masked. Masked pixels are shown in black in figure 3.9, as is land.

While most of our *in situ* data were collected before the SeaWiFS satellite was operational, the July 1998 satellite image included the period of our last cruise. *In situ*, measured reflectance ratios (*R(412) / R(555)*) at three stations during that cruise were compared with the corresponding *R(412) / R(555)* values calculated from the satellite image (table 3.1).

The stations were chosen to represent mid-shelf, shelf break and offshelf waters. The calculated reflectance ratios were within 11 - 22 % of the measured values. All of the calculated values were lower than the measured ones, possibly because of the systematic underestimate of water-leaving radiance at 412 nm by current satellite algorithms.

Measured and predicted K_d values were also compared. Values of K_d measured at 323, 338, and 380 nm at three stations during the July 1998 cruise were compared with those calculated at the nearest pixel from the monthly-binned, July 1998 SeaWiFS image, as for the reflectance ratios (table 3.1).

K_d values determined in August 1997 in the Gulf Stream were also compared with those calculated for the nearest pixel in August 1998 (table 3.1). The modelled K_d at 323 nm was within 10% of the measured value at each station. The modelled values of K_d at 338 and 380 nm were within 30% of the measured values at the mid-shelf station.

Station	Station Location	Satellite Image Pixel Location	In situ R 412 / R 555	Modelled R 412 / R 555	%R diff. (model-in situ) / in situ)	Wave-length (nm)	In situ K_d (m^{-1})	Modelled K_d (m^{-1})	% Kd diff. (model - in situ) / in situ	In situ K_d slope (nm^{-1})	Modelled K_d slope (nm^{-1})	% slope difference (model - in situ) / in situ
M9807-7	38.36N 74.47W	38.26N 74.43W	0.8268	0.6722	-19	323	1.092	1.195	9	0.0155	0.0178	15
						338	0.7216	0.9424	31			
						380	0.3801	0.4942	30			
M9807-37	38.00N 74.04W	37.85N 74.03W	1.911	1.696	-11	323	0.4049	0.4437	10	0.0182	0.0185	2
						338	0.2785	0.3342	20			
						380	0.1377	0.1568	14			
M9807-14	37.12N 72.93W	36.84N 73.03W	2.267	1.779	-22	323	0.4463	0.4216	-6	0.0229	0.0183	-20
						338	0.3237	0.3168	-2			
						380	0.122	0.1478	21			
M9708-15	36.02N 72.285W	36.33N 72.23W	7.460	6.294	-16	323	0.1053	0.1091	3	0.0200	0.0215	8
						338	0.0797	0.07699	-3			
						380	0.0338	0.03188	-6			

Table 3.1. Comparison of K_d values determined *in situ* and calculated from a SeaWiFS ocean colour image. For the M9807 stations, both the measurements and the satellite image were taken in July, 1998. The K_d values for station M9708-15 (Gulf Stream) were calculated from in situ measurements in August 1997 and from a satellite image of August 1998.

The modelled values improved with distance from shore, and were within 6% of measured values in the Gulf Stream. At the mid-shelf and shelf break stations the modelled K_d values were all higher than the actual values, probably again as a result of the problem with the atmospheric correction in the presence of particles or of a high concentration of CDOM.

An exponential regression was fit to the three UV K_d values (both modelled and determined *in situ*; table 3.1) at each station. The slope of the natural logarithm of spectral K_d (hereafter referred to as the " K_d slope") determined using the modelled K_d values was within 20% of that determined from the *in situ* K_d values at every station. Clearly, the relationships presented above give a good estimate of *in situ* UV attenuation, at least in the Mid-Atlantic Bight in the summer.

Figure 3.9 shows a distinct seasonal change in UV attenuation. $K_d(323)$ appears to have decreased by about 50% from May to August in the Mid-Atlantic Bight, possibly by photobleaching or because of lower terrestrial runoff in August. Attenuation at the other

UV wavelengths follows the same pattern, as does CDOM absorptivity (data not shown), which is tied directly to K_d in the equations used to generate the images.

3.4 Discussion

The relationships between reflectance and K_d seem to be robust for all five cruises, over the whole summer in the Mid-Atlantic Bight, and in June in the Bering Sea. They are consistent over a wide range of water types, from turbid, inshore waters to clear, oligotrophic, offshore waters. It seems likely that they will be widely applicable to different oceans and different seasons, although they require further testing in the winter and in other locations.

A linear relationship fits the a_{CDOM} *vs.* K_d data at 338 and 323 nm. (A linear relationship can also be applied to the data at 380 nm, but with less confidence; figure 3.7) CDOM absorptivity appears to vary directly with the total attenuation. This seems reasonable for the open ocean, where most of the CDOM comes from the decomposition of phytoplankton (Kalle, 1966), the only other open ocean component whose UV absorption varies seasonally. Some of the scatter in figure 3.7 might be due to the variety of times of day and latitudes at which the K_d measurements were made, which would probably change the geometry of the irradiance entering the water.

K_d is not the same as total absorption. While we measure attenuation by comparing irradiance at two depths separated by a known vertical distance, photons do not all travel

straight down. It is important to account for the average pathlength travelled by a photon as it is scattered down through the water column. This is usually accomplished using $\bar{\mu}_d$, the average cosine of the downwelling irradiance distribution (Kirk, 1983).

$$a(\lambda) = K_d(\lambda) \times \bar{\mu}_d(\lambda) \qquad (3.18)$$

where $a(\lambda)$ is total absorptivity (m^{-1}). It is unclear what value should be used for $\bar{\mu}_d$ in the UV. Previous authors have published measurements which show that a_{CDOM} in the UV appears to be greater than $K_d \times \bar{\mu}_d$ using values for $\bar{\mu}_d$ appropriate for visible radiation. Morris *et al.* (1995) reported this problem in the clearest lakes in their study and explained it as a result of scattering. DeGrandpre *et al.* (1996) found the same result in the Mid-Atlantic Bight. They attributed the discrepancy to low apparent K_d due to wave focussing, and also suggested that light in oligotrophic water might be less diffuse than is usually assumed. Another possible explanation was that particles in the spectrophotometer cells artificially increased apparent absorbance. However, the absorbance spectra presented here were corrected for scattering in the spectrophotometers as described in Chapter 2 (equation 2.6). The relationships between a_{CDOM} and K_d presented in equations 3.6 to 3.8 show that if $\bar{\mu}_d$ in equation 3.18 were taken to be approximately 0.7 as is usual for visible radiation (see Ciotti *et al.*, 1999), a_{CDOM} would be greater than total absorptivity even after the scattering correction.

There is evidence to suggest that $\bar{\mu}_d(UV)$ may be higher than the values usually used for diffuse visible radiation. Kirk (1983) showed with Monte Carlo simulations that $\bar{\mu}_d$

increased as the ratio of scattering, $b(\lambda)$ (m^{-1}), to total absorption, $a(\lambda)$ (m^{-1}) decreased, and approached 1 as $b(\lambda) / a(\lambda)$ approached 0 for vertically incident light. Bannister (1992) also showed that $\bar{\mu}_d$ depended on $b(\lambda) / a(\lambda)$ and on depth. For $b(\lambda) / a(\lambda)$ =1 and vertically incident sunlight, for example, Bannister calculated a $\bar{\mu}_d$ of about 0.97 at the surface, and 0.9 as it approached the asymptotic value at depth. For sunlight incident at 30°, $\bar{\mu}_d$ approached 0.95 at the surface; for sunlight incident at 60°, $\bar{\mu}_d$ approached 0.85 at the surface. The ratio $b(\lambda) / a(\lambda)$ must be lower for UV than for visible radiation: absorbance increases exponentially with decreasing wavelength, while scattering only increases proportionally with wavelength to the power of 0-1 (Gordon *et al.*, 1988) or 2 (Sathyendranath *et al.*, 1989). Figures 3.10 and 3.11 show a comparison of the spectral dependence of *b* and *a*. So, from Bannister's models, $\bar{\mu}_d$ of 0.9 - 0.97 is quite possible. Berwald *et al.* (1995) modelled the dependence of $\bar{\mu}_d$ on depth, absorption, and scattering, also for vertically incident radiation. J. Berwald kindly provided us with a spreadsheet model that calculated $\bar{\mu}_d$ for several UV wavelengths using parameters extrapolated from visible values (water absorbance and scattering, scattering by small particles, scattering by large particles, particulate absorbance). Using these parameters and realistic coastal and open ocean values for chlorophyll concentrations and a_{CDOM} (table 3.2), $\bar{\mu}_d$ for 350 nm varied between 0.90 and 0.96. (While the extrapolation of some of the model parameters into the UV may not have been entirely rigorous, there were no measured values available (J. Berwald, personal communication.)) Gordon (1989a) calculated theoretical values for the distribution function ($1/\bar{\mu}_d$) just beneath the surface of the ocean for several visible wavelengths and solar zenith angles. He did not calculate any values for UV, but from his calculation it can be seen that $\bar{\mu}_d$(440nm) is

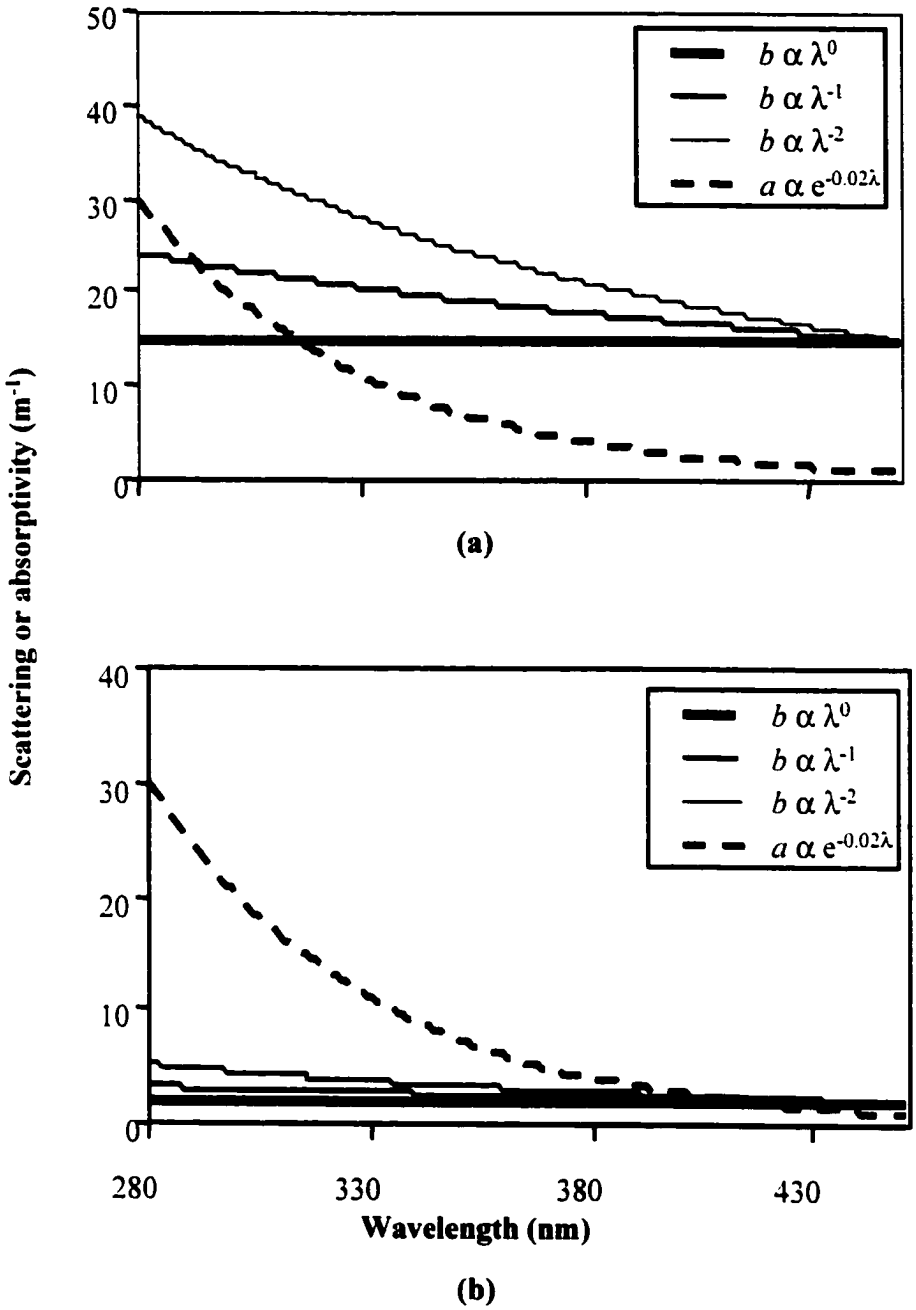

Figure 3.10. Spectral dependence of scattering and absorptivity where scattering is proportional to λ^0, λ^{-1} or λ^{-2}, absorptivity is proportional to $e^{-0.02\lambda}$, and $a(450)=1$. (a) with b/a (450 nm) = 15; (b) with b/a (450 nm) = 2.

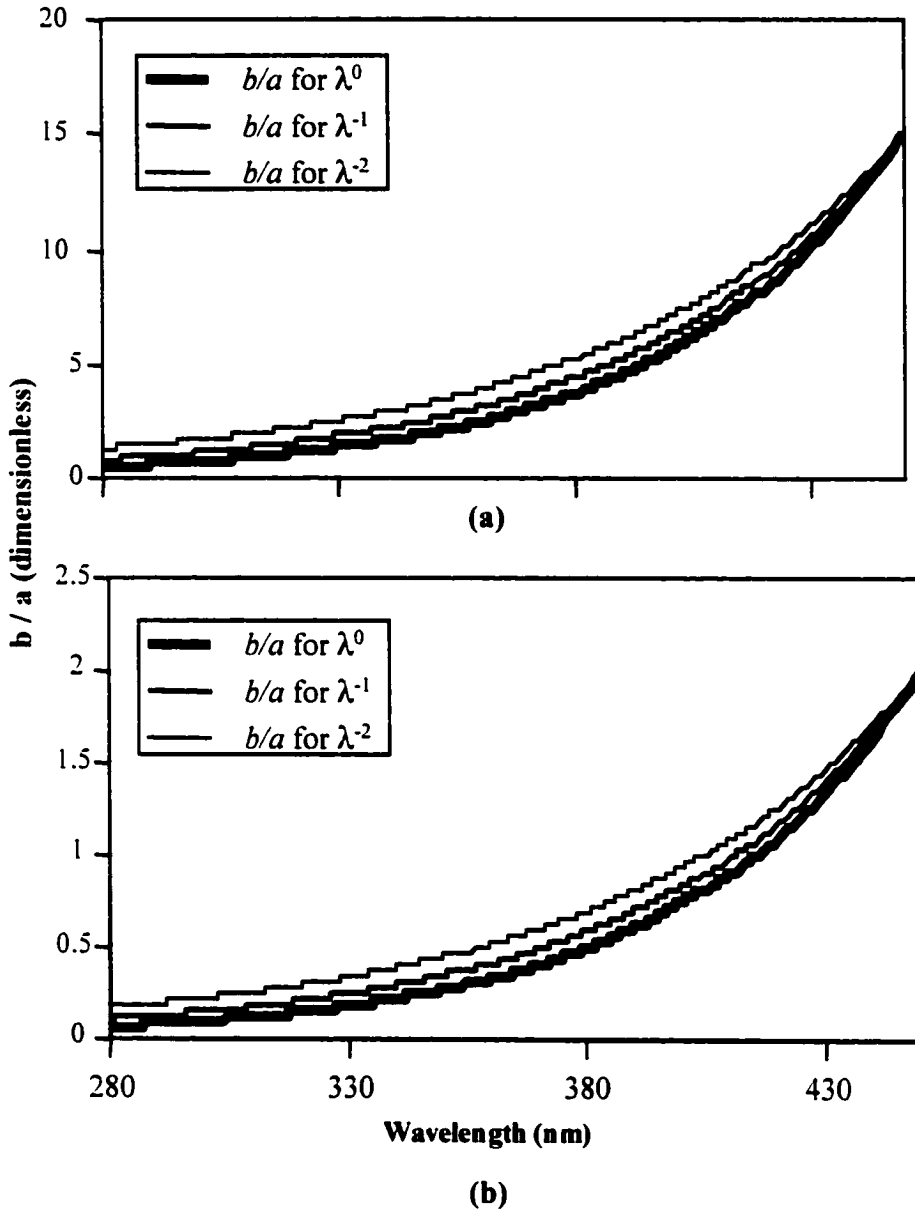

Figure 3.11 Spectral dependence of b/a, where scattering is proportional to λ^0, λ^{-1}, or λ^{-2}, absorptivity is proportional to $e^{-0.02\lambda}$, and $a(450)=1$.
(a) where $b/a(450)=15$; (b) where $b/a(450)=2$.

	Wavelength (nm)	Calculated $\bar{\mu}_d$
Offshore		
$a_{CDOM}(300nm) = 0.3\ m^{-1}$	300	0.97
$[chl] = 0.1\ mg\ l^{-1}$	350	0.90
	400	0.86
Coastal		
$a_{CDOM}(300nm) = 2\ m^{-1}$	300	0.98
$[chl] = 1\ mg\ l^{-1}$	350	0.96
	400	0.92

Table 3.2. Examples of $\bar{\mu}_d$ calculated using J. Berwald's model for offshore and coastal water. Note that some assumptions have not been tested for UV radiation, and many parameters were simply extrapolated from visible values.

greater than 0.9 just beneath the surface of the water for solar zenith angles of 0 - 30°. This section is not intended to give a precise value for $\bar{\mu}_d$ *(UV)*, but simply to show that it is possible that it is between 0.9 and 1. Clearly this is a problem that requires further study.

Accepting that $\bar{\mu}_d$ might be close to 1 for UV radiation, the variation in the ratios a_{CDOM} / K_d reported at 323, 338, and 380 nm requires some explanation. It might have resulted from wavelength-dependent variation of $\bar{\mu}_d$ or of the b / a ratio, or from absorption by other components, such as the photo-protective mycosporine-like amino acid pigments, MAAs. These pigments are produced by some phytoplankton and absorb most strongly between 300 and 360 nm (Karentz *et al.*, 1991; Vernet and Whitehead, 1996). This interaction could represent a limitation to the remote determination of CDOM absorptivity, since, in a phytoplankton bloom which produces a high concentration of MAAs, the relationships developed here might not apply. The particularly high ratio reported for 380 nm should be used with caution, due to the lower correlation coefficient of that relationship ($r^2 = 0.66$). In general, where particle loads are typically low, as in most parts of the ocean, it seems that absorbance by CDOM is responsible for essentially all of the UV atttenuation. This result is consistent with previous meaurements made in the Bering Sea (A. Ciotti, personal communication). Also, while Smith and Baker (1981) presented results that suggested that pure water also absorbed a significant proportion of UV photons in the open ocean, their measurements were made on ocean water that probably contained CDOM. More recent measurements by Pope and Fry (1997) on

commercially distilled water show significantly less absorption by pure water, although unfortunately, they only measured absorption at wavelengths 380 nm and longer.

3.5 Summary

This chapter presents empirical relationships between the *in situ* downwelling attenuation coefficient at several ultraviolet wavelengths and *in situ* visible reflectance, and between the downwelling attenuation coefficient and the absorptivity of coloured dissolved organic matter at the same ultraviolet wavelengths. These relationships apply over a wide range of water types, in two oceans. Coloured dissolved organic matter is responsible for essentially all ultraviolet attenuation in the ocean in the summer in the areas studied. The *in situ* ultraviolet downwelling attenuation coefficients are also related to visible reflectance calculated from satellite images. The average cosine for downwelling UV irradiance may be between 0.9 and 1.

Chapter 4. DIC Photoproduction Estimates

4.1 Introduction

Previous authors have noted that there must be a process in the ocean which remineralizes about 10^{13} moles of terrestrially-derived dissolved organic carbon, DOC, every year (for example Kieber *et al.*, 1989; see Chapter 1) for which there is currently no quantified sink. Kieber *et al.* (1989) suggested that the missing sink might be photochemical oxidation, but they were unable to quantify the importance of the process at that time. Miller and Zepp (1995) and Kieber and Mopper (2000) made estimates of the rate of photochemical DOC remineralization to DIC, the carbon photoproduct produced at the highest rate, but without a DIC quantum yield spectrum, both approaches required many simplifying assumptions.

Miller and Zepp (1995), for example, measured the production rate of DIC under full-spectrum radiation in a solar simulator. They then scaled the measured absorptivity-normalized production rate to an average *in situ* rate using a calculated annual irradiance spectrum and the calculated absorptivity at 350 nm of "global average river water". The resulting average near surface rate of conversion of DOC to DIC calculated for 40°N was 7.5×10^{-7} moles C l^{-1} $hour^{-1}$, which they pointed out made the photochemical oxidation of DOC a significant sink for organic carbon in the ocean.

Kieber and Mopper (2000) calculated a global, annual rate of DIC photoproduction. They had found that the ratio of DIC/CO produced during full spectrum irradiations of open ocean water was about 8, so they multiplied a global estimate of CO production (see chapter 5) by that factor. They estimated that 1.1×10^{15} g C (about 0.9×10^{14} moles) were remineralized to DIC each year.

The method presented in this chapter combines the spectral quantum yield data and optical relationships presented in previous chapters with satellite images and a solar model to make a more quantitative estimate of DIC photoproduction in the Mid-Atlantic Bight and in the whole ocean.

4.2 Methods

Water column production estimates

Both vertically-resolved and whole water column DIC photoproduction rates were estimated. To calculate a depth profile for DIC photoproduction at stations for which quantum yield spectra were determined, the modelled surface scalar irradiance was propagated down through the water column using an attenuation spectrum, $K_d(\lambda)$, calculated from the measured K_d values with two single exponential fits (figure 4.1: r^2=0.97-0.99 for UV and 412 nm section, n=4; r^2=0.94-0.99 for visible section, n=4). At each depth (1 m intervals), the product of spectral scalar irradiance and the measured spectral CDOM absorptivity and quantum yield spectra gave spectral DIC production

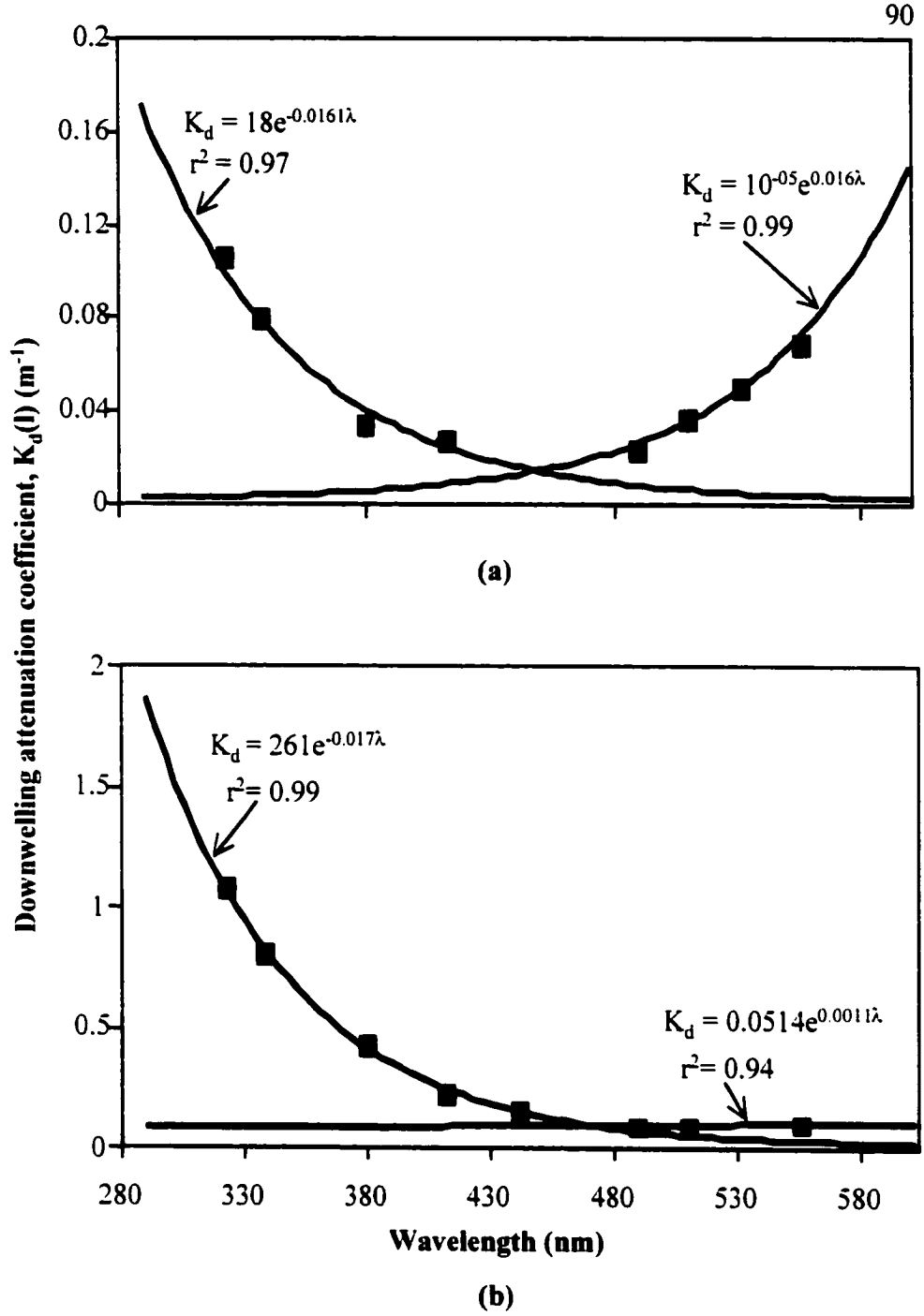

Figure 4.1. Exponential fits to measured K_d points: (a) stn 16 (offshore); (b) stn 5 (coastal).

(equation 2.5). The sum of the depth-resolved production down to 200 m at each station represented the whole water column production rate. This method requires *in situ* measurements of $a_{CDOM}(\lambda)$, $K_d(\lambda)$ and $\phi(\lambda)$. Obviously, it is not a practical way to make calculations over a large area.

Using representative, measured quantum yield spectra, it is possible to calculate a whole water column rate of photoproduction in an area without measuring values of $a_{CDOM}(\lambda)$, $K_d(\lambda)$ or $\phi(\lambda)$ at each station, as explained below. This method invokes two assumptions. The first is that all the solar radiation which passes into the water is absorbed somewhere within the water column. This is reasonable, since a comparison of measured values of $E_d(\lambda)$ with $L_u(\lambda)$, shows that only about 0.1 - 2% of the irradiance entering the ocean at any wavelength is reflected back out again. With this assumption, if CDOM is the precursor material for DIC photoproduction, it is necessary only to know what proportion of the incident irradiance is absorbed by CDOM, rather than the actual absorptivity of CDOM, and equation (2.5) becomes (after Cullen *et al.*, 1997):

$$\frac{dDIC}{dt} = \int_{\lambda} E_0(\lambda, 0-) \frac{a_{CDOM}(\lambda)}{a(\lambda)} \phi(\lambda) d(\lambda) \qquad (4.1)$$

where $dDIC/dt$ is the DIC production rate per unit area (moles DIC $m^{-2}month^{-1}$), $E_0(\lambda, 0-)$ is scalar irradiance incident just beneath the surface of the ocean (moles photons m^{-2} $month^{-1}$ nm^{-1}), $a_{CDOM}(\lambda)$ and $a(\lambda)$ are CDOM absorptivity (m^{-1}) and total absorptivity

(m^{-1}) respectively, and $\phi(\lambda)$ is the apparent quantum yield (moles DIC (mole photons)$^{-1}$). The second assumption is that all the photochemically active radiation (mostly UV) absorbed within the water column is absorbed by CDOM, i.e., $a_{CDOM}/a = 1$. This assumption is based on data presented in Chapter 3. If $a_{CDOM}/a = 1$, then equation 4.1 simplifies to:

$$\frac{dDIC}{dt} = \int_{\lambda} E_d(\lambda, 0-)\phi(\lambda)d\lambda \qquad (4.2)$$

Thus, to calculate whole water column DIC photoproduction rates, it is necessary only to know the scalar irradiance just beneath the ocean's surface and which pooled quantum yield spectrum to apply at each location.

Regional DIC photoproduction estimate made using SeaWiFS images

Using the assumptions described above, the calculation of DIC photoproduction from SeaWiFS imagery required the selection of a pooled quantum yield spectrum for each pixel, and an appropriate solar spectrum. Attenuation at 323 nm, $K_d(323)$, provided a convenient way to distinguish the quantum yield zones. SeaWiFS images of monthly-binned, normalized water-leaving radiance, $nL_w(\lambda)$ at 412 and 555 nm in the Mid-Atlantic Bight for July 1998 at 9 km x 9 km resolution (figure 3.8) were used to determine $K_d(323)$, as described in chapter 3. (The nL_w images were from the SeaWiFS data set available following reprocessing in August-September 1998.) The quantum yield zones

were divided according to two apparent natural breaks in $K_d(323)$ with location. The inshore zone was where $K_d(323)$ was ≥ 2 m^{-1}; the coastal zone where $2 > K_d(323) \geq 0.2$ m^{-1}; and the open ocean zone where $K_d(323) < 0.2$ m^{-1}. Figure 4.2 shows the resulting quantum yield zones in the Mid-Atlantic Bight for July 1998. Gregg and Carder's (1990) solar irradiance model, as modified by Arrigo (1994), provided a monthly, clear sky, scalar irradiance spectrum just below the sea surface for the wavelength range 295 - 480 nm. Irradiance (moles photons $m^{-2}s^{-1}nm^{-1}$) was calculated at fifteen minute intervals for every day in July and then summed to calculate the total monthly scalar irradiance. The Mid-Atlantic Bight lies mainly between 36°N and 40°N, so the average of the monthly spectral irradiance calculated at each of these two latitudes was applied to the whole Mid-Atlantic Bight. For most of the wavelength range, the two spectra were within 2% of one another, although through most of the UVB they were about 5% different, and at 295 nm 16% different. The TOMS data set provided a measured average ozone thickness over the area for July 1998 (350 DU; TOMS, 1999) to use in the model with default meteorological parameters (wind speed 0 m/s; 100% relative humidity; air temperature 30°C; atmospheric pressure 100 kPa). The resulting monthly scalar irradiance spectrum is shown in figure 4.3 (a).

The clear sky irradiance model neglects the effects of clouds. Clouds affect both the magnitude and spectral distribution of irradiance (Bartlett *et al.*, 1998). The Bartlett *et al.* (1998) model, extrapolated into the UV where it was not actually constrained by Bartlett *et al.*, was used to determine the effect of clouds over the Mid-Atlantic Bight for July 1998. In this model clear sky spectral irradiance is multiplied by a "cloud factor", which

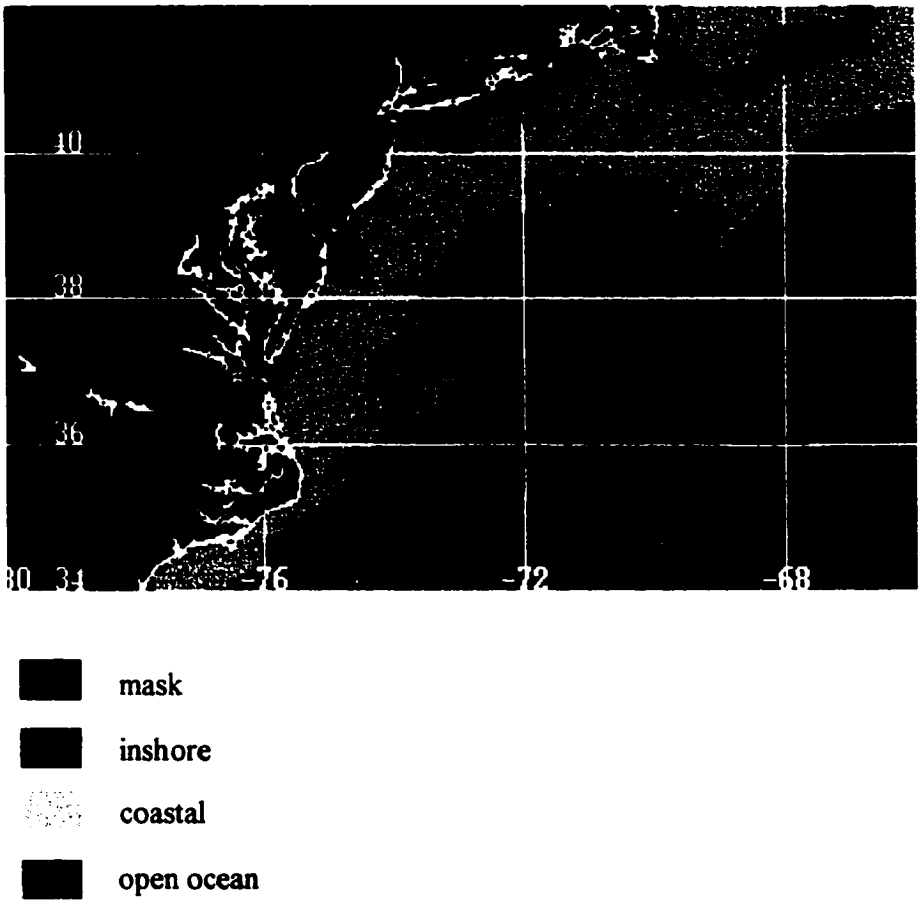

Figure 4.2. Quantum yield zone map for Mid-Atlantic Bight, July 1998

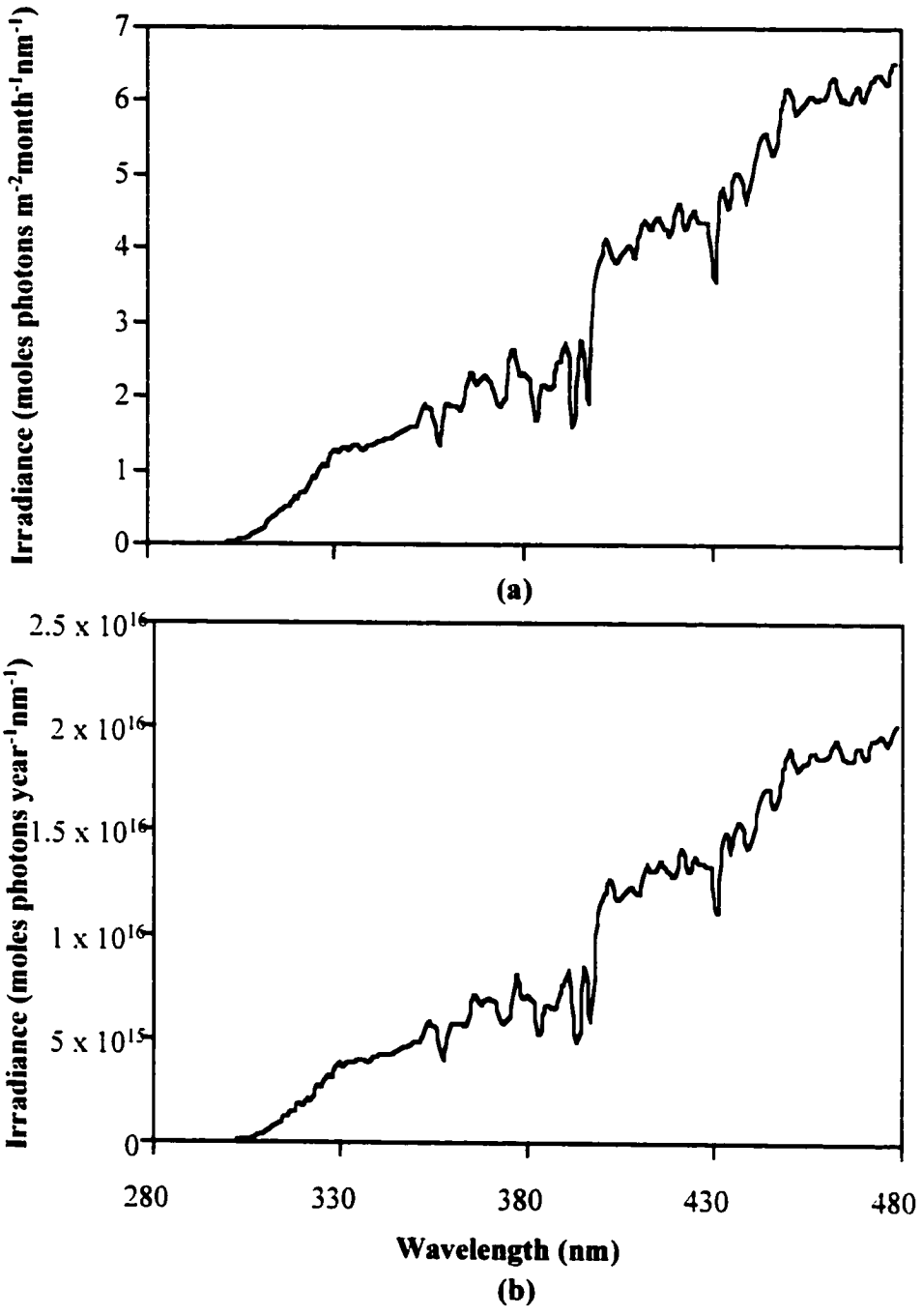

Figure 4.3. Solar irradiance spectra (calculated, as described in the text, from Gregg and Carder, 1989). (a) Monthly, clear sky, scalar irradiance at 40°N for July 1998, ozone 350 DU; (b) Total global, annual, clear sky, spectral irradiance just below the sea surface.

accounts for the change in the magnitude of irradiance due to clouds, and by a "spectral cloud effect", which weights the spectral distribution of irradiance. In general clouds reduce the magnitude of irradiance at every wavelength but attenuate shorter wavelength radiation less than that at longer wavelengths. Calculation of both the cloud factor and the spectral cloud effect requires the fraction of sky covered by cloud. Unfortunately there were no direct cloud cover data available for the time of this study, so an indirect measure from satellite imagery was used.

The number of days during July 1998 that each 1 km x 1 km pixel was covered by cloud was determined from daily images of *nLw(490)* in the Mid-Atlantic Bight (GAC level 2). (The July 1998 cloud cover was calculated from the SeaWiFS data version available in November 1999; that for the other months was from the January 2000 version.) The distribution of the number of days of cloud masking is shown in figure 4.4. The ratio of the number of cloudy days at each pixel to the total number of days in July (31) was used to represent the average cloud cover fraction for that pixel for the cloud correction.

This method of determining the cloud fraction was not entirely satisfactory for two reasons. Firstly, the satellite passed at approximately the same local time (about noon) each day, which biased the cloud cover measurement toward a mid-day cloud cover fraction; and secondly, most of the pixel had to be covered by cloud that was opaque to the satellite's sensors to be counted, so that only cloud cover over a wide area was included. Warren *et al.* (1988) compiled an atlas of shipboard cloud cover estimates averaged over 1952 to 1981 for each month, which showed that in the Mid-Atlantic Bight

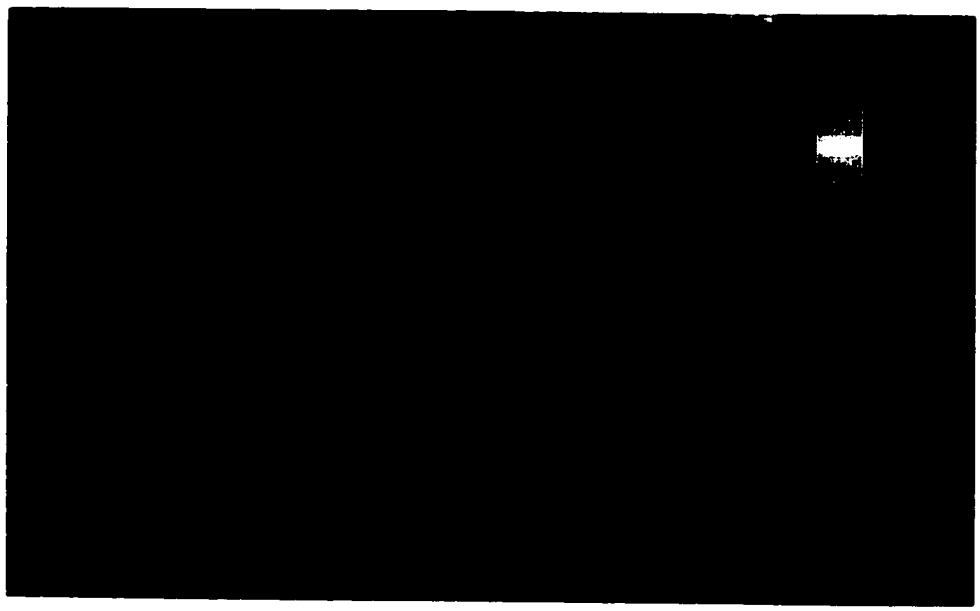

Figure 4.4. Number of days of opaque cloud cover in the Mid-Atlantic Bight July, 1998, calculated as described in the text

the average percent cloud cover was approximately 50% in July, while the method described above resulted in cloud cover only up to 25% per pixel. The atlas is also subject to some biases, which will not be discussed here, but it does suggest that the estimate made in this chapter systematically underestimates average cloud cover.

Table 4.1 shows all the possible values for DIC photoproduction calculated as the product of spectral zone pooled quantum yield and cloud-corrected incident irradiance for cloud fractions from 0/31 to 31/31. The image of DIC photoproduction in the Mid-Atlantic Bight in July 1998 (figure 4.5c) is the result of the combination of the actual values for quantum yield zone and cloud fraction determined from figures 4.2 and 4.4, respectively. The same procedure was followed to calculate DIC photoproduction in the Mid-Atlantic Bight in October, January, and April to demonstrate seasonal changes (figure 4.5). (Masked pixels in figure 4.5 represent those at which $nL_w(412)$ or $nL_w(555)$ was below the cutoff value. See Chapter 3.)

Global annual oceanic DIC photoproduction estimate

To calculate an annual rate of photochemical conversion of DOC to DIC, the quantum yield spectra determined in the Mid-Atlantic Bight and in Bedford Basin during the spring and summer were assumed to apply equally well to the whole ocean in every season. It was also assumed, as explained above, that all the photochemically active radiation that entered the water column was absorbed by CDOM. To make the calculation, the world was divided into eighteen 10° latitude bands. The sea surface area within each band was calculated (table 4.2) using data from the Combined Ocean

Number of cloudy days (/31)	Inshore Zone	Coastal Zone	Open Ocean Zone
0	0.038	0.230	1.10
1	0.038	0.230	1.10
2	0.038	0.230	1.10
3	0.038	0.230	1.00
4	0.038	0.230	1.00
5	0.038	0.230	1.00
6	0.038	0.230	1.00
7	0.038	0.230	1.00
8	0.038	0.230	1.00
9	0.038	0.230	1.00
10	0.037	0.220	1.00
11	0.037	0.220	1.00
12	0.037	0.220	1.00
13	0.037	0.220	1.00
14	0.037	0.220	0.99
15	0.036	0.210	0.98
16	0.036	0.210	0.96
17	0.036	0.210	0.95
18	0.035	0.200	0.93
19	0.035	0.200	0.91
20	0.034	0.200	0.88
21	0.033	0.190	0.86
22	0.032	0.180	0.83
23	0.032	0.180	0.79
24	0.030	0.170	0.76
25	0.029	0.160	0.72
26	0.028	0.150	0.68
27	0.026	0.140	0.63
28	0.024	0.130	0.58
29	0.022	0.120	0.52
30	0.020	0.110	0.46
31	0.017	0.090	0.39

Table 4.1. Calculated DIC production rate (moles DIC m^{-2} $month^{-1}$) for July 1998 in the Mid-Atlantic Bight, with all combinations of quantum yield zone and fractional cloud cover.

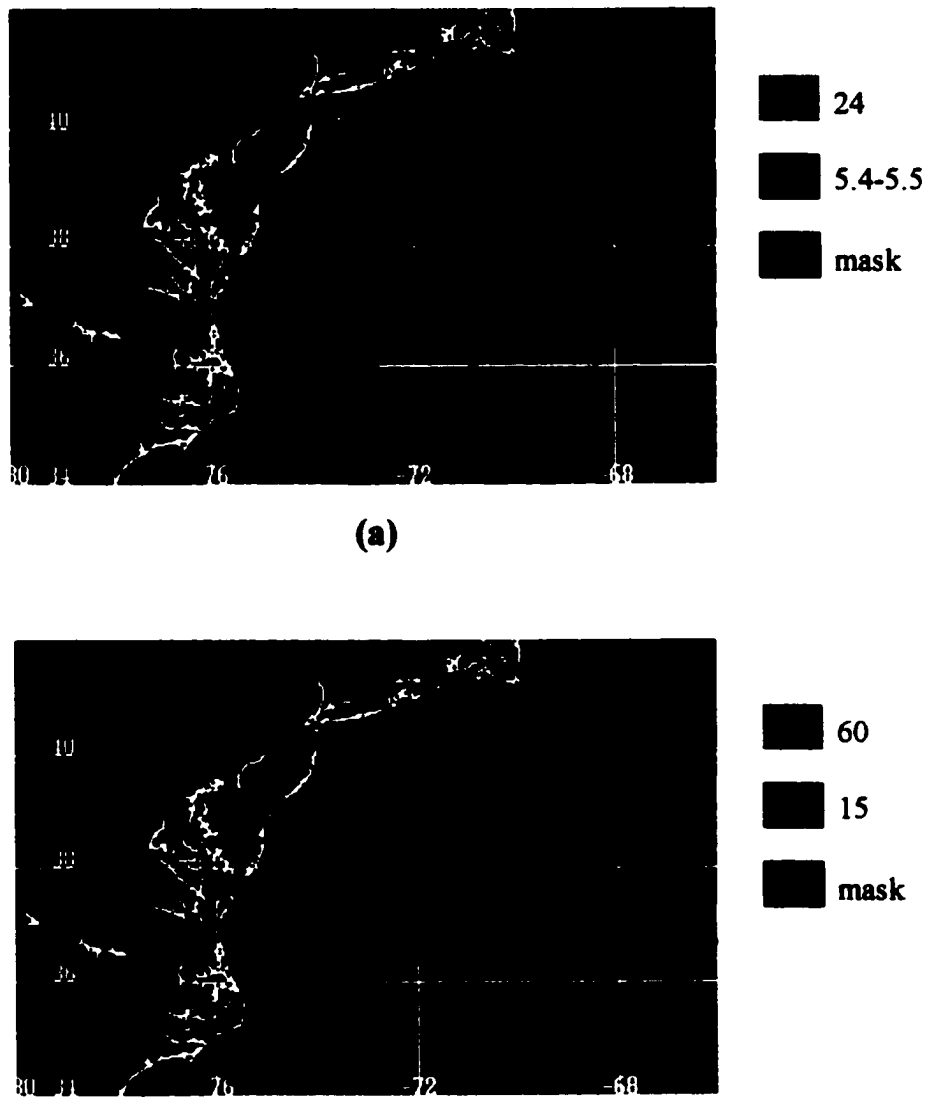

(a)

(b)

Figure 4.5. Monthly rate of photochemical production of DIC in the Mid-Atlantic Bight (10^{-2} moles DIC m^{-2} $month^{-1}$): (a) January, 1998; (b) April, 1998.

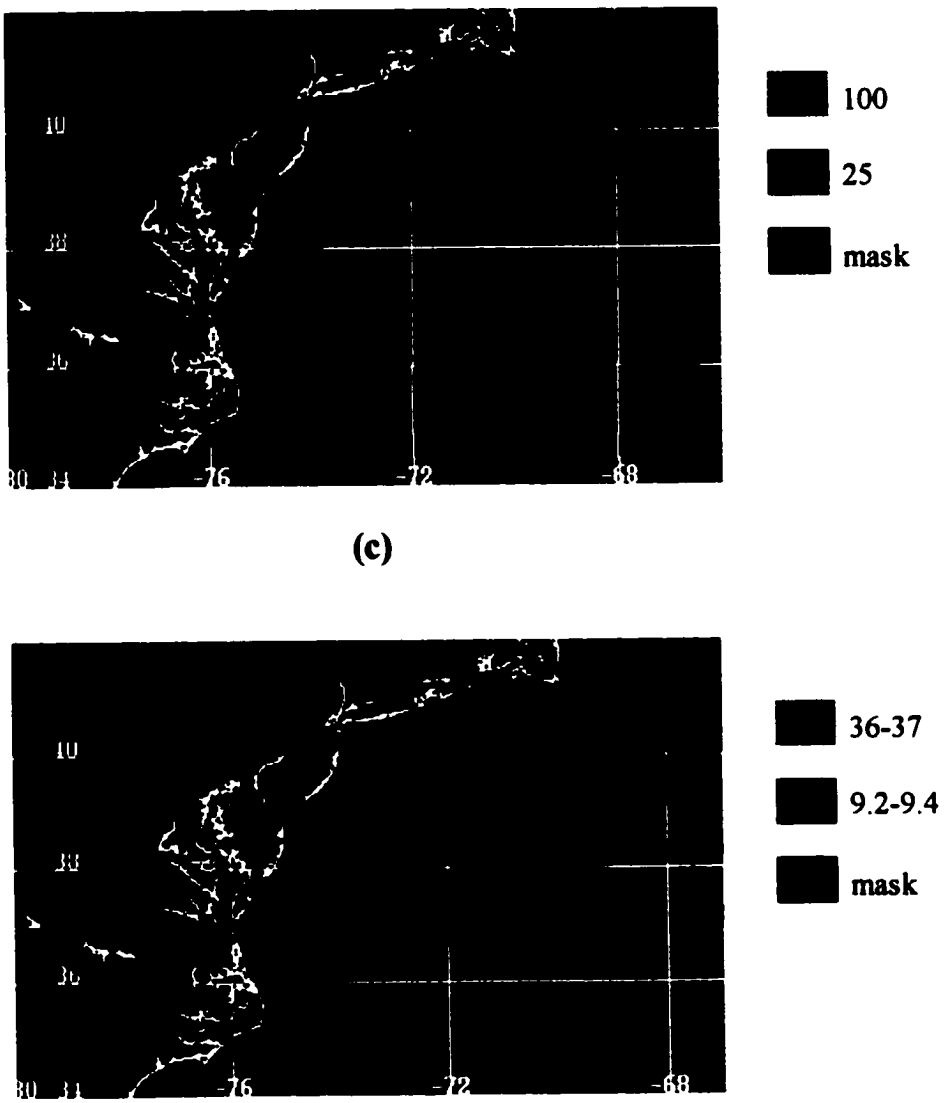

(c)

(d)

Figure 4.5. Monthly rate of photochemical production of DIC in the Mid-Atlantic Bight (10^{-2} moles DIC m^{-2} $month^{-1}$): (c) July, 1998; (d) October, 1998

Latitude Band	Sea Surface Area in Band (km^2)
90°S - 80°S	0
80°S - 70°S	3.11×10^{06}
70°S - 60°S	1.68×10^{07}
60°S - 50°S	2.55×10^{07}
50°S - 40°S	3.07×10^{07}
40°S - 30°S	3.25×10^{07}
30°S - 20°S	3.12×10^{07}
20°S - 10°S	3.37×10^{07}
10°S - 0°	3.40×10^{07}
0° - 10°N	3.45×10^{07}
10°N - 20°N	3.16×10^{07}
20°N - 30°N	2.51×10^{07}
30°N - 40°N	2.09×10^{07}
40°N - 50°N	1.45×10^{07}
50°N - 60°N	1.07×10^{07}
60°N - 70°N	4.69×10^{06}
70°N - 80°N	7.85×10^{06}
80°N - 90°N	3.59×10^{06}

Table 4.2. Sea surface area in each 10° latitude band used for global irradiance calculation.

Atmosphere Data Set (COADS, 1999). The annual scalar irradiance calculated from the Gregg and Carder (1990) model (as modified by Arrigo, 1994) at each band's central latitude (i.e at 55°N for the 50°N-60°N band) was calculated as described earlier for the monthly spectrum - scalar irradiance (moles photons m^{-2} s^{-1} nm^{-1}) at fifteen minute intervals was summed over the whole year. The annual irradiance was then multiplied by the sea surface area in that latitude band to obtain an estimate of the annual spectral scalar irradiance just below the surface of the ocean in each band. The summed irradiance in all the latitude bands provided an estimate of the global, annual, clear sky, scalar irradiance spectrum that passes into the ocean (figure 4.3 (b)). This estimate neglected the effect of clouds.

The global annual irradiance spectrum was multiplied by both the open ocean and the coastal pooled DIC spectral quantum yield. These two products represented the global annual rate of DIC production assuming that the respective quantum yield spectrum applied to the whole world. Then, assuming that about 7% of the world's ocean overlies continental shelf and that the remainder is open ocean (following Andrews *et al.*, 2000). the two products were weighted accordingly and summed to estimate the annual photochemical production rate of DIC for the whole ocean.

4.3 Results

Figure 4.6 shows depth profiles of DIC photoproduction calculated for two stations using measured attenuation coefficients, absorptivity, and quantum yield spectra and modelled

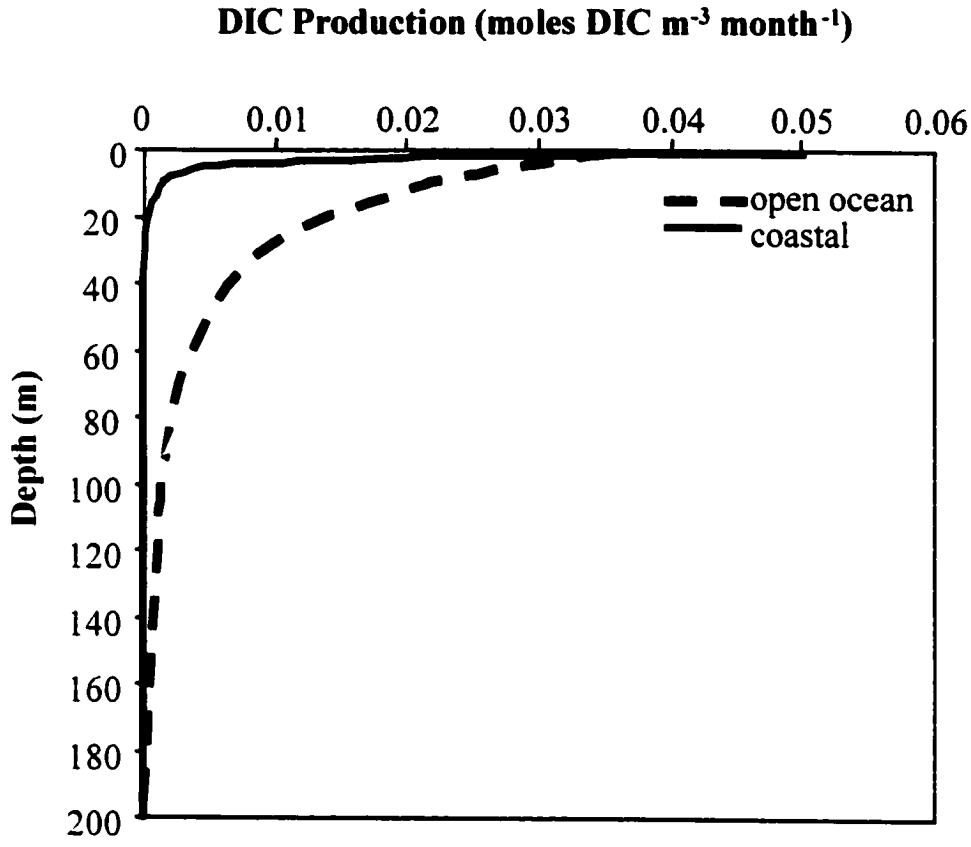

Figure 4.6. Monthly DIC production rate by depth for an open ocean station and a coastal station in the Mid-Atlantic Bight, August 1998.

monthly, clear sky, scalar irradiance. While the production rate at the coastal station is higher in the top 60 cm, total production summed at 1 m intervals over the top 200m of the ocean is much higher at the open ocean station (table 4.3). Both profiles demonstrate roughly exponential decay of production with depth, as a result of the shapes of the attenuation spectra used to determine the light field.

The whole water column DIC production rate was calculated at five stations, using the modelled irradiance and the appropriate pooled DIC quantum yield spectra. Table 4.3 compares the results of the water column calculation method with those calculated using *in situ* quantum yield, $a_{CDOM}(\lambda)$ and $K_d(\lambda)$ at each station. In general, the two estimates were closer for the open ocean station than for the coastal and inshore ones. This was probably the result of the higher variability among quantum yield spectra in the coastal and inshore zones. The water column method is more appropriate for calculations of average production over a large area than at a single station, since the pooled quantum yield spectra represent zone averages.

On a regional scale, the whole water column estimate showed that in July 1998, photoproduction in the Mid-Atlantic Bight was about 1 mole DIC $m^{-2}month^{-1}$ in the open ocean zone, and about a quarter of that in the coastal zone (figure 4.5 (a)). A comparison of figures 4.2, 4.4 and 4.5 demonstrates that the choice of quantum yield spectrum dominates the calculated DIC production rate; the effect of clouds, at least in that location at that time of year, is insignificant in comparison.

Station	DIC Production (0-200m)	DIC Production (whole water column)
Open ocean (M9708-16As)	0.89	1.0
Coastal (M9708-08)	0.18	0.23
Coastal (M9705-05)	0.12	0.23
Inshore (F9805-03)	0.037	0.04
Inshore (F9805-04)	0.059	0.04

Table 4.3. Comparison of DIC production rate (moles DIC m^{-2} $month^{-1}$) calculated using modelled clear-sky, monthly, scalar irradiance spectrum for July at 40°N: over the top 200 m calculated at 1 m intervals using measured *in situ* downwelling attenuation coefficient, quantum yield, and absorptivity spectra *vs.* over the whole water column using zone pooled quantum yield spectra.

The October, January, and April images of the Mid-Atlantic Bight show a seasonal change in the distribution of DIC photoproduction related to a change in transparency of the coastal water, as shown in figure 4.5. DIC photoproduction per unit area was higher in the summer, as expected, due to the higher incident irradiance. The calculated rate of photoproduction was further increased in the summer by the increased transparency of the water; this resulted in an interpreted increase in photochemical efficiency due to the application of the open ocean quantum yield spectrum over a wider area. Whether that increased efficiency is real remains to be tested with additional determinations of quantum yield in samples taken during other seasons.

From the global calculation described earlier, a direct photochemical loss rate of 10^{15} moles of DOC $year^{-1}$ is estimated. Using the standard deviations of the coefficients of the zone pooled quantum yield spectra calculated in chapter 2 and the stated error of the irradiance model (± 6.6%), a standard deviation for the global production estimate was calculated. The calculation was made numerically, by varying the coefficient and irradiance values up to their standard deviations through 1000 iterations using Matlab®, and calculating the standard deviation of the resulting DIC production values. As a result, the calculated range of values for global annual DIC photoproduction is 0.7 - 4.1 x 10^{15} moles C $year^{-1}$.

Discussion

Miller and Zepp (1995) calculated an average near surface DIC production rate for 40°N using "global average river water" of 0.75 μmoles C l^{-1} $hour^{-1}$. For comparison, a similar rate was calculated using the inshore zone pooled quantum yield spectrum, the annual scalar irradiance at 40°N from the Gregg and Carder model, and the absorptivity spectrum from the most inshore station (F9805-01) scaled up to 15.4 m^{-1} at 350 nm to match the colour of water assumed by Miller and Zepp (1995). The result was very similar to that of Miller and Zepp. An average near-surface DIC production rate for 40°N of 0.4 μmoles C l^{-1} $hour^{-1}$was calculated. However, the inshore zone pooled quantum yield spectrum does not apply to most of the study area and probably not to most of the ocean. Near-surface DIC production rates calculated for the coastal and open ocean zone, using real CDOM absorptivity spectra and the appropriate zone pooled quantum yield spectra were 0.04 μmoles C l^{-1} $hour^{-1}$ for the coastal zone and 0.03 μmoles C l^{-1} $hour^{-1}$ for the open ocean zone, an order of magnitude lower than the calculated inshore rate. While these near-surface rates are interesting for comparison with the earlier estimate, they do not reflect the whole water column production rates that can be calculated from the spectrally-resolved information in this thesis.

Kieber and Mopper (2000) calculated a global, annual DIC photoproduction rate of 0.9 x 10^{14} moles by assuming that DIC was produced at about 8 times the rate of CO throughout the ocean. That rate is clearly lower than the 10^{15} moles reported in this thesis. However, if they had used a DIC/CO production ratio of 60 instead of 8, as discussed in Chapter 5, their value would have been about 7 x 10^{14} moles C per year,

which, for a global estimate, is quite close to the 10^{15} moles C per year rate calculated here.

Using the whole water column method, the global annual photoproduction rate of DIC seems to be high, relative to the missing sink for terrestrial organic carbon mentioned in the introduction (~10^{13} moles per year). It is an overestimate for several reasons. For example, this estimate is made for a full year of clear-sky irradiance; a full year of total global coverage by opaque cloud would reduce it by a factor of 2-3, according to Bartlett *et al.*'s (1998) cloud model. Also, the assumption that 100% of the photochemically active radiation is absorbed by CDOM is reasonable for UV wavelengths, but since the open ocean quantum yield spectrum has a fairly shallow slope, light with a wavelength as long as 450 nm might be important. At that wavelength, there is significant competition for photons by phytoplankton, although Siegel (2000) stated that for most of the open ocean, CDOM was responsible for 50-60% of light absorption at 440 nm, and Yentsch (1996) reported that CDOM absorbed 80-90% of the light at short, visible wavelengths in the coastal waters of the Gulf of Maine in the spring. Therefore, a correct a_{CDOM}/a ratio could reduce the production further by up to a factor of two. Additionally, most of the world's sediment input to the ocean comes from rivers draining south-east Asia and the Pacific Islands (Gross and Gross, 1996), and most of the fresh water input is near the equator (Libes, 1992), while the samples came from the north-western Atlantic. If that terrestrially-influenced water is less efficient at producing DIC photochemically than the open ocean portion of the north-western Atlantic, then the production estimate should be lower for that reason also. More quantum yield determinations from other parts of the

world in different seasons will be necessary to reduce the uncertainty of the global annual DIC production estimate.

Another possible source of error is that the slope of the open ocean zone pooled quantum yield spectrum, which is applied to most of the world in this calculation, might be too shallow. The pooled spectrum is based only on three measured spectra, although those three are very similar to one another (figure 2.9). It would tend to overestimate DIC production if the slope were too shallow and included too much visible radiation. However, the product of the global annual irradiance spectrum and the inshore pooled quantum yield spectrum, which is much steeper and lower than the open ocean one, still gives an annual DIC production rate of 10^{14} moles C $year^{-1}$. A calculation of DIC production using the open ocean quantum yield spectrum, but only considering radiation at wavelengths shorter than 400 nm results in an annual rate on the order of 10^{15} moles C $year^{-1}$. Consequently, while more quantum yield determinations in open ocean water will be necessary to preclude this possibility, it seems unlikely that the method described above overestimates the global production rate by including too much visible radiation.

The estimate of global annual DIC photoproduction could be improved in the future in several ways. As mentioned earlier, more DIC quantum yield spectra are needed to characterize the variability of efficiency with location and season. Also, instead of assuming that the irradiance spectrum at the centre of each 10° latitude band applied to the whole band and using modelled, clear-sky irradiance, it would be useful to apply measured irradiance spectra on the finest scale available, and to calculate the DIC

production rate separately for each small area. The calculation at each location could also use the correct quantum yield spectrum depending on the local water type instead of making a global approximation of 7% coastal, 93% open ocean. Geographic Information System, GIS, software would probably be quite useful in making such detailed calculations.

While this calculation admittedly overestimates DIC production due to the effects of clouds and of competition for photons at visible wavelengths, those two effects would not reduce it by the factor of 100 needed to match the estimated missing sink for terrestrial DOC. However, most of the photochemical oxidation taking place in the open ocean probably involves DOC formed *in situ* from the degradation products of marine phytoplankton, a source not considered in the aforementioned models. If 10^{15} moles of DOC are indeed lost each year to DIC, then photochemical oxidation is also a significant source of DIC to the surface ocean, comparable to the rate of DIC uptake by new production (1.5×10^{15} moles C $year^{-1}$, Carr *et al.*, 2000).

Summary

The combination of satellite imagery with experimentally-determined quantum yield spectra and empirical optical relationships represents a quantitative method for calculating the photochemical production of dissolved inorganic carbon in the ocean. Dissolved inorganic carbon production rates calculated in this way are comparable to those calculated at individual stations from *in situ* measurements of absorptivity, quantum

yield, and downwelling attenuation coefficient. However, because the zone pooled quantum yield spectra represent regional averages, the whole water column calculation method is more appropriate for large areas than for individual stations. The near-surface dissolved inorganic carbon production rate is higher at inshore stations because of the higher concentration of coloured dissolved organic matter, but the shallower slope of the quantum yield spectrum for open ocean water results in a higher water column production rate in that zone. The global, annual rate of dissolved inorganic carbon photoproduction is on the order of 10^{15} moles carbon $year^{-1}$, which is sufficient to account for the whole missing sink for terrestrial dissolved organic carbon as well as much of the dissolved organic carbon produced in the open ocean. Dissolved inorganic carbon is produced photochemically at a rate comparable to its annual rate of uptake by new production.

Chapter 5. Comparison with other photoproducts

5.1 Introduction

The accurate calculation of oceanic photochemical reaction rates requires a known quantum yield spectrum. Quantum yield spectra have been determined for a number of photoproducts prior to this thesis work. While DIC is the most rapidly produced carbon photoproduct resulting from the breakdown of CDOM (Miller and Zepp, 1995), many other chemically and biologically reactive species are also formed, as described in Chapter 1.

In particular, three of those products, CO, H_2O_2 and CS_2, are of interest for their reactions in sea water. Carbon monoxide is a volatile gas which, when emitted to the atmosphere, reacts with hydoxyl radical and affects the buildup of greenhouse gases, such as methane (Valentine and Zepp, 1993) and carbon dioxide (Erickson, 1989). It is also a substrate for bacteria (Moran and Zepp, 1997). The photochemical formation of CO in the ocean is thought to contribute significantly to its total atmospheric budget (Valentine and Zepp, 1993). Hydrogen peroxide reacts strongly with organic matter and may be an important source of free radicals (Sikorski and Zika, 1993). Its distribution is so strongly tied to its photochemical production at the surface of the ocean that it can be used as a tracer for mixing (Zika *et al.*, 1985). In the troposphere, CS_2 reacts to form COS, a source of long-lived atmospheric aerosols which can affect the world's radiation budget (Xie *et al.*, 1998). The photochemical formation of CS_2 in the surface ocean seems to

provide much of the flux of CS_2 to the atmosphere (Xie *et al.*, 1998). Clearly, it is important to study the rates and distributions of formation of CO, H_2O_2 and CS_2.

The method described in Chapter 4 for determining regional DIC photoproduction can be applied to any photochemical product whose spectral quantum yield is known. This chapter compares the DIC quantum yield spectra reported in Chapter 2 for sea water with those determined by previous authors in lake and river water, and with those of CO, H_2O_2, and CS_2.

5.2 Methods

The method described in Chapter 4 was used to calculate monthly total water column production rates for CO, H_2O_2, and CS_2 in the Mid-Atlantic Bight for July 1998 and to calculate a global, annual photoproduction rate for each. Where discrete quantum yield data points were given instead of a full spectrum, a single exponential decay line was fitted through the points (figure 5.1). Quantum yield data were taken from Moore (1999; lake DIC), Gao and Zepp (1998; river DIC), Miller *et al.* (2000; H_2O_2 spectrum), Moore *et al.* (1993; discrete H_2O_2 points), Ziolkowski (unpublished; ocean CO), Valentine and Zepp (1993; river CO), and Xie *et al.* (1998; CS_2).

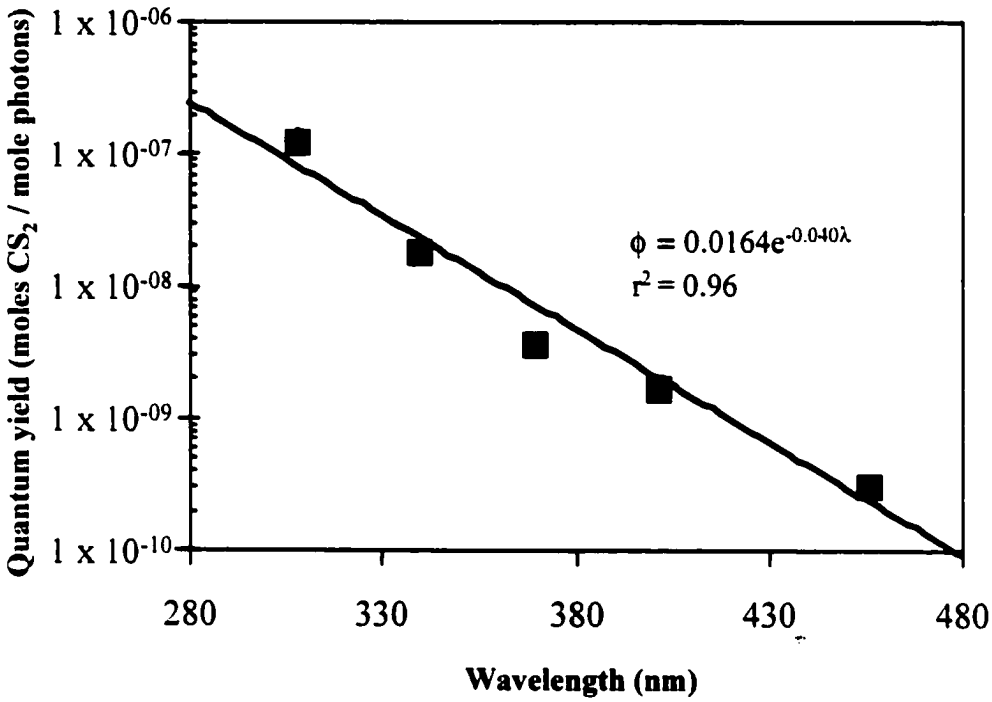

Figure 5.1. Exponential fit to Xie et al., 1998 CS_2 quantum yield points for DIC production calculation

5.3 Results

Figure 5.2 shows the quantum yield spectra or points for all products discussed in this chapter. DIC is the most efficiently produced, and the quantum yield spectrum for H_2O_2 is the next highest. The CO quantum yield spectrum is about an order of magnitude lower than the DIC ones, and the CS_2 spectrum is about three orders of magnitude lower.

It is difficult to assess the combined effects of magnitude and shape of quantum yield on photochemical production rate simply by looking at the quantum yield spectra, so monthly water column production rates were calculated for all the products in the Mid-Atlantic Bight for July 1998, from the satellite images previously used to calculate regional DIC production (figure 5.3; table 5.1). The values given in table 5.1 were calculated using the monthly, clear sky, scalar irradiance at 40°N. Global, annual production rates were also calculated (table 5.2).

5.4 Discussion

As previously predicted from laboratory experiments, DIC is produced far more quickly in the ocean than is any other photoproduct with a known quantum yield. Its production certainly represents the most rapid direct photochemical loss of organic carbon. The effect of clouds on the other products is more marked than it is on DIC, because the efficiency of their production is believed to be independent of location. With the assumptions made in this calculation - particularly that all the photochemically active radiation is absorbed by CDOM, which is the precursor material for all the reactions

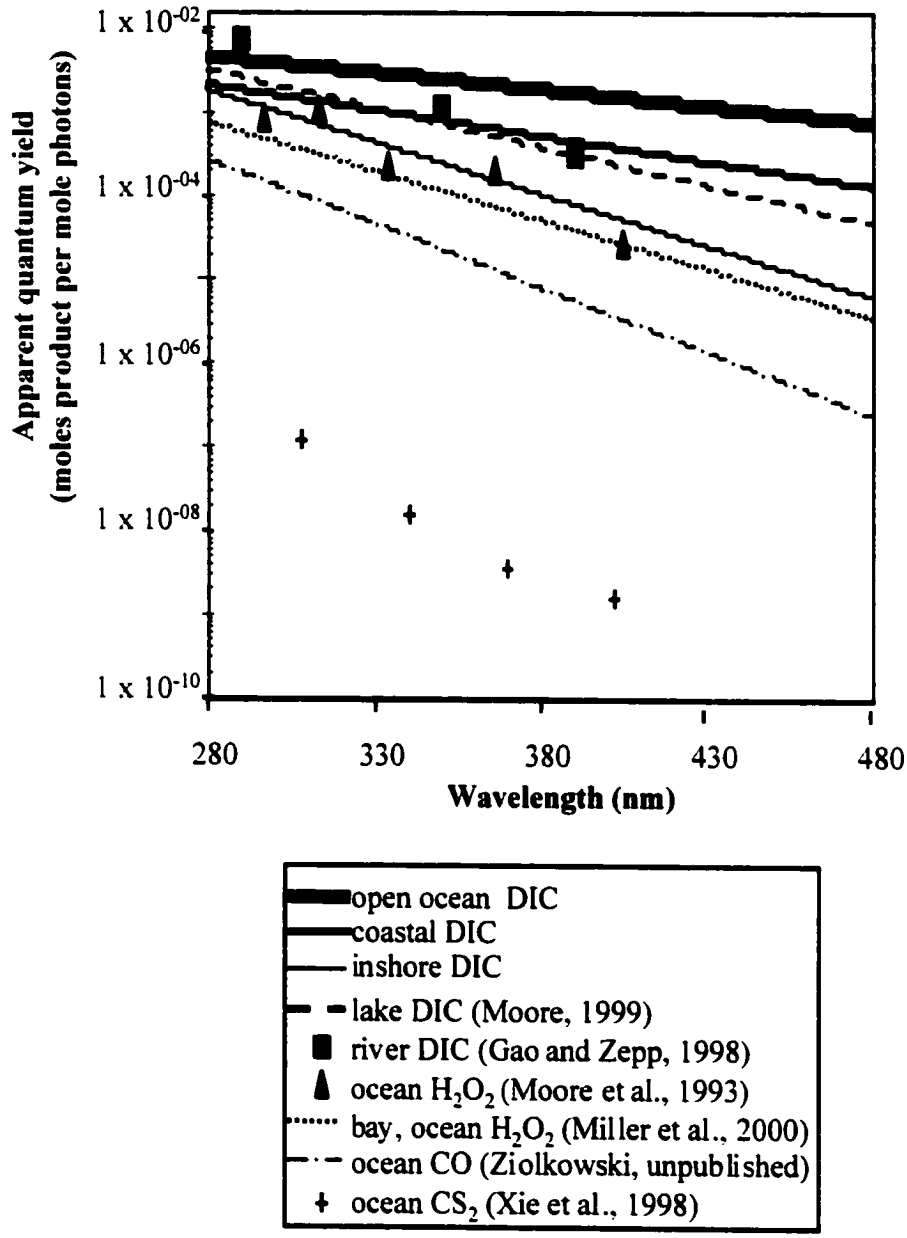

Figure 5.2. Comparison of DIC pooled zone quantum yield spectra with quantum yield spectra for DIC from a river and a lake and for other products.

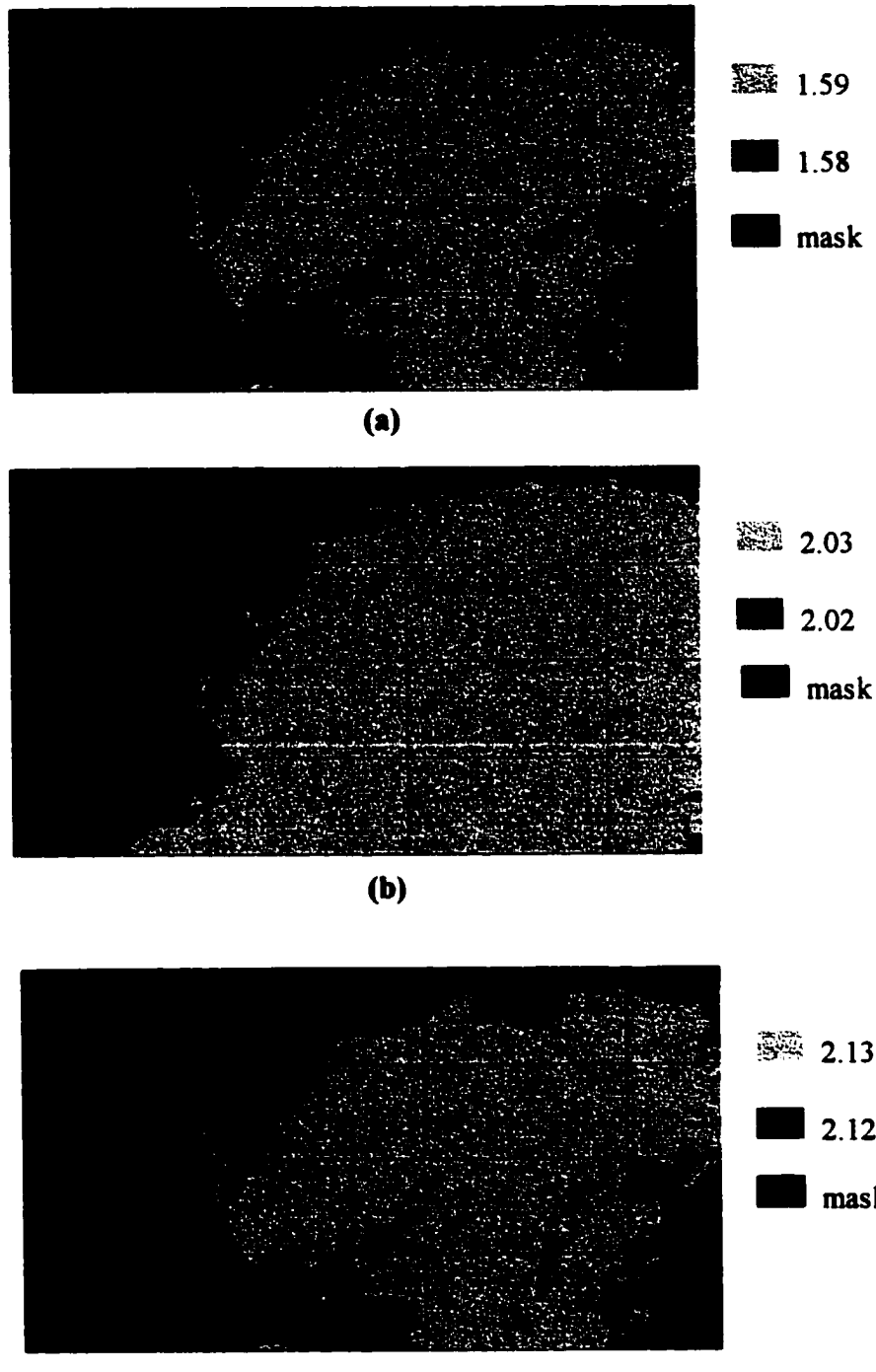

Figure 5.3. Monthly production rates in the Mid-Atlantic Bight, July 1998: (a) CO (10^{-2} moles CO m^{-2} $month^{-1}$); (b) H_2O_2 (10^{-2} moles H_2O_2 m^{-2} $month^{-1}$); (c) CS_2 (10^{-6} moles CS_2 m^{-2} $month^{-1}$).

Product	Monthly water column production rate	Monthly open ocean DIC rate / product rate	Monthly coastal DIC rate / product rate	Monthly inshore DIC rate / product rate
DIC (open ocean)	1.0			
DIC (coastal)	2.4×10^{-1}			
DIC (inshore)	3.8×10^{-2}			
CO	1.6×10^{-2}	63	15	2.4
H_2O_2	3.3×10^{-2}	30	7.3	1.2
CS_2	2.1×10^{-6}	4.8×10^{5}	1.1×10^{5}	1.8×10^{4}

Table 5.1. Comparison of monthly production rates (moles product m^{-2} $month^{-1}$) for DIC using all zone pooled quantum yield spectra with CO, H_2O_2 and CS_2, July 1998, Mid-Atlantic Bight, clear sky, scalar irradiance at 40°N.

Product	Global annual production rate	Global DIC production rate / product rate
CO	3.8×10^{13}	58
H_2O_2	5.9×10^{13}	37
CS_2	6.3×10^{9}	3.5×10^{5}

Table 5.2. Global, annual production rates (moles product $year^{-1}$) for CO, H_2O_2 and CS_2 and comparison with global annual DIC production rate.

studied here - for a given irradiance spectrum, the variation in quantum yield alone determines the variation in production rate for the various products. The regional production rate images for CO, H_2O_2 and CS_2 in figure 5.3 show little of the spatial variability in production rate which is so marked in the DIC production images (figure 4.6), because those products are thought to have only one quantum yield spectrum each.

DIC is produced about twice as quickly as CO in the inshore zone; it is produced at about 15 times the CO production rate in coastal water, and 60 times as quickly in open ocean water. The range of these ratios is similar to that measured in the laboratory by Miller and Zepp (1995; DIC / CO = 10-65) and brackets the ratios reported by Kieber *et al.* (2000; DIC / CO = 8-20). The ratio of monthly water column photoproduction of DIC to that of H_2O_2 ranges from 1.2 inshore to about 30 in the open ocean. CS_2 is produced from 18 000 times to 480 000 times more slowly than DIC in the Mid-Atlantic Bight in July.

The global annual estimate of CS_2 photoproduction presented here compares well with the estimate made by Xie *et al.* (1998). Based on Xie *et al.*'s (1998) estimate of 36 μmoles S m^{-2} $year^{-1}$ and a global sea surface area of 3.61 x 10^{14} m^2, their results predict a global annual CS_2 photoproduction rate of 6.5 x 10^9 moles CS_2 $year^{-1}$. Using the water column production method presented in this thesis with Xie *et al.*'s quantum yield spectrum the calculated rate is 6.3 x 10^9 moles CS_2 $year^{-1}$.

The global, annual estimate of CO production also compares quite well with that made by Kieber and Mopper (2000) by extrapolation from measured, full-spectrum, near-surface

production rates. Kieber and Mopper calculated that about 1.1×10^{13} moles of CO were produced photochemically each year, as compared with the 3.8×10^{13} moles per year estimated in this chapter.

The methods presented in this thesis will allow the remote estimation of whole water column and depth-resolved production rates for any photochemical product of CDOM that has a known quantum yield spectrum.

Chapter 6. Conclusions

The goal of this thesis was to make a quantitative estimate of the direct photochemical source of dissolved inorganic carbon, DIC, in the ocean. The photochemical production of DIC represents the most rapid direct photochemical loss of dissolved organic carbon, DOC, so in this thesis its production is used as a proxy for DOC loss. The objectives set out in Chapter 1 have been reached by determining the first quantum yield spectra for the photochemical production of DIC in sea water; relating *in situ* attenuation and CDOM absorptivity to remotely sensed ocean colour; determining the proportion of total absorptivity due to CDOM, at least for the UV; and combining all of that information to make quantitative estimates of DIC production.

Spectral quantum yield of DIC for any given sample was well represented by a single exponential decay line. The spectra fell into three broad categories: inshore, coastal and open ocean, defined roughly either by salinity or by ocean colour. The magnitude of quantum yield increased with distance from shore, while the slope shallowed, which together increased the efficiency of DIC photoproduction in the open ocean relative to inshore production. This increased production offshore might represent a selective loss of highly-absorbing, non-DIC producing chromophores either by photobleaching or by microbial degradation. Fading in a solar simulator increased the efficiency of DIC photoproduction by increasing the magnitude of the quantum yield spectrum, although the slope of the spectrum steepened. More measurements of quantum yield are required

to determine whether the three zone pooled spectra reported in this thesis apply equally well to other areas of the ocean in other seasons.

The downwelling attenuation coefficient for UV radiation, $K_d(UV)$, can be predicted from *in situ* or remotely-determined visible reflectance measurements. While these relationships have not been tested in the winter or in the southern hemisphere, they seem to be robust over a wide range of water types in the Atlantic Ocean and the Bering Sea from May to August. The absorptivity of CDOM, a_{CDOM}, is linearly related to K_d at corresponding UV wavelengths. It is responsible for almost all of the attenuation at 323 and 338 nm, and probably at 380 nm as well. The average cosine of downwelling UV irradiance may be between 0.9 and 1, considerably higher than that determined for visible radiation. This suggestion is supported by several lines of evidence besides the very high ratio of a_{CDOM} to K_d for UV radiation.

The clear sky monthly areal rate of DIC photoproduction in the Mid-Atlantic Bight in 1998 ranged from 0.2 moles $m^{-2}month^{-1}$ in January to 1 mole $m^{-2}month^{-1}$ in July. While the whole water column rate of DIC production increases offshore due to the increased quantum yield, the near-surface rate is higher inshore, because of the higher absorptivity of CDOM. The global annual DIC photoproduction rate is approximately 10^{15} moles DIC $year^{-1}$. This value is high enough to account for the whole missing sink for terrestrially-derived DOC in the ocean. It is actually higher than the annual input of terrestrial DOC to the ocean, which probably reflects the importance of the photochemical transformation of autochthonous DOC formed from the degradation of

phytoplankton and other organic material. The rate of DIC photoproduction is also comparable to the annual rate of DIC uptake in new production by phytoplankton.

DIC is produced at a higher rate than CO, H_2O_2 and CS_2, both in surface waters and over the whole water column. The ratio of global annual DIC production to that of CO is about 60; the ratio of the two monthly production rates ranges from 2 for inshore water to 62 for open ocean water, a range similar to that determined experimentally by Miller and Zepp (1995) and bracketing that found by Kieber *et al.* (2000). The ratio of monthly DIC production to monthly CO production in coastal water is about 15, which matches closely the average value determined by Miller and Zepp (1995) and by several subsequent studies. The global rate of CS_2 photoproduction calculated using the whole water column production method matches that given by Xie *et al.* (1998).

The approach presented in this thesis can be used to calculate the vertically-resolved and whole water column rates of any photochemical reaction with a known quantum yield spectrum on any scale represented by remotely-sensed ocean colour data. It is a valuable tool for studying photochemical reactions on a global scale.

Appendix 1. From Aristotle to SeaWiFS: 2300 years of ocean optics

Introduction

In the fourth century B. C., Aristotle noticed that sea water was blue and very transparent, while river water was yellowish and murky (Louis, 1991). We have spent the last 2300 years trying to figure out why. We have also wondered how we might predict those changes. Although there has been speculation for centuries, such questions could not be answered empirically without instruments - instruments that could measure light in the ocean, separate it into different colours, or help to observe the tiny plants and other constituents of sea water. Contrary to popular belief, the 1960s did not mark the beginning of quantitative work in ocean optics. With the advent of useful instruments and techniques in the late 1800s and early 1900s, people began to make measurements that could explain Aristotle's observations. Throughout the twentieth century, improved methods have led to an increasingly detailed understanding of the processes controlling the distribution of light in the ocean. Here, I will describe the approaches and motivations of some of the many investigators who have studied ocean colour and transparency. I will also show how remote sensing, using aeroplanes and satellites, has allowed scientists to apply the knowledge of the causes of optical variability in the ocean to the interpretation of biological, chemical, and physical processes on a global scale.

Transparency of the ocean

Aristotle suggested that suspended particles in river water might explain why it was less clear than ocean water, even though, according to the ideas of the time, it was "purer" and less dense (Louis, 1991). Unfortunately, the discussion soon became mired in arguments about the purity of different types of water, and Aristotle's insights were not pursued further. The discussion of ocean optics was limited for some time to incidental observations by people who were really interested in something completely different. Ships' captains, while exploring unknown seas and looking for new trading routes, sometimes commented in their log books about the clarity of the ocean. In 1676, for example, Captain John Hood noted that the water in the Still Sea near Novaya Zemlya, as well as being the densest and saltiest he had ever seen (or tasted), was probably the clearest in the world; he could see shells on the bottom at a depth of 80 fathoms, about 160 m (Krümmel, 1907).

In the mid-1800s people began to measure light penetration in the ocean out of curiosity. On land, photometry was becoming popular, both among academics, especially astronomers who wanted to measure the brightness of stars, and among the gas inspectors who were measuring the intensity of street lamps (Johnston, 1996). There was an ongoing controversy over which photometric method to use. In the ocean, however, a rough estimate of transparency required only an object to submerge and a string to retrieve it.

The first recorded deliberate measurement was made in 1815 by Captain Kotzebue, who lowered a piece of red material into the ocean and measured the depth at which it disappeared (Krümmel, 1907). The first optical expedition was mounted a few years later on board the Coquille, during which Captain Duperrée lowered a white plate into the water at a number of stations (Krümmel, 1907). Krümmel reports several other, similar measurements made during the mid-1800s. The purpose of these early expeditions is unclear. They are mentioned without primary source references in Otto Krümmel's Handbuch der Ozeanographie (1907).

Michael Faraday used a similar technique in 1855 to demonstrate graphically the pollution of the Thames River in England (Cadée, 1996). He reported to the local newspaper that he had torn up pieces of white card and dropped them into the river in several locations. When the cards sank edge-first, he noted that the lower edge of the card disappeared before the upper edge was even below the surface of the water.

In the mid-1800s, Father Angelo Secchi, an Italian Jesuit priest, became interested in how sunlight affected the earth. Despite a hostile political climate which resulted in a period of Jesuit exile from Rome, Secchi made major advances in stellar spectroscopy and geophysics under the patronage of Pope Pious IX, and published about 700 articles and books (Brück, 1979). He was particularly interested in the physics of the sun. In 1865, Secchi turned his attention to the problem of the penetration of sunlight through sea water. He argued that, while all the measurements of the depth of penetration of light made in the ways described above were interesting, they were not really very useful.

Previous authors had not reported either the solar elevation or the degree of cloudiness, so it was impossible to generalize from their observations. Alessandro Cialdi and Angelo Secchi (1865) made systematic measurements of light penetration during a cruise on board the papal corvette *l'Immacolata Concezione*. They used several different disks, the largest being 3.73 m in diameter and made out of a circle of iron covered with white-varnished sail material. The others were a 40 cm diameter white plate and several 40 cm iron circles covered with the sail material. Secchi reported that the largest disk worked best because its image stayed together deeper, although subsequent work with Secchi disks has usually involved smaller versions. At each station, Cialdi and Secchi made replicate measurements of light penetration and simultaneously measured the solar zenith angle with a sextant, so that the measurements could be converted into equivalent depths for vertically incident sunlight. They explained that a depth measured using the disk method was not the depth of light extinction; on the contrary, light had to travel twice the depth of the submerged object to return to the observer's eye. Further, they noted that light must travel even further into the ocean than twice the disk depth, because the disk disappeared when the only colours of light left to reflect off it were the same colour as the surrounding ocean. Secchi speculated that blue and purple light could penetrate to great depths. It was probably the rigorousness of these observations that led to Secchi's name being given to the kind of disk used by generations of oceanographers to measure the penetration of light, despite the fact that the other investigators mentioned above had developed the technique first.

Although such techniques were available in the mid-1800s, they were not apparently widely used. There were no optical measurements made during the famous *Challenger* Expedition of 1872-1876, for example, although some of the scientists involved certainly wondered about the depth of light penetration: it was already well known that phytoplankton required light to survive, so when Comte degli Antelminelli found diatoms in the guts of benthic echinoids in deep water, he wondered whether there was enough light at the bottom of the ocean to support photosynthesis (Murray, 1886).

The development of photography in the mid-1800s provided scientists with another tool to measure the penetration of light in the ocean. In 1884 H. Fol and E. Sarasin (cited in Holmes, 1957) exposed photographic plates under water to measure the penetration of light. They had some success, but the method was considered quite unreliable, and was soon replaced by other instruments (Pettersson, 1934). Niels Højerslev (1994) has written an extensive history of the development of optical oceanographic instrument design in Scandinavia that describes many of these instruments in detail.

In 1922 Victor Shelford and F. W. Gail adapted a Kunz gas-filled photoelectric cell for use in the ocean and used it to measure light penetration in Puget Sound. H. H. Poole and W. R. G. Atkins modified the Shelford and Gail design for use in the rougher waters of the English Channel near Plymouth, as part of the Plymouth Laboratory's investigation of primary production. They carried out a number of very useful experiments and introduced some innovations still used in optical measurements in the 1990s. They used an amplified telephone to detect unbalanced current, instead of a galvanometer, because it

was more stable at sea (Poole, 1925; Poole and Atkins, 1926) and attached a diffuser over the photoelectric cell to simplify path-length calculations. They were able to correct the measurements at depth for changes in light intensity at the surface by using a surface reference radiometer. With such techniques available, it became possible to try to quantify the effect of light on photosynthesis, a link that had been made only qualitatively before.

In 1933 Penelope Jenkin made measurements that linked photosynthesis with light penetration in the ocean for the first time (Jenkin, 1937). Photosynthesis by marine plants was of considerable interest to people who wanted to understand the productivity of the sea (ibid.). The International Council for the Exploration of the Sea (I.C.E.S.) had been formed in 1902, with the main goal of carrying out research to benefit the fisheries of the member states (Mills, 1989, p. 14n). Britain had directed much of its share of the I.C.E.S. money to the Plymouth laboratory for studies of productivity in the English Channel and in the North Sea (Mills, 1989, p. 200), and had appointed W. R. G. Atkins there as physiologist (Mills, 1989, p. 201). It was Atkins who suggested to Jenkin that she undertake the simultaneous measurement of light and photsynthesis in the English Channel (Mills, 1989, p. 225). In 1928 S. M. Marshall and A. P. Orr had published a method that used oxygen production as a measure of the rate of photosynthesis by marine plants, and a number of investigators (for example Poole and Atkins, 1926) had measured the penetration of different colours of light into the ocean. It was expected that the intensity of available light would affect photosynthesis in the ocean, but no one had measured light and photosynthesis together, to test the hypothesis. On board the M. B. A.

steam trawler Salpo, in 1933 and in 1934, Jenkin did just that. While she performed the photosynthesis part of the experiment, Atkins and Poole measured light in the water, using a photocell with coloured filters. As well as showing that light controlled the photosynthetic rate of marine plants, Jenkin hoped to find that light measurements could be used as a proxy for the much more time-consuming measurements of photosynthesis.

During the cruise Jenkin exposed diatoms to light at different depths in the water, measured the light at those depths, and then measured the oxygen production at each depth. She used a monospecific culture of *Coscinodiscus excentricus*, a centric diatom that she had collected from the English Channel in the early spring and kept in culture for five months. She placed six bottles of diatoms and culture medium at each depth - three clear glass bottles open to light incident from all directions, two bottles that were blackened all over except on one side, and one totally dark bottle. The bottles were placed into wire baskets attached to a fixed cable and left for a number of hours. Light energy was measured as the sum of all illumination from 380 to 720 nm; the ultraviolet and infrared portions of the spectrum were excluded, as Jenkin felt that their influence would be minimal, and even if significant, would be confined to a small area in the uppermost portion of the water column. The dark bottle at each depth was included as a correction for respiration, which was thought to be constant, regardless of the level of incident light; the oxygen loss in the dark bottle was added to the oxygen increase measured in the light bottles, to obtain total production numbers.

From these experiments Jenkin concluded that photosynthesis depended strongly on available light; oxygen production increased with increasing incident daylight. Although it was already known that chlorophyll absorbed red light most strongly, Jenkin reported that red light could not limit photosynthesis, since the rate of oxygen production scaled with total energy, while red light was very quickly attenuated. She found that total light energy decreased roughly exponentially with depth, and that photosynthesis did too, except near the surface, where it appeared to be somewhat inhibited. She concluded that intense light must itself be the limiting factor, as the inhibition was less noticeable in the partially blackened bottle, and more noticeable during the midday irradiation than during the earlier and later experiments. As a result of the general increase in oxygen production with increasing light, and of the surface inhibition, the depth of maximum oxygen production was about 5m below the surface of the water. Jenkin also calculated a compensation depth at which photosynthesis exactly balanced respiration over 24 hours, and produced a plot of photosynthesis vs. irradiance, of a kind still used very commonly in the 1990s. Her experiment was significant as the first to combine measurements of photosynthesis with simultaneous measurements of light, and her light and dark bottle procedure is still used today for determining the rate of primary production.

The photoelectric method described earlier, though quantitative, was considered rather complicated and unwieldy (Pettersson, 1934), because it required an external amplifier to make the tiny currents strong enough to measure. Recognizing that submarine daylight was essential to primary production in the ocean, Hans Pettersson felt that a more accurate measure of its penetration was required. Although the new cuprous oxide cells

which he used had a number of problems of their own - losing sensitivity after exposure to intense light, for example - Pettersson (1934) used one in a submarine actinometer that he constructed with colleagues. He used the actinometer to measure both light from above and that scattered back from below, and obtained continuous records of submarine daylight at various depths for a year, including some measurements made beneath a 20 cm sheet of ice. G. Evelyn Hutchinson described the use of Petterson's transmissometer as well as several other instruments in studies of lake transparency in his comprehensive 1957 treatise on limnology.

Since those early measurements of light penetration, there has been an explosion of work on the subject; more precise silicon diodes have replaced photocells for light detection (Satlantic Inc. home page, April 1999), and instruments are more streamlined and more precise than those of the 1930s, but the same optical properties - irradiance, scattering, and absorption - are still measured, mainly to help to relate remotely sensed properties to the physical, chemical and biological states of the ocean (see "Interpretation and Modelling of Remotely Sensed Data" section).

Many recent authors have been especially interested in the transparency of the ocean to ultraviolet (UV) radiation, because of its damaging effect on phytoplankton (Smith and Baker, 1980; Behrenfeld *et al.*, 1993). For example, Donald Morris *et al.* (1995) measured UV penetration through lakes and related it to the concentration of dissolved organic carbon.

Besides measuring the depth of light penetration, many scientists have tried to determine the importance of suspended particles to changes in water transparency. Prince Albert of Monaco was aware of previous work on ocean transparency, and wanted to confirm previous results and to test the effects of particles on transparency. He made some estimates of the effect of particle load in 1905 (Thoulet, 1905). He stirred some very fine kaolinite clay into water, made standard dilutions of the suspension, and then tested what pathlength of each was required to make a candle flame behind the flask disappear. He determined that particles alone could make water completely opaque.

George Clarke (1933) was interested in the effect of light on the vertical distribution and migration of phytoplankton. To quantify the variability of the incident light, he investigated the effects of latitude, time of day, sea state, and particles on the intensity of irradiance in the ocean. He included a range of UV and visible wavelengths, from 346 to 526 nm. Rather oddly, Clarke determined that the first three variables he tested had no significant effect on the absolute depth of penetration of light, but that suspended matter in northern water was probably responsible for its decreased transparency relative to that found in the south, and particularly in the Sargasso Sea; in the Sargasso Sea he detected light down to 180 m. He also introduced to marine optics the unit microwatts per cm^2 for irradiance. This unit replaced the older metercandle, which did not include UV radiation or have the flexibility to be used at different depths under water at which the spectrum was very different from that at the surface. Microwatts/ cm^2 could be used at any depth, provided that the range of wavelengths included was specified. It is still commonly used today.

Hans Pettersson (1934) tested the hypothesis that particles were responsible for changes in transparency. He lowered a transparency meter that he had designed down through the water oriented horizontally, so that he could measure the transmission of light through 15 cm depth parcels. He also constructed a scattering meter. Pettersson reasoned that if particles were responsible for decreases in transparency in certain layers of water, then there should be an accompanying increase in upward scatter at those depths. Simultaneous sea water collection showed that particles did indeed change the transparency of water, but that dissolved organic matter had a strong effect too. (In 1957 Nils Jerlov pointed out that transparency meters were subject to inaccuracies due to scattering out of the light path, particularly in clear, open ocean water where the light path had to be very long to make a measurement. He presented a new transparency meter that used multiple reflection off concave mirrors set close together, so that a total light path of about 10 m could be obtained with losses only to inefficiency of reflection by the mirrors.) Wayne Burt (1958) agreed that particles were very important to light attenuation. He measured transparency at a number of depths with a quartz prism spectrophotometer, and found that it increased suddenly below about 100 m. He interpreted this change as the result of decreased particle size below the surface mixed layer.

The effect of absorbance will be discussed in the next section with respect to colour, but it is worth mentioning here that absorbance also affects transparency. Any light that is absorbed is unavailable to be scattered. Wilson Powell and George Clarke, for example,

discovered that absorbance near the surface of the ocean was important to transparency. In 1936 they quantified the reflection of light off the surface of the ocean to settle a dispute about the varying estimates of "surface loss" by reflection. They hoped that they would find a strong relationship between physical conditions easily measured at the sea's surface and submarine daylight, so that in the future they would be able to model the underwater light field instead of having to measure it directly. They found that reflection depended strongly on sun angle and sea state, and that the proportion reflected back from the surface could vary from 3 to 9 % while the sun was more than 30 degrees above the horizon, and could increase considerably for more oblique sun angles. They determined, however, that the "surface losses" of up to 60 % reported by previous authors were due not to reflection at the surface but to absorption by a particularly opaque layer of water just beneath the surface.

Nils Jerlov (1953) made measurements to determine the relative influence of dissolved and particulate matter on transparency, using both a transparency meter and a Tyndall meter to measure scattering. He related scattering to particulate absorbance and determined dissoved absorbance from the difference between absorbance by particles + dissoved matter and absorbance by particles alone. This calculation required reliance on an empirical relationship between scattering and absorption which Jerlov pointed out was parobably only locally applicable, but it represented a successful method of separating the effects of different components on transparency. One interesting result of this study was the discovery that terrestrially-derived, coloured dissolved matter behaved conservatively and could be used as a tracer for mixing.

In 1957 Jerlov presented a new transparency meter that was less affected by the selective absorbance of light by coloured dissolved organic matter

It is now relatively easy to measure irradiance throughout and below the euphotic zone, either in discrete bandwidths or over an integrated range of visible wavelengths, but the topic still has some appeal: P. Wolf and G. C. Cadée (1994) recently published a stinging response to an earlier paper in which the authors claimed to have measured light to the greatest depth ever - a Secchi depth of 79 m. Wolf and Cadée pronounced that Captain John Hood's record of about 160 m was still the deepest measurement of light penetration ever made, and that the authors should have been aware of the earlier literature (although it seems that Clarke might have beaten Hood's record in 1933). And the Secchi disk still has its proponents: in 1986, Rudolph Preisendorfer published a review paper that described how to make quantitative measurements using a Secchi disk, and even coded the "ten laws of the Secchi disk" into mathematical form. He did not recommend using a Secchi disk where more precise, electronic measurements were appropriate, but pointed out that there was a very long record of Secchi disk measurements available for comparison in long-term studies. Marlon Lewis *et al.* (1988) made use of part of that data base of Secchi depth measurements to calculate mean transparency fields in the ocean. From variations in mean transparency, they were able to identify areas of major upwelling and show temporal variation in fronts of new production.

Colour of the Ocean

Certainly, people besides Aristotle must have noticed before the nineteenth century that the ocean was not the same colour everywhere or all the time; they evidently recognized by the early seventeenth century that the colour of the ocean was affected by its components, as Shakespeare's MacBeth lamented that if he tried to wash his blood-stained hands in the ocean they would "the multitudinous seas incarnadine". But other than an occasional reference to the sea's turning to blood, or looking like it, there is no easily discovered reference to the cause of ocean colour before the work of John Aitken in the late 1800s. Aitken went to the Mediterranean Sea to determine why its water was so blue and why the colour was not always the same. He wanted to know whether absorbance of red by water was responsible, or whether the colour of particles or impurities in the water determined the colour. Without any complicated equipment, he tested the absorbance hypothesis in several ways: he looked at submerged white objects through a glass-ended tube, directly through the water, and inside a blackened tube. He also submerged several coloured objects, including oranges and lemons, and observed their underwater colour. All the results, including the apparent unripening of the fruit, showed that the water transmitted blue preferentially and absorbed red. He also determined, however, that the brightness of the colour depended on the size and colour of suspended particles.

Just to be sure that the red absorption was due to water itself and not to any impurity, he distilled water and condensed it in several containers made out of different materials to test whether the resulting water always looked blue. It did, and Aitken was quite satisfied

with the result. He commented: "The addition of impurities to water seems generally to change its colour from blue to green or yellow... No attempt was made to find out what the discolouring substances in water are. The task would evidently be an endless one, and of little value." (Aitken, 1882)

Apparently, other scientists disagreed with Aitkens' assessment of the value of future work, so the inquiry into the cause of ocean colour did not end in 1882.

During the first decade of the 1900s, both Germans and Norwegians conducted experiments related to the spring diatom bloom, which led F. Schütt, during a speech in 1904, to comment that the colour of the water was determined by its physical structure and by the physiology of the organisms living in it (Mills, 1989, p. 123). Phytoplankton were found to turn the water green (although a detailed absorbance spectrum had to wait until Charles Yentsch's work in 1960). The realization that phytoplankton did not absorb all colours equally drove the efforts in the 1920s and 1930s to determine the rates of attenuation of different colours of light through sea water. Isaac Newton in 1686 had published the results of his optical experiments, showing that white light was made up of all the colours of the rainbow, and that individual colours could be separated from the rest by refraction. This information, together with the work by James Maxwell and Heinrich Hertz on the wave theory of light in the late 1800s (Serway *et al.*, 1989) allowed scientists to design experiments that used selective cutoff filters to measure the penetration of light of different colours through the ocean. (Arab scientists in the

thirteenth century had done similar experiments on refraction (Park, 1997), but their work was slow to reach Europe.)

The photocells used in the 1920s and 1930s to measure the penetration of light into the ocean (see "transparency" section) were also useful for measuring the penetration of different colours of light. Victor Shelford and Jakob Kunz (1926) used photoelectric cells covered with plates of coloured glass to measure the penetration of red, yellow, blue and green light through the ocean. They commented that spherical coloured glass filters would be better, and even tried putting their photocells into coloured light bulbs, but without success. The best shape for a filter, they said, would be a hemisphere that covered the top of a photocell, so that it could collect light incident at a wider range of angles. They also found that, after the attenuation due to pure water had been subtracted, something absorbed the short wavelengths of light, leaving green and yellow at depth. C. L. Utterback and J. W. Boyle (1933) and R. H. Oster and George Clarke (1935) also made measurements of red, blue and green light penetration *in situ*, with similar results.

Narrow bandwidth filters eventually replaced the older, broad band filters used by experimenters such as Atkins and Poole in the 1930s, in order to measure light in more precisely defined wavebands, but John Tyler (1959) pointed out a problem associated with these new filters. Sea water acts as a strong monochromator, eventually absorbing the short and long wavelengths, and leaving a narrow band of light centred on 510 nm. Many of the narrow band filters, he said, let in so much stray light from other wavelengths that once the water had filtered out all of the light at the wavelength to be

measured, the detector would still measure a significant amount of 510 nm light. The leakage might only be a small percentage of the total measured light at the surface, but it could be 100 % of the signal at depth. Such waveband leakage is still a problem at times in the 1990s, but the narrow band filters have been too valuable to discard, so people continued to use them (improved as much as possible) after Tyler's warning.

Wayne Burt (1958) measured light penetration through sea water in 13 wavebands over a range of 400 to 800 nm and down to 1170 m depth. He found that transmission increased with increasing wavelength, although he did not specify the depth to which he was able to measure any of the wavelengths. He attributed the rapid attenuation of short wavelengths to a high concentration of "yellow substance", which presumably absorbed the blue and violet light.

Field measurements like those of Shelford and Kunz and of Burt were complemented by laboratory studies of absorption. E. O. Hurlburt (1926) measured absorption of visible radiation by three open ocean water samples using a monochromator in the laboratory. It is not clear what spectral resolution he managed, but he seems to have made the very first direct measurements of absorption by sea water. His interest in the subject was somewhat different from that of his contemporaries, however. Hurlburt made the interesting observation that, if sunlight passed through an atmosphere which contained the equivalent of 40 meters of water (salt or fresh) its spectrum would coincide exactly with the sensitivity curve of the human eye. Hurlburt speculated from this observation that eyes developed their sensitivity (in animals other than humans, of course) during the

warmer Paleozoic era, when the atmosphere contained much more water vapour than it does today.

In 1927 Hurlburt went on to determine absorption coefficients for UV radiation in sea water and the proportions of that absorption due to each of the principal salts. It is difficult to compare his absorption numbers to more recent results because of the lack of units in his published work, but in general, Hurlburt reported that UV was attenuated more quickly than visible radiation through both sea water and fresh water. Magnesium chloride and calcium sulphate contributed significantly to the absorption of UV, while the other salts absorbed very little. In another speculation about the ancient earth, Hurlburt commented that it seemed unlikely that the atmosphere and ocean should be most transparent to the most intense parts of the solar spectrum (the visible portion) just by coincidence; he suggested that visible radiation might have effectively burned its way through whatever chromophores had originally absorbed it. Neither of his ideas about the ancient earth seems to have been discussed widely, but they remain interesting speculations.

In the late 1930s there was some disagreement about how much of the attenuation of light in sea water was due to suspended particles and how much to the dissolved components, termed "color". Following Hurlburt, George Clarke and Harry James (1939) made some measurements of light absorption by sea water in 1938. They used a monochromator with a one meter sample pathlength, and measured the absorption due to different components of sea water from a number of locations over a range of 365 to 800 nm.

Clarke and James filtered their water through "coarse" and "fine" filters and compared the colours of the filtrates to help to settle the dispute. They determined that for longer wavelengths (473 to 800 nm) particles were responsible for almost all of the absorption, since the filtered sea water samples had almost the same absorption as distilled water in that region of the spectrum. In contrast, they found that blue and ultraviolet radiation were absorbed strongly by something in solution. They speculated that this material might have come from the disintegration of phytoplankton, an idea supported by later work (for example Kalle, 1966; Druffel *et al.*, 1992). While collecting their samples, Clarke and James deployed a submarine photometer, so that they could compare the transparency of sea water *in situ* with that measured in the laboratory. They had hoped to find that laboratory absorbance measurements would provide a convenient proxy for *in situ* attenuation of light, but unfortunately, their preservation method changed the sample colour too much for such comparisons to be practical at that time.

By 1975 it had become apparent that there were many corrections needed before laboratory absorption measurements could be related directly to *in situ* attenuation. Niels Højerslev (1975) described an absorption meter that could be used in the ocean. While it seemed like a very useful tool, it has never been widely used. However, similar instruments have been developed since. Annick Bricaud *et al.* (1995) reported a data set that combined for the first time *in situ* attenuation, absorption, scattering and backscattering at several visible wavelengths.

By the 1960s it was fairly widely accepted that the blue colour of the open ocean was due to scattering of the shortest wavelengths of light and absorption of the longest, and that inshore waters turned green because of the influence of dissolved organic matter (Yentsch 1960). But although phytoplankton were known to be affected by the colour of incident light, the effect of phytoplankton on ocean colour was not clear.

In 1960 the contribution of phytoplankton to spectral attenuation could be quantified precisely for the first time. Charles Yentsch (1960) published a spectrum of particulate phytoplankton absorbance. He determined that phytoplankton absorbance shifted the reflectance of water from blue to green because of its strong absorption at 443 nm. The higher absorbance peak at 680 nm did not affect the colour of the water appreciably at the phytoplankton concentrations found in natural waters, because of the much stronger absorption of red light by water. He also noted that most of the coloured material seemed to be contained in cells that did not pass through a 5 μm filter (Yentsch, 1962). This was a much larger pore size than is generally used today, but it helped to standardize the measurement of phytoplankton absorbance.

In 1982 Charles Yentsch and Clarice Yentsch reported that phytoplankton also absorbed UV radiation under some circumstances. Probably as a trait left over from the formation of the earth's early atmosphere, some phytoplankton have the ability to accumulate a pigment that acts as a sort of sunscreen against UV. W. C. Dunlap and B. E. Chalker (1986) and Deneb Karentz *et al.* (1991) identified the sun screens as a class of protein, the mycosporine-like amino acids. It is still unclear how much the sunscreen-producing

phytoplankton might influence the light field of the ocean, although Maria Vernet and K. Whitehead (1996) demonstrated that mycosporine-like amino acids were released from cultured phytoplankton and caused a significant increase in the UV absorbance of the surrounding medium.

Carl Lorenzen (1972) described the contribution of phytoplankton to light absorption in the ocean for different euphotic zone depths. He discovered that their effect was greatest where the euphotic zone was shallow; absorption by water dominated where the euphotic zone was deep. Studies of the complex interaction between mixing, phytoplankton, and light are still under way in the 1990s, though now usually related more to phytoplankton damage by UV (Cullen and Neale, 1994).

Annick Bricaud *et al.* (1981) reported that dissolved organic matter might affect ocean colour as much as phytoplankton did in a different region of the spectrum. They presented absorbance spectra that showed that dissolved organic matter absorbed UV most strongly, and visible radiation less so. Their measurements confirmed that the absorbance spectrum could be described as an exponential decay with wavelength, as it was often described in models. This information has been very useful to subsequent optical and chemical oceanographers. They found that the slope of the log-linearized spectrum did not vary very much, so that, knowing the absorbance at one wavelength, one could apply an average slope to calculate the absorbance at all the other wavelengths over the UV and visible spectrum. They pointed out that this could be very useful in the open ocean, since the absorbance of visible radiation by dissolved organic matter was

quite weak there, and few oceanographers had spectrophotometers with sufficiently long pathlengths to measure it. Since that time, however, a number of authors have disputed the claim that the absorbance slope was constant, and there have been many attempts to characterize the changes in the magnitude and slope of the absorbance spectrum of coloured dissolved organic matter with location (for example, Green and Blough, 1994; Højerslev, 1998), season (for example, DeGrandpre *et al.*, 1996; Vodacek *et al.*, 1997), and salinity (Blough et al., 1993). So far, there has been no consensus. and often people use a single slope for CDOM absorptivity (either the one calculated by Bricaud *et al.* or other values) in models.

Interpretation and Modelling of Remotely Sensed Data

From the late 1800s until the mid-1900s, the focus of optical research in the ocean was on the direct measurement of water transparency, and of absorbance and scattering by various components. But the question underlying all that research was: "Why was the ocean the colour it was, and what made its colour and transparency vary?" Since the mid-1900s, people have begun to interpret optical variations as indications of physical, chemical, and biological processes in the ocean, and to apply that knowledge to remotely sensed data. At the same time, a lot of modelling papers have been published. People have made models to describe the effect of particle size on scattering (for example Brown and Gordon, 1974; Bricaud and Morel (1986) and others), the effect of ship perturbance on optical measurements made nearby (Gordon, 1985), and especially, the relationship between inherent (properties of the water and consituents) and apparent (properties that

also depend on the light field) optical properties as affected by a plethora of factors (for example, Gordon *et al.*, 1975; Gordon, 1976, 1991; Baker and Smith, 1982, Kirk, 1984, and Roessler and Perry, 1995; Ciotti et al., 1999). Many of the models have been very useful, and have given us new insights, but in general, the models are not well-integrated into the stream of work that has answered the questions posed in this chapter. Optical modelling, therefore, will not be discussed further in this paper, except where it applies directly to the interpretation of remote sensing.

The earliest remote sensing data was collected by aeroplane. Charles Cox and Walter Munk (1954) took aerial photographs of the sea's surface while a ship measured wind speed and sea below them. They calculated statistics of the surface glitter using the photographs, and compared them to the actual sea state at the time they were taken. From this relationship they found that they could use glitter as a proxy of sea surface slope and for wind speed.

Remote sensing of ocean colour on a global scale became possible with the advent of artificial satellites carrying light reflectance sensors. Patterns were visible in the clouds, and in 1964 the American National Aeronautics and Space Administration (NASA) launched the first weather satellite, Nimbus 1, to take photographs of cloud cover to relate to local weather (NASA's Mission to Planet Earth home page, April 1999). A succession of weather satellites followed, each with more advanced sensors than the last. In 1978, NASA launched Nimbus 7, a weather satellite that carried the Coastal Zone Color Scanner (CZCS). CZCS measured the reflectance of different wavelengths of light

from the ocean's surface, making remote sensing of ocean colour possible. The reason for NASA's current interest in ocean colour and the justification for launching another ocean colour satellite after CZCS stopped working is to be able to predict long-term trends in climate change and to find patterns that will help to predict sudden changes in weather. For example, they would like to be able to predict floods and harsh winters in time to warn and to help the people affected (NASA's Mission to Planet Earth home page, April, 1999). Ocean colour, as earlier work has shown, reflects the physical, chemical, and biological conditions of the ocean, so it is a natural parameter to study in relation to climate change.

In 1981, Rosswell W. Austin and T. J. Petzold made a significant contribution to the use of remote optical measurements when they published empirical relationships between the ratio of reflectance at two visible wavelengths measured by CZCS and the *in situ* attenuation of light at an intermediate wavelength. Howard Gordon *et al.* (1983) published atmospheric correction algorithms which, when used with Austin and Petzold's relationship, allowed the calculation of chlorophyll concentration in surface waters. Trevor Platt and Shubha Sathyendranath (1988) showed that the surface chlorophyll concentrations calculated from satellite images could be used to calculate primary productivity per unit area. The CZCS satellite was no longer operational by this time, but the model was intended for use with a satellite to be launched later. They also proposed that there should be large scale field studies to ground-truth the algorithm.

By the late 1980s it had become apparent that the errors in the chlorophyll estimates, though not enormous, were not decreasing. Something else was interfering with the estimates made from reflectance data. Kendall Carder *et al.* (1989) showed that the CZCS algorithms often gave chlorophyll concentrations that were too high in areas where there was a high concentration of coloured dissolved organic matter. They pointed out that the earlier assumptions - that absorption at 443 nm by dissolved organic matter was very low and that it covaried with chlorophyll - were incorrect in many places, especially downstream from areas of high primary productivity. They suggested that this might explain the incorrect chlorophyll estimates. David Siegel and Anthony Michaels (1995) agreed, and calculated that in some areas coloured dissolved organic matter could account for up to 60% of the observed absorption. Algorithms for quantifying absorption by dissolved organic matter from remote reflectance measurements are still being developed. The SeaWiFS satellite launched in August 1997 (SeaWiFS home page, March, 1999) will provide more data for testing and improving calculated relationships.

Conclusion

Since the mid-1800s the study of light in the ocean has been driven largely by interest in the controls on primary production. More recently, the focus has shifted to the prediction of global climate change. In the late 1990s we seem to have convincing explanations for most of the variations in the colour and transparency of the ocean. As Aitken concluded in 1882, colour is determined by absorption, and the intensity of colour by scattering. Both scattering and absorption affect transparency. Phytoplankton, dissolved organic

matter, detritus, and water itself all contribute to the colour of sea water. We can even plot the spectral effect of each component on ocean colour (Kirk, 1983). The discovery of the causes of ocean colour and transparency required the development of a number of instruments and the curiosity and techniques to use them. Remote sensing has allowed us to begin to apply the knowledge we have gained to the description of ocean processes on a global scale. And it has only taken 2300 years.

Appendix 2. Fits to absorbance spectra

The plots on the next four pages represent the raw absorbance data (AU) used to calculate the quantum yield spectra in Chapter 2. The exponential fits to the data were used only to provide offset values which were subsequently subtracted from each spectrum. The fits were not used in any other calculations. The offsets were subtracted to correct for scattering and refractive index differences as described in Chapter 2. This method was used instead of the older correction method, which involved subtracting the absorbance at a particular wavelength or the average over a range of wavelengths (for example. Green and Blough, 1994) from the whole spectrum.

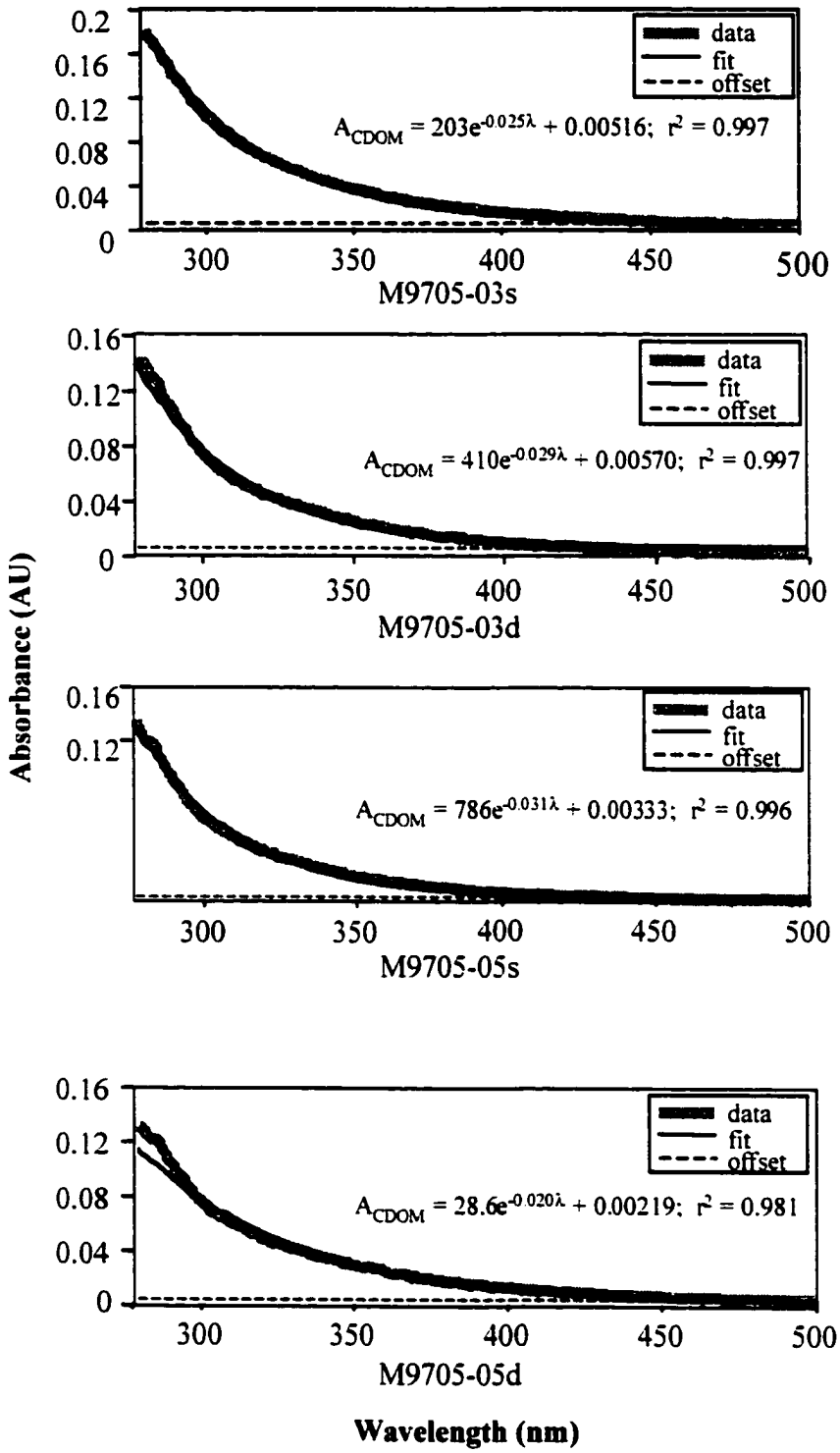
0.2
0.16
0.12
0.08
0.04
0
data
fit
offset
$A_{CDOM} = 203e^{-0.025\lambda} + 0.00516$; $r^2 = 0.997$
300
350
400
450
500
M9705-03s
0.16
0.12
0.08
0.04
0
data
fit
offset
$A_{CDOM} = 410e^{-0.029\lambda} + 0.00570$; $r^2 = 0.997$
300
350
400
450
500
M9705-03d
Absorbance (AU)
0.16
0.12
data
fit
offset
$A_{CDOM} = 786e^{-0.031\lambda} + 0.00333$; $r^2 = 0.996$
300
350
400
450
500
M9705-05s
0.16
0.12
0.08
0.04
0
data
fit
offset
$A_{CDOM} = 28.6e^{-0.020\lambda} + 0.00219$; $r^2 = 0.981$
300
350
400
450
500
M9705-05d
Wavelength (nm)

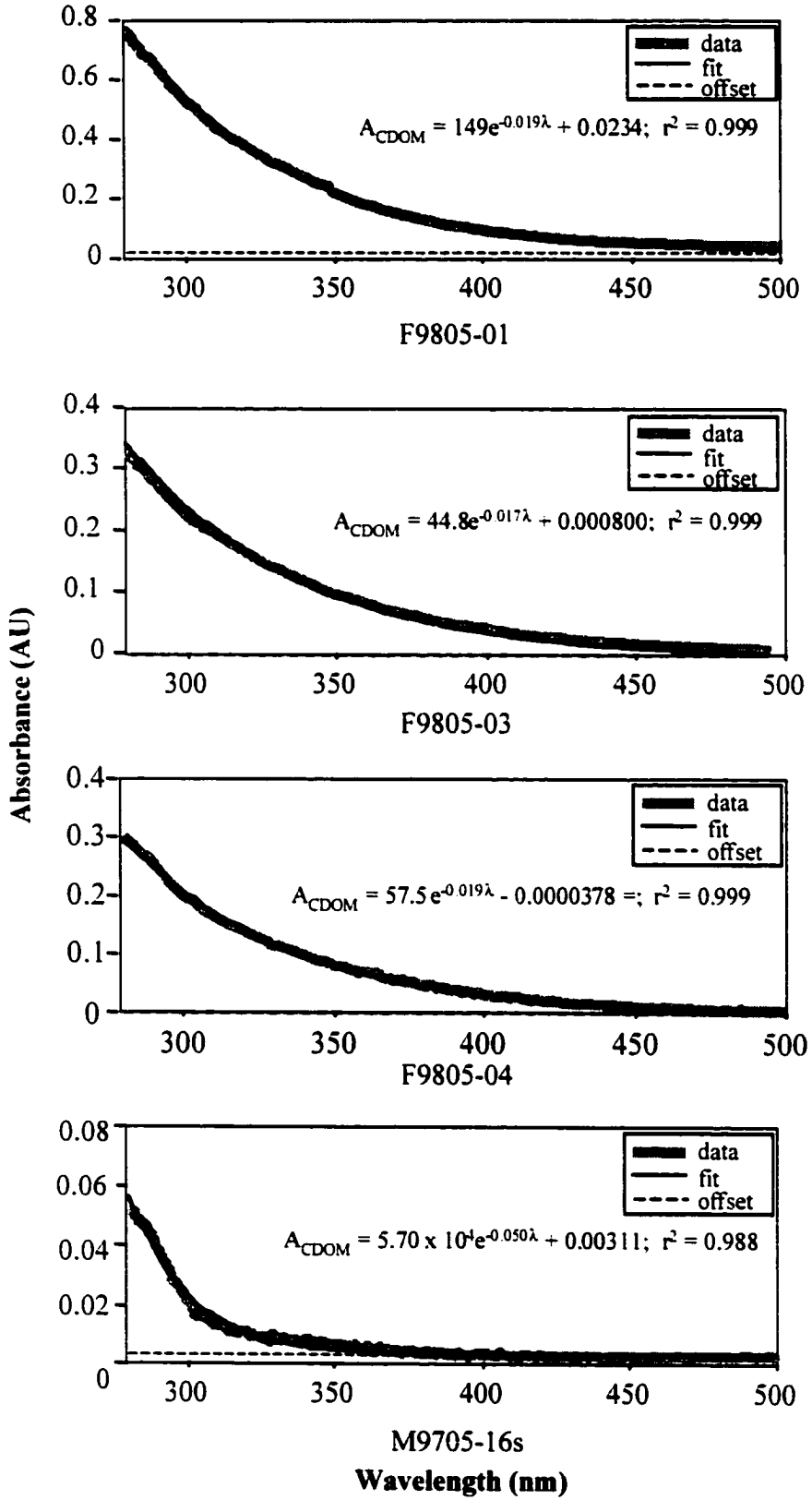
0.8
0.6
0.4
0.2
0
data
fit
offset
$A_{CDOM} = 149e^{-0.019\lambda} + 0.0234$; $r^2 = 0.999$
300
350
400
450
500
F9805-01
0.4
0.3
0.2
0.1
0
data
fit
offset
$A_{CDOM} = 44.8e^{-0.017\lambda} + 0.000800$; $r^2 = 0.999$
300
350
400
450
500
F9805-03
Absorbance (AU)
0.4
0.3
0.2
0.1
0
data
fit
offset
$A_{CDOM} = 57.5e^{-0.019\lambda} - 0.0000378$ =; $r^2 = 0.999$
300
350
400
450
500
F9805-04
0.08
0.06
0.04
0.02
0
data
fit
offset
$A_{CDOM} = 5.70 \times 10^{-4}e^{-0.050\lambda} + 0.00311$; $r^2 = 0.988$
300
350
400
450
500
M9705-16s
Wavelength (nm)

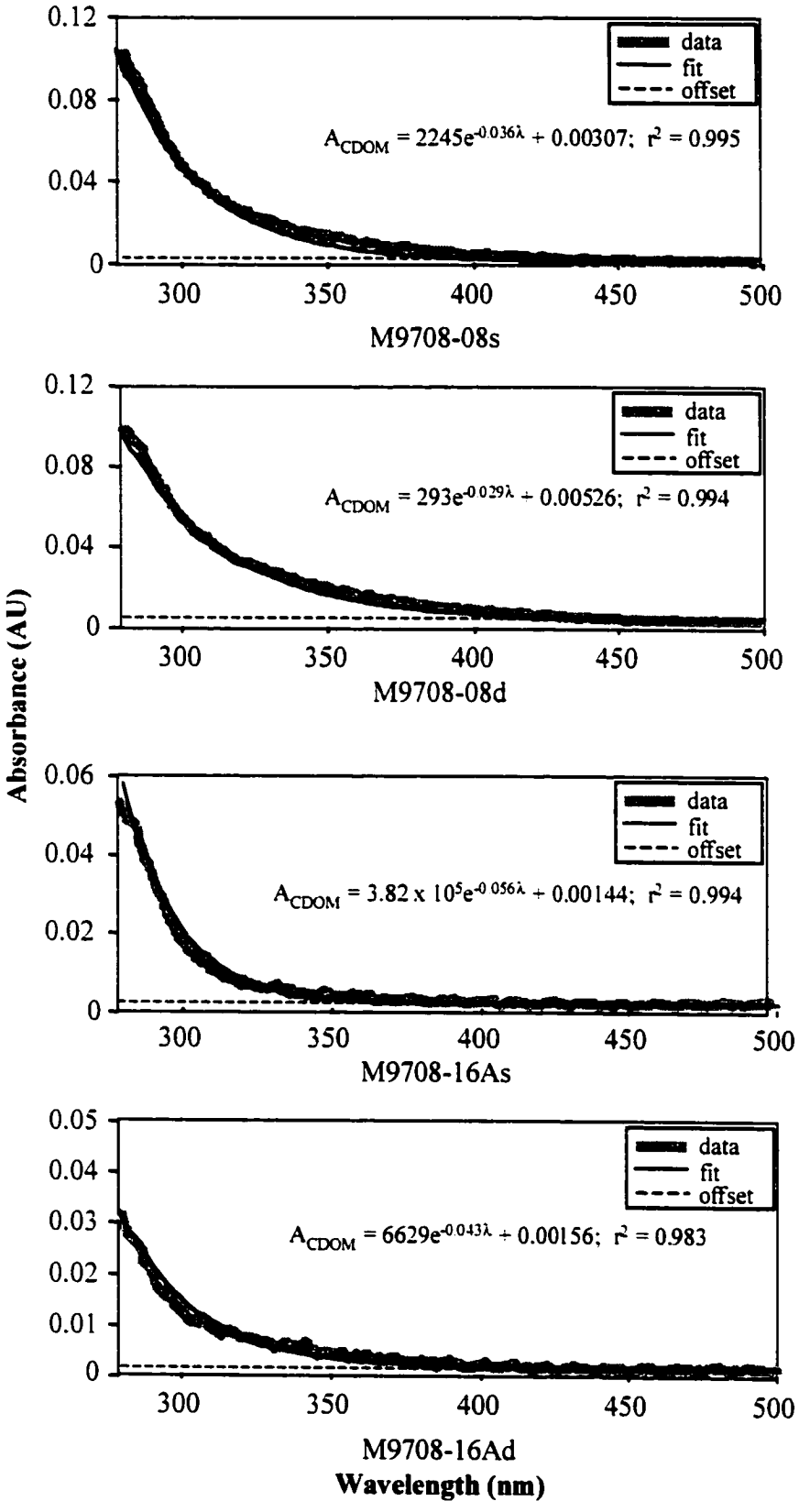
0.12
0.08
0.04
0
data
fit
offset
$A_{CDOM} = 2245e^{-0.036\lambda} + 0.00307$; $r^2 = 0.995$
300
350
400
450
500
M9708-08s
$A_{CDOM} = 293e^{-0.029\lambda} + 0.00526$; $r^2 = 0.994$
M9708-08d
Absorbance (AU)
0.06
0.02
$A_{CDOM} = 3.82 \times 10^5 e^{-0.056\lambda} + 0.00144$; $r^2 = 0.994$
M9708-16As
0.05
0.03
0.01
$A_{CDOM} = 6629e^{-0.043\lambda} + 0.00156$; $r^2 = 0.983$
M9708-16Ad
Wavelength (nm)

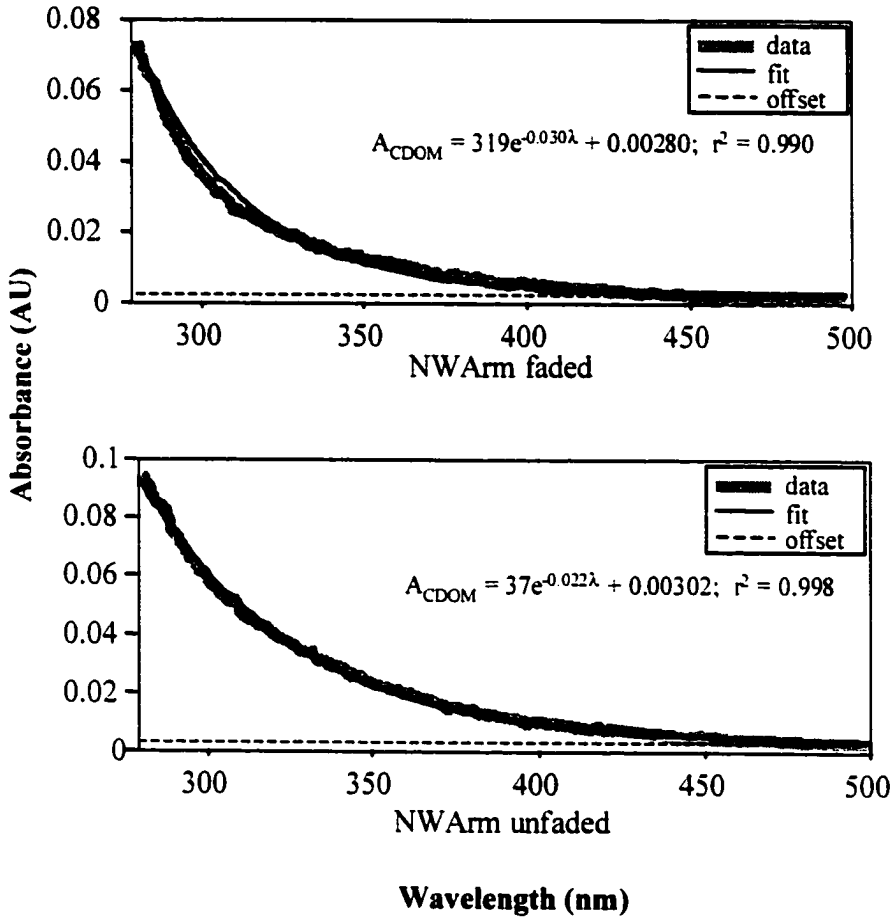
0.08
0.06
0.04
0.02
0
data
fit
offset
$A_{CDOM} = 319e^{-0.030\lambda} + 0.00280$; $r^2 = 0.990$
300
350
400
450
500
NWArm faded
0.1
0.08
0.06
0.04
0.02
0
data
fit
offset
$A_{CDOM} = 37e^{-0.022\lambda} + 0.00302$; $r^2 = 0.998$
300
350
400
450
500
NWArm unfaded
Absorbance (AU)
Wavelength (nm)

References

Aiken, J., Moore, G.F. and Holligan, P.M. 1992. Remote sensing of oceanic biology in relation to global climate change. Journal of Phycology 28(5): 579-590.

Aitken, J. 1882. On the colour of the Mediterranean and other waters. Proceedings of the Royal Society of Edinburgh 1881-1882: 472-483.

Allard, B., Borén, H., Pettersson, C. and Zhang, G. 1994. Degradation of humic substances by UV irradiation. Environment International 20(1): 97-101.

Amador, J.A., Alexander, M. and Zika, R.G. 1989. Sequential photochemical and microbial degradation of organic molecules bound to humic acid. Applied and Environmental Microbiology 55(11): 2843-2849.

Ammerman, J.W., Fuhrman, J.A., Hagstrom, A. and Azam, F. 1984. Bacterioplankton growth in sea water: I growth kinetics and cellular characteristics in seawater cultures. Marine Ecology Progress Series 18: 31-39.

Amon, R.M. and Benner, R. 1996. Photochemical and microbial consumption of dissolved organic carbon and dissolved oxygen in the Amazon River system. Geochimica et Cosmochimica Acta 60(10): 1783-1792.

Amon, R.M.W. and Benner, R. 1994. Rapid cycling of high-molecular-weight dissolved organic matter in the ocean. Nature 369: 549-552.

Anderson, T.R. and Williams, P.J. 1999. A one-dimensional model of dissolved organic carbon cycling in the water column incorporating combined biological-photochemical decompostion. Global Biochemical Cycles 13(2): 337-349.

Andreae, M.O. and Ferek, R.J. 1992. Photochemical production of carbonyl sulfide in seawater and its emission to the atmosphere. Global Biogeochemical Cycles 6(2): 175-183.

Andrews, S. S., Caron, S. and Zafiriou, O. C. 2000. Photochemical oxygen consumption in marine waters: a major sink for colored dissolved organic matter? Limnology and Oceanography 45(2): 267-277.

Armstrong, F.A.J., Williams, P.M. and Strickland, J.D.H. 1966. Photo-oxidation of organic matter in sea water by ultra-violet radiation, analytical and other applications. Nature 211: 481-483.

Arrigo, K.R. 1994. Impact of ozone depletion on phytoplankton growth in the Southern Ocean: Large-scale spatial and temporal variability. Marine Ecology Progress Series 114(1-2): 1-12.

Arrigo, K.R. and Brown, C.W. 1996. Impact of chromophoric dissolved organic matter on UV inhibition of primary productivity in the sea. Marine Ecology Progress Series 140: 207-216.

Atkins, W.R.G. 1932. Solar radiation and its transmission through air and water. Journal du Conseil pour l'Exploration de la Mer 7(2): 171-121.

Austin, R.W. and Petzold, T.J. 1981. The determination of the diffuse attenuation coefficient of sea water using the coastal zone color scanner. In: R.F. Gower (Editor). Oceanography from Space, Plenum Publishing.

Azam, F. and Hodson, R.E. 1977. Size distribution and activity of marine microheterotrophs. Limnology and Oceanography 22(3): 492-501.

Backlund 1992. Degradation of aquatic humic material by ultraviolet light. Chemosphere 25(12): 1869-1878.

Baker, K.S. and Smith, R.C. 1982. Bio-optical classification and model of natural waters. 2. Limnology and Oceanography 27(3): 500-509.

Balzani, V. and Carassitti, V. 1970. Photochemistry of Coordination Compounds. Academic Press, New York, London.

Bannister, T.T. 1992. Model of the mean cosine of underwater radiance and estimation of underwater scalar irradiance. Limnology and Oceanography 37(4): 773-780.

Bartlett, J.S., Ciotti, A.M., Davis, R.F. and Cullen, J.J. 1998. The spectral effect of clouds on solar irradiance. Journal of Geophysical Research 103(C13): 31017-31031.

Baxter, R.M. and Carey, J.H. 1983. Evidence for photochemical generation of superoxide ion in humic waters. Nature 306: 575-576.

Behrenfeld, M. 1993. Effects of ultraviolet-B radiation of primary production along latitudinal transects in the South Pacific Ocean. Marine Environmental Research 35(349-363).

Bertilsson, S. and Tranvik, L.J. 1998. Photochemically produced carboxilic acids as substrates for freshwater. Limnology and Oceanography 43(5): 885-895.

Berwald, J., Stramski, D., Mobley, C.D. and Kiefer, D.A. 1995. Influences of absorption and scattering on vertical changes in the average cosine of the underwater light field. Limnology and Oceanography 40(8): 1347-1357.

Blough, N.V., Zafiriou, O.C. and Bonilla, J. 1993. Optical absorption spectra of waters from the Orinoco River outflow: Terrestrial input of colored organic matter to the Caribbean. Journal of Geophysical Research 98(C2): 2271-2278.

Blough, N.V. and Zepp, R.G. 1995. Reactive oxygen species in natural waters. In: C.S. Foote, J.S. Valentine, A. Greenberg and J.F. Leibman (Editors), Active Oxygen in Chemistry. Chapman and Hall.

Bontempi, P. S. and Yoder, J. A. 1999. Permanent and transient spatial patterns in chlorophyll a as remotely sensed by CZCS, OCTS, and SeaWiFS. *Abstract in* Limnology and Oceanography: Navigating the Next Century: Abstract Book, American Society of Limnology and Oceanography (ASLO) meeting, Santa Fe, New Mexico, p. 28.

Bricaud, A. and Morel, A. 1986. Light attenuation and scattering by phytoplanktonic cells: a theoretical modeling. Applied Optics 25(4): 571-580.

Bricaud, A., Morel, A. and Prieur, L. 1981. Absorption by dissolved organic matter of the sea (yellow substance) in the UV and visible domains. Limnology and Oceanography 26(1): 43-53.

Bricaud, A., Roesler, C. and Zaneveld, R.V. 1995. In situ methods for measuring the inherent optical properties of ocean waters. Limnology and Oceanography 40(2): 393-410.

Brown, O.B. and Gordon, H.R. 1974. Size-refractive index distribution of clear coastal water particulates from light scattering. Applied Optics 13(12): 2874-2881.

Budac, D. and Wan, P. 1992. Photocarboxylation: mechanism and synthetic utility. Journal of Photochemistry and Photobiology 67: 135-166.

Bunce, N.J. and Chittim, B.G. 1979. Proposal for a photoreactivity index for aquatic pollutants. Chemosphere (11/12): 853-854.

Burt, W.V. 1958. Selective transmission of light in tropical Pacific waters. Deep-Sea Research 5: 51-61.

Bushaw, K.L., Zepp, R. G., Tarr, M. A., Schulz-Jander, D., Bourbonniere, R. A., Hodson, R. E., Miller, W. L., Bronk, D. A., and Moran, M. A. 1996. Photochemical release of biologically available nitrogen from aquatic dissolved organic matter. Nature 381: 404-407.

Cadée, G.C. 1996. Michael Faraday and his "Secchi disks". Archives of Natural History 23(2): 291-294.

Carder, K.L., Steward, R.G., Harvey, G.R. and Ortner, P.B. 1989. Marine humic and fulvic acids: Their effects on remote sensing of ocean chlorophyll. Limnology and Oceanography 34(1): 68-81.

Carr, M. E., Sato, O. T. and Polito, P. S. 2000. Estimating oceanic new production from annual heat storage measured by satellite altimeter. *Abstract in* Eos, Transactions, American Geophysical Union 80(49) suppl., 2000 Ocean Sciences Meeting, San Antonio, Texas, p. 27.

Carson, R. 1962. Silent Spring. H. Hamilton, London, 304 pp.

Chen, Y., Khan, S. U., and Schnitzer, M. 1978. Ultraviolet irradiation of dilute fulvic acid solutions. Soil Science Society of America Journal 42: 292-296.

Cialdi, M. and Secchi, A. 1865. Sur la transparence de la mer. Comptes Rendus des Seances, 17 July 1865: 100-104.

Ciotti, A.M., Cullen, J.J. and Lewis, M.R. 1999. A semi-analytical model of the influence of phytoplankton community structure on the relationship between light attentuation and ocean color. Journal of Geophysical Research 104(C1): 1559-1578.

Clarke, G.L. 1933. Observations on the Penetration of daylight into Mid-Atlantic and coastal waters. Biological Bulletin 65: 317-337.

Clarke, G.L., Ewing, G.C. and Lorenzen, C.J. 1970. Spectra of backscattered light from the sea obtained from aircraft as a measure of chlorophyll concentration. Science 167: 1119-1121.

Clarke, G.L. and James, H.R. 1939. Laboratory analysis of the selective absorption of light by sea water. Journal of the Optical Society of America 29: 43-55.

Clarke, G.L. and Oster, R.H. 1934. The penetration of the blue and red components of daylight into Atlantic coastal waters and its relation to phytoplankton metabolism. Biological Bulletin 67: 59-75.

COADS 1999. http://www.cdc.noaa.gov/coads/. Last updated December 14, 1999. Verified May 12, 2000. Maintained by Sandy Lubker (sjl@cdc.noaa.gov).

Coble, P.G. 1996. Characterization of marine and terrestrial DOM in seawater using excitation-emission matrix spectroscopy. Marine Chemistry 51(4): 325-346.

Cooper, W.J., Zika, R.G., Petasne, R.G. and Fischer, A.M. 1989. Sunlight-induced photochemistry of humic substances in natural waters: major reactive species. In: I.H. Suffet and P. McCarthy (Editor), Aquatic Humic Substances: Influence on Fate and Treatment of Pollutants. American Chemical Society, pp. 332-362.

Cooper, W.J., Zika, R.G., Petasne, R.G. and Plane, J.M.C. 1988. Photochemical formation of H_2O_2 in natural waters exposed to sunlight. Environmental Science and Technology 22(10): 1156-1160.

Cotterell, A. 1993. The Penguin Encyclopedia of Classical Civilizations. Viking, London.

Cox, C. and Munk, W. 1955. Measurement of the roughness of the sea surface from photographs of the sun's glitter. Journal of the Optical Society of America 44(11): 838-850.

Cullen, J.J., Davis, R.F., Bartlett, J.S. and Miller, W.L. 1997. Toward remote sensing of UV attenuation, photochemical fluxes, and biological effects of UV in surface waters. *Abstract in* Current and Emerging Issues in Aquatic Science: Program and Abstracts. American Society of Limnology and Oceanography, ASLO 97 Aquatic Sciences Meeting, Santa Fe, New Mexico, p. 137.

Cullen, J.J. and Neale, P.J. 1994. Ultraviolet radiation, ozone depletion, and marine photosynthesis. Photosynthesis Research 39: 303-320.

Cullen, J. J. and Neale, P. J. 1997. Biological weighting functions for describing the effects of ultraviolet radiation on aquatic systems. *In,* The Effects of Ozone Depletion on Aquatic Ecosystems, ed. D. P. Hader, R. G. Landes Company, 97-118.

DAAC 1999. http://daac.gsfc.nasa.gov/. Updated May 10, 2000. Verified May 12, 2000. Maintained by web curator (web-curator@daac.gsfc.nasa.gov).

De Haan, H. 1993. Solar UV-light penetration and photodegradation of humic substances in peaty lake water. Limnology and Oceanography 38(5): 1072-1076.

De Wolf, P. and Cadée, G.C. 1994. Water visibility record robust after 3 centuries. EOS 75(9): 99.

Degli Antelminelli, C.A.F.C. 1886. Report on the diatomaceae collected by HMS Challenger during the years 1873-1876., The Voyage of HMS Challenger: Botany. vol 2. prepared under the superintendance of John Murray, Rome, Rome.

DeGrandpre, M.D., Vodacek, A., Nelson, R.K., Bruce, E.J. and Blough, N.V. 1996. Seasonal seawater optical properties of the U.S. Middle Atlantic Bight. Journal of Geophysical Research 101(C10): 22,727-22,736.

Deuser, W.G. 1988. Whither organic carbon. Nature 332: 396-397.

Dickson, M.L. and Wheeler, P.A. 1993. Chlorophyll a concentrations in the North Pacific: Does a latitudinal gradient exist? Limnology and Oceanography 38(8): 1813-1818.

Dobbs, R.A., Wise, R.H. and Dean, R.B. 1972. The use of ultra-violet absorbance for monitoring the total organic carbon content of water and wastewater. Water Research 6: 1173-1180.

Doerffer, R. and Fischer, J. 1994. Concentrations of chlorophyll, suspended matter, and gelbstoff in case II waters derived from satellite coastal zone color scanner data with inverse modeling methods. Journal of Geophysical Research 99(C4): 7457-7466.

Draper, W.M. 1985. Determination of wavelength-averaged, near UV quantum yields for environmental chemicals. Chemosphere 14(9): 1195-1203.

Druffel, E.R.M., Williams, P.M., Bauer, J.E. and Ertel, J.R. 1992. Cycling of dissolved and particulate organic matter in the open ocean. Journal of Geophysical Research 97(C10): 15,639-16,659.

Dunlap, W. C. and Chalker, B. E. 1986. Identification and quantification of near-UV absorbing compounds (S-320) in a hermatypic scleractinian. Coral Reefs 5: 1-5.

Erickson, D. J. III 1989. Ocean to atmosphere carbon monoxide flux: global inventory and climate implications. Global Biogeochemical Cycles 3(4): 305-314.

Ertel, J.R., Hedges, J.I. and Perdue, E.M. 1984. Lignin signature of aquatic humic substances. Science 223: 485-487.

Fenton, N., Priddle, J., and Tett, P. 1994. Regional variations in bio-optical properties of the surface waters in the Southern Ocean. Antarctic Science 6(4): 443-448.

Ferek, R.J. and Andreae, M.O. 1983. The supersaturation of carbonyl sulfide in surface waters of the Pacific Ocean off Peru. Geophysical Research Letters 10(5): 393-396.

Ferrari, G. M., Dowell, M. D., Grossi, S., and Targa, C. 1996. Relationship between the optical propoerties of chromophoric dissolved organic matter and total concentration of dissolved organic carbon in the southern Baltic Sea region. Marine Chemistry 55: 299-316.

Finden, D.A.S., Tipping, E., Jaworski, G.H.M. and Reynolds, C.S. 1984. Light-induced reduction of natural iron(III) oxide and its relevance to phytoplankton. Nature 309(783-784).

Foster, P. and Morris, A.W. 1974. Ultra-violet absorption characteristics of natural waters. Water Research 8: 137-142.

Fraser, R.S., Mattoo, S., Yeh, E.-N. and McClain, C.R. 1997. Algorithm for atmospheric and glint corrections of satellite measurements of ocean pigment. Journal of Geophysical Research 102(D14): 17,107-17,118.

Gao, H. and Zepp, R.G. 1998. Factors influencing photoreactions of dissolved organic matter in a coastal river of the southeastern United States. Environmental Science and Technology 32(19): 2940-2946.

Geller, A. 1986. Comparison of mechanisms enhancing biodegradability of refractory lake water constituents. Limnology and Oceanography 31(4): 755-764.

Gordon, H.R. 1976. Radiative transfer in the ocean: A method for determination of absorption and scattering properties. Applied Optics 15(11): 2611-2613.

Gordon, H.R. 1985. Ship perturbations of irradiance measurements at sea. 1: Monte Carlo simulations. Applied Optics 24(23): 4172-4182.

Gordon, H.R. 1989. Can the Lambert-Beer law be applied to the diffuse attenuation coefficient of ocean water? Limnology and Oceanography 34(8): 1389-1409.

Gordon, H.R. 1989. Dependence of the diffuse reflectance of natural waters on the sun angle. Limnology and Oceanography 34(8): 1484-1489.

Gordon, H.R. 1991. Absorption and scattering estimates from irradiance measurements: Monte Carlo simulations. Limnology and Oceanography 36(4): 769-777.

Gordon, H.R. 1995. Remote sensing of ocean color: a methodology for dealing with broad spectral bands and significant out-of-band response. Applied Optics 34(36): 8363-8374.

Gordon, H.R., Brown, O. B., Evans, R. H., Brown, J. W., Smith, R. C., Baker, K. S., and Clark, D. K. 1988. A semianalytic radiance model of ocean color. Journal of Geophysical Research 93: 10909-10924.

Gordon, H.R., Brown, O.B. and Jacobs, M.M. 1975. Computed relationships between the inherent and apparent optical properties of a flat homogenous ocean. Applied Optics 14(2): 417-427.

Gordon, H.R. and Clark, D.K. 1981. Clear water radiances for atmospheric correction of coastal zone color scanner imagery. Applied Optics 20: 4175-4180.

Gordon, H.R., Clark, D. K., Brown, J. W., Brown, O. B., Evans, R. H., and Broenkow, W. W. 1983. Phytoplankton pigment concentrations in the Middle Atlantic Bight: comparison of ship determinations and CZCS estimates. Applied Optics 22(1): 20-36.

Gordon, H.R. and McCluney, W.R. 1975. Estimation of the depth of sunlight penetration in the sea for remote sensing. Applied Optics 14(2): 413-416.

Granéli, W., Lindell, M. and Tranvik, L. 1996. Photo-oxidative production of dissolved inorganic carbon in lakes of different humic content. Limmnology and Oceanography 41(4): 698-706.

Green, S.A. and Blough, N.V. 1994. Optical absorption and fluorescence properties of chromophoric dissolved organic matter in natural waters. Limnology and Oceanography 39(8): 1903-1916.

Gregg, W.W. and Carder, K.L. 1990. A simple spectral solar irradiance model for cloudless maritime atmospheres. Limnology and Oceanography 35(8): 1657-1675.

Gross, M.G. and Gross, E. 1996. Oceanography: A View of Earth. Prentice Hall, Upper Saddle River, 472 pp.

Haag, W.R. and Hoigné, J. 1985. Photo-sensitized oxidation in natural water via OH radicals. Chemosphere 14(11/12): 1659-1671.

Hamilton, R.D. 1963. Photochemical processes in the inorganic nitrogen cycle of the sea. Limnology and Oceanography 9: 107-111.

Harvey, G.R., Boran, D.A., Chesal, L.A. and Tokar, J.M. 1983. The structure of marine fulvic and humic acids. Marine Chemistry 12: 119-132.

Hedges, J.I. 1987. Organic matter in sea water. Nature 330: 205-206.

Hedges, J.I., Hatcher, P.G., Ertel, J.R. and Meyers-Schulte, K.J. 1992. A comparison of dissolved humic substances from seawater with Amazon River counterparts by 13C-NMR spectrometry. Geochimica et Cosmochimica Acta 56: 1753.

Herman, J.R., Krotov, N., Celarier, E., Larko, D. and Labow, G. 1999. Distributions of UV radiation at the Earth's surface from TOMS-measured UV-backscattered radiances. Journal of Geophysical Research 104(D10): 12,059-12,076.

Hochman, H.T., Müller-Karger, F.E. and Walsh, J.J. 1994. Interpretation of the coastal zone color scanner signature of the Orinoco River plume. Journal of Geophysical Research 99(C4): 7443-7455.

Hoge, F. E., Williams, M. E., Swift, R. N., Yungel, J. K., and Vodacek, A. 1995. Satellite retrieval of the absorption coefficient of chromophoric dissolved organic matter in continental margins. Journal of Geophysical Research 100(C2): 24847-24854.

Højerslev, N. 1975. A spectral light absorption meter for measurements in the sea. Limnology and Oceanography 20(6): 1024-1034.

Højerslev, N. 1994. A history of early optical oceanographic instrument design in Scandinavia. *In* Ocean Optics, ed. R. Spinrad, Oxford University Press, Oxford, 118-147.

Holmes, R.W. 1957. Solar radiation, submarine daylight, and photosynthesis. Geological Society of America: Memoir 67(1): 109-128.

Huot, Y. 1999. Damage to DNA in bacterioplankton: a model of damage by ultraviolet radiation and its repair as influenced by vertical mixing. M.Sc. Thesis, Dalhousie University, Halifax, 96 pp.

Hurlburt, E.O. 1926. The transparency of ocean water and the visibility curve of the eye. Journal of the Optical Society of America 13: 553-556.

Hurlburt, E.O. 1927. The penetration of ultraviolet light into pure water and sea water. Journal of the Optical Society of America 17: 15-22.

Hurlburt, E.O. 1945. Optics of distilled water and natural water. Journal of the Optical Society of America 35(11): 698-705.

Hutchinson, G. E. 1957. A Treatise on Limnology. John Wiley and Sons, New York.

Inn, E.C.Y. 1972. CO quantum yield in the photosynthesis of CO_2. Journal of Geophysical Research 77(10): 1991-1993.

Jeffrey, W. H., Pledger, R. J., Aas, P., Hager, S., Von Haven, R., and Mitchell, D. L. 1996. Diel and depth profiles of DNA photodamage in bacterioplankton exposed to ambient solar ultraviolet radiation. Marine Ecology Progress Series 137:283-291.

Jerlov, N.G. 1950. Ultra-violet radiation in the sea. Nature 166(4211): 111-112.

Jerlov, N. G. 1953. Influence of suspended and dissolved matter on the transparency of sea water. Tellus 5: 59-65.

Jerlov, N. G. 1957. A transparency-meter for ocean water. Tellus 9: 229-233.

Jerome, J.H. and Bukata, R.P. 1998. Tracking the propagation of solar ultraviolet radiation: Dispersal of ultraviolet photons in inland waters. Journal of Great Lakes Research 24(3): 666-680.

Johannessen, S. C., Miller, W. L., and Cullen, J. J. 1999. Photochemistry from space: integrating field data with theory. *Abstract in* Limnology and Oceanography: Navigating the Next Century: Abstract Book, American Society of Limnology and Oceanography (ASLO) meeting, Santa Fe, New Mexico, p. 94.

Johnston, S.F. 1996. Making light work: Practices and practitioners of photometry. History of Science 34: 273-302.

Kahru, M. and Mitchell, B. G. 2000. Seasonal and non-seasonal variability of satellite-derived chlorophyll and CDOM concentration in the California Current. *Abstract in* Eos, Transactions, American Geophysical Union 80(49) suppl., 2000 Ocean Sciences Meeting, San Antonio, Texas, p. 63.

Kaiser, E. and Herndl, G. J. 1997. Rapid recovery of marine bacterioplankton after inhibition by UV radiation in coastal waters. Applied and Environmental Microbiology 63(10): 4026-4031.

Kalle, K. 1966. The problem of the Gelbstoff in the sea. Oceanography and Marine Biology Annual Review 4: 91-104.

Karentz, D., McEuen, F.S., Land, M.C. and Dunlap, W.C. 1991. Survey of mycosporine-like amino acid compounds in Antarctic marine organisms: potential protection from ultraviolet exposure. Marine Biology 108: 157-166.

Kettle, A.J. 1994. A model of the temporal and spatial distribution of carbon monoxide in the mixed layer. M.Sc. Thesis, Woods Hole Oceanographic Institute, Massachussetts Institute of Technology, Woods Hole.

Kieber, D.J., McDaniel, J. and Mopper, K. 1989. Photochemical source of biological substrates in seawater: implications for carbon cycling. Nature 341: 637-639.

Kieber, D.J. and Mopper, K. 1987. Photochemical formation of glyoxylic and pyruvic acids in seawater. Marine Chemistry 21: 135-149.

Kieber, D. J. and Mopper, K. 2000. Photochemical formation of dissolved inorganic carbon in seawater and its impact on the marine carbon cycle. Surface Ocean Lower Atmosphere Study (SOLAS) Open Science Workshop, Kiel, Germany.

Kieber, D. J., Mopper, K., and Qian, J. 2000. Photochemical formation of dissolved inorganic carbon in seawater and its impact on the marine carbon cycle. *Abstract in* Eos, Transactions, American Geophysical Union 80(49) suppl., 2000 Ocean Sciences Meeting, San Antonio, Texas, p. 128.

Kieber, R. J., Zhou, X., and Mopper, K. 1990. Formation of carbonyl compounds from UV-induced photodegradation of humic substances in natural waters: fate of riverine carbon in the sea. Limnology and Oceanography 35(7): 1503-1515.

Kirk, J. T. 1983. Light and Photosynthesis in Aquatic Ecosystems. Cambridge University Press, Cambridge.

Kirk, J.T. 1991. Volume scattering function, average cosines, and the underwater light field. Limnology and Oceanography 36(3): 455-467.

Kirk, J.T. 1984. Dependence of relationship between inherent and apparent optical properties of water on solar altitude. Limnology and Oceanography 29(2): 350-356.

Kirk, J.T. 1994. Optics of UV-B radiation in natural waters. Archiv fur Hydrobiologie Beiheft 43: 1-16.

Klugh, A.B. 1927. Light penetration into the Bay of Fundy and into Chamcook Lake, New Brunswick. Ecology 8(1): 90-93.

Kotzias, D., Herrman, M., Zsolnay, A., Beyerle-Pfnür, R., Parlar, H., and Korte, F. 1987. Photochemical aging of humic substances. Chemosphere 16(7): 1463-1468.

Kotzias, D., Herrman, M., Zsolnay, A., Russi, H. and Korte, F. 1986. Photochemical reactivity of humic materials. Naturwissenschaften 73: 35-36.

Krümmel, O. 1907. Handbuch der Ozeanographie. Verlag von J. Engelhorn, Stuttgart.

Lewis, M. R., Kuring, N. and Yentsch, C. 1988. Global patterns of ocean transparency. Implications for the new production of the open ocean. Journal of Geophysical Research 93(C6): 6843-6856.

Li, W.K. and Dickie, P.M. 1985. Metabolic inhibition of size-fractionated marine plankton radiolabelled with amino acids, glucose, bicarbonate, and phosphate in the light and dark. Microbial Ecology 11: 11-24.

Libes, S.M. 1992. An Introduction to Marine Biogeochemistry. John Wiley and Sons, Inc., Toronto, 734 pp.

Lindell, M. J., Granéli, W., and Tranvik, L. J. 1995. Enhanced bacterial growth in response to photochemical transformation of dissolved organic matter. Limnology and Oceanography 40(1): 195-199.

Longworth, J.W. 1982. On light, colors, and the origins of spectroscopy. In: J.D. Regan and J.A. Parrish (Editors), The Science of Photomedicine. Plenum Press, New York, pp. 21-67.

Lorenzen, C.J. 1972. Extinction of light in the ocean by phytoplankton. Journal du Conseil Internationale pour l'Exploration de la Mer 34(2): 262-267.

Louis, P. 1993. Aristote: Problemes Tome II (translated into French by P. Louis from a work attributed to Aristotle and written in the third or fourth century B.C.). Les Belles Lettres, Paris.

Malcolm, R. L. 1990. The uniqueness of humic substances in each of soil, stream and marine environments. Analytica Chimica Acta 232: 19-30.

McCormick, N.J. 1992. Asymptotic optical attenuation. Limnology and Oceanography 37(7): 1570-1578.

McCormick, N.J. 1995. Mathematical models for the mean cosine of irradiance and the diffuse attenuation coefficient. Limnology and Oceanography 40(5): 1013:1018.

Meybeck, M. 1982. Carbon, nitrogen and phosphorus transport by world rivers. American Journal of Science 282: 401-450.

Meyers-Schulte, C.J. and Hedges, J.I. 1986. Molecular evidence for a terrestrial component of humic matter dissolved in ocean water. Nature 321: 61-63.

Michaels, A.F., Bates, N.R., Buesseler, K.O., Carlson, C.A. and Knap, A.H. 1994. Carbon-cycle imbalances in the Sargasso Sea. Nature 372(6506): 537-540.

Miles, C. J. and Brezonik, P. L. 1981. Oxygen consumption in humic-colored waters by a photochemical ferrous-ferric catalytic cycle. Environmental Science and Technology 15(9): 1089-1095.

Miller, G.C. and Zepp, R.G. 1978. Effects of suspended sediments on photolysis rates of dissolved pollutants. Water Research 13: 453-459.

Miller, G.W., Kieber, D.K. and Mopper, K. 2000. Action spectra and temperature dependence for the photochemical formation of hydrogen peroxide in seawater: laboratory and field results. *Abstract in* Eos, Transactions, American Geophysical Union 80(49) suppl., 2000 Ocean Sciences Meeting, San Antonio, Texas, p. 146.

Miller, W. 1998. Effects of UV radiation on aquatic humus: Photochemical principles and experimental considerations. Ecological Studies 133: 125-143.

Miller, W.L. 1994. Recent advances in the photochemistry of natural dissolved organic matter. In: G.R. Helz (Editor), Aquatic and Surface Photochemistry. Lewis Publishers, CRC Press, Boca Raton, pp. 111-128.

Miller, W.L. and Kester, D. 1994. Photochemical iron reduction and iron bioavailability in seawater. Journal of Marine Research 52: 325-343.

Miller, W.L. and Kester, D.R. 1994. Peroxide variations in the Sargasso Sea. Marine Geochemistry 48: 17-19.

Miller, W.L., King, D.W., Lin, J. and Kester, D.R. 1995. Photochemical redox cycling of iron in coastal seawater. Marine Chemistry 50: 63-77.

Miller, W.L. and Moran, M.A. 1997. Interaction of photochemical and microbial processes in the degradation of refractory dissolved organic matter from a coastal marine environment. Limnology and Oceanography 42(6): 1317-1324.

Miller, W.L. and Zepp, R.G. 1995. Photochemical production of dissolved inorganic carbon from terrestrial organic matter: Significance to the oceanic organic carbon cycle. Geophysical Research Letters 22(4): 417-420.

Mills, E. 1989. Biological Oceanography: An Early History, 1870-1960. Cornell University Press, New York.

Moore, C.A., Farmer, C.T. and Zika, R.G. 1993. Influence of the Orinoco river on hydrogen peroxide distribution and production in the Eastern Caribbean. Journal of Geophysical Research 98(C2): 2289-2298.

Moore, R.J. 1999. Photochemical degradation of coloured dissolved organic matter in two Nova Scotian lakes. M.Sc. Thesis, Dalhousie University, Halifax.

Moore, R.M. and Zafiriou, O.C. 1994. Photochemical production of methyl iodide in seawater. Journal of Geophysical Research 99(D8): 16,415-16,420.

Mopper, K. 1977. Sugars and uronic acids in sediment and water from the Black Sea and North Sea with emphasis on analytical techniques. Marine Chemistry 5(4-6): 585-603.

Mopper, K. and Zhou, X. 1990. Hydroxyl radical photoproduction in the sea and its potential impact on marine processes. Science 250: 661-664.

Mopper, K., Zhou, X., Kieber, R.J., Kieber, D.J., Sikorski, R.J., and Jones, R.D. 1991. Photochemical degradation of dissolved organic carbon and its impact on the oceanic carbon cycle. Nature 353: 60-62.

Moran, M.A. and Zepp, R.G. 1997. Role of photochemistry in the formation of biologically labile compounds from dissolved organic matter. Limnology and Oceanography 42: 1307-1316.

Morel, A. 1978. Available, usable, and stored radiant energy in relation to marine photosynthesis. Deep-Sea Research 25: 673-688.

Morel, A. 1988. Optical modeling of the upper ocean in relation to its biogenous matter content (Case I waters). Journal of Geophysical Research 93(C9): 10,749-10,768.

Morel, A. and Prieur, L. 1977. Analysis of variations in ocean color. Limnology and Oceanography 22(4): 709-722.

Morris, D.P. and Hargreaves, B.R. 1997. The role of photochemical degradation of dissolved organic carbon in regulating the UV transparency of three lakes on the Pocono Plateau. Limnology and Oceanography 42(2): 239-249.

Morris, D.P., Zagarese, H., Williamson, C. E., Balseiro, E. G., Hargreaves, B. R., Modenutti, B., Moeller, R., and Queimalinos, C. 1995. The attenuation of solar UV radiation in lakes and the role of dissolved organic carbon. Limnology and Oceanography 40(8): 1381-1391.

Mortimer, C. H. 1988. Discoveries and testable hypotheses arising from Coastal Zone Color Scanner imagery of southern Lake Michigan. Limnology and Oceanography 33(2): 203-226.

Naganuma, T, Konishi, S., Inoue, T., Nakane, T., and Sukizaki, S. 1996. Photodegradation or photoalteration? Microbial assay of the effect of UV-B on dissolved organic matter. Marine Ecology Progress Series 135: 309-310.

NASA Mission to Planet Earth, 1999. http://www.earth.nasa.gov/whatis/index.html. Updated November 11, 1998. Verified May 12, 2000. Maintained by SAIC Information Services (kyocum@hq.nasa.gov).

Nelson, N. 1997. Watching the world from above. Annual Report of the Bermuda Biological Station Research 1997: 11-12.

Nelson, N.B., Siegel, D.A. and Michaels, A.F. 1998. Seasonal dynamics of colored dissolved material in the Sargasso Sea. Deep-Sea Research 45(6): 931-957.

Newton, Sir I. 1686. Optics. In: R.M. Hutchins (Editor), Great Books of the Western World 34. Newton, Huygens, 1971. Encyclopaedia Britannica Inc., pp. 377-550.

Nissenbaum, A. and Kaplan, I.R. 1972. Chemical and isotopic evidence for the in-situ origin of marine humic substances. Limnology and Oceanography 17(4): 570-582.

Norrman, B., Zweifel, U.L., Hopkinson, C.S.J. and Fry, B. 1995. Production and utilization of dissolved organic carbon during an experimental diatom bloom. Limnology and Oceanography 40(5): 898-907.

Opsahi, S. and Benner, R. 1997. Distribution and cycling of terrigenous dissolved organic matter in the ocean. Nature 386: 480-482.

Oster, R.H. and Clarke, G.L. 1935. The penetration of red, green, and violet components of daylight into Atlantic waters. Journal of the Optical Society of America 25: 84-91.

Park, D. 1997. The Fire Within the Eye. Princeton University Press, Princeton.

Parsons, T.R., Maita, Y. and Lalli, C.M. 1984. A Manual of Chemical and Biological Methods for Seawater Analysis. Pergammon Press, Toronto.

Pettersson, H. 1935. Submarine daylight and the transparency of sea water. Journal du Conseil Internationale pour l'Exploration de la Mer 10: 48-65.

Platt, J.R. 1964. Strong inference. Science 146(3642): 347-353.

Platt, T. and Sathyendranath, S. 1988. Oceanic primary production: Estimation by remote sensing at local and regional scales. Science 241: 1613-1620.

Poole, H.H. 1925. On the photo-electric measurement of submarine illumination. Scientific Proceedings, Royal Dublin Society 18(9): 99-115.

Poole, H.H. and Atkins W.R.G., 1926. On the penetration of light into sea water. Journal of the Marine Biology Association 14(1): 177-198.

Pope, R.M. and Fry, E.S. 1997. Absorption spectrum (380-700 nm) of pure water. II. Integrating cavity measurements. Applied Optics 36(3): 8710-8723.

Poutanen, E.-L. and Morris, R.J. 1983. A study of the formation of high molecular weight compounds during the decomposition of a field diatom population. Estuarine, Coastal and Shelf Science 17: 189-196.

Powell, W.M. and Clarke, G.L. 1936. The reflection and absorption of daylight at the surface of the ocean. Journal of the Optical Society of America 26: 111-120.

Preisendorfer, R.W. 1986. Secchi disk science: Visual optics of natural waters. Limnology and Oceanography 31(5): 909-926.

Ratte, M., Bujok, O., Spitzy, A. and Rudolph, J. 1998. Photochemical alkene formation in seawater from dissolved organic carbon: Results from laboratory experiments. Journal of Geophysical Research 103(D5): 5707-5717.

Roesler, C.S. and Perry, M.J. 1995. In situ phytoplankton absorption, fluorescence emmission, and particulate backscattering spectra determined from reflectance. Journal of Geophysical Research 100(C7): 13,279-13,294.

Rundel, R.D. 1983. Action spectra and estimation of biologically effective UV radiation. Physiologia Plantarum 58: 360-366.

Salonen, K. and Vahätälo, A. 1994. Photochemical mineralisation of dissolved organic matter in Lake Skjervatjern, 4. Nordic Symp. on Humic Substances, 7-9 Jun 1993, Loen, Norway.

Sarmiento, J.L. and Bender, M. 1994. Carbon biogeochemistry and climate change. Photosynthesis Research 39(209-234).

Sarmiento, J.L. and Sundquist, E.T. 1992. Revised budget for the oceanic uptake of anthropogenic carbon dioxide. Nature 356: 589-593.

Sathyendranath, S., Prieur, L. and Morel, A. 1989. A three-component model of ocean colour and its application to remote sensing of phytoplankton pigments in coastal waters. International Journal of Remote Sensing 10: 1373-1394.

Satlantic 1999. http://www.satlantic.com/. Updated 2000. Verified May 12, 2000. Maintained by webmaster (webmaster@satlantic.com).

Scully, N.M., Vincent, W.F., Lean, D.R.S. and MacIntyre, S. 1998. Hydrogen peroxide as a natural tracer of mixing in surface layers. Aquatic Science 60(2): 169-186.

SeaWiFS 1999. http://seawifs.gsfc.nasa.gov/SEAWIFS.html. Verified May 12, 2000. Maintained by Gene Feldman (gene@seawifs.gsfc.nasa.gov).

Serway, R.A., Moses, C.J. and Moyer, C.A. 1989. Modern Physics. Saunders College Publishing, Toronto.

Shelford, V.E. and Kunz, J. 1926. The use of photo-electric cells of different alkali metals and color screens in the measurement of light penetration into water. Transactions of the Wisconsin Academy of Science, Arts and Letters 22: 283-298.

Siegel, D. A. 1999. Orthogonal views of the global ocean biosphere using SeaWiFS. *Abstract in* Limnology and Oceanography: Navigating the Next Century: Abstract Book, American Society of Limnology and Oceanography (ASLO) meeting, Santa Fe, New Mexico, p. 163.

Siegel, D.A., Maritorena, S., Nelson, N.B. and Lorenzi-Kaiser, M. 2000. Global ocean distribution of colored organic materials. *Abstract in* Eos, Transactions, American Geophysical Union 80(49) suppl., 2000 Ocean Sciences Meeting, San Antonio, Texas, p. 63.

Siegel, D.A. and Michaels, A.F. 1996. Quantification of non-algal light attenuation in the Sargasso Sea: Implications for biogeochemistry and remote sensing. Deep-Sea Research II 43(2/3): 321-345.

Sikorski, R.J. and Zika, R.G. 1993. Modeling mixed-layer photochemistry of H_2O: Physical and chemical modeling of distribution. Journal of Geophysical Research 98(C2): 2329-2340.

Sikorski, R.J. and Zika, R.G. 1993. Modeling mixed-layer photochemistryof H_2O: Optical and chemical modeling of production. Journal of Geophysical Research 98(C2): 2315-2328.

Smith, R.C. and Baker, K.S. 1979. Penetration of UV-B and biologically effective dose rates in natural waters. Photochemistry and Photobiology 29: 311-323.

Smith, R.C. and Baker, K.S. 1981. Optical properties of the clearest natural waters (200-800 nm). Applied Optics 20(2): 177-184.

Smith, S.V. and Hollibaugh, J.T. 1993. Coastal metabolism and the oceanic organic carbon balance. Reviews of Geophysics 31(1): 75-89.

Smith, R. C., Prézelin, B. B., Baker, K. S., Bidigare, R. R., Boucher, N. P., Coley, T., Karentz, D., MacIntyre, S., and Matlick, H. A. 1992. Ozone depletion: ultraviolet radiation and phytoplankton biology in Antarctic waters. Science 255(5047): 952-959.

Spokes, L.J. and Liss, P.S. 1996. Photochemically induced redox reactions in seawater. Marine Geochemistry 54: 1-10.

Stockner, J.G., Klut, M.E. and Cochlan, W.P. 1990. Leaky filters: a warning to aquatic ecologists. Canadian Journal of Fisheries and Aquatic Sciences 47: 16-23.

Thomas, D. N. and Lara, R. J. 1995. Photodegradation of algal derived dissolved organic carbon. Marine Ecology Progress Series 116: 309-310.

Thoulet, J. 1905. Etude sur la transparence et la couleur des eaux de mer. In: Albert 1er, Prince Souverain de Monaco (Editor), Résultats des Campagnes Scientifiques Accomplies sur son Yacht. Imprimerie de Monaco, Monaco.

TOMS 1999. http://toms.gsfc.nasa.gov. Updated April 4, 2000. Verified May 12, 2000. Maintained by Russell Wooldridge (wooldridge@qhearts.gsfc.nasa.gov).

Turner, P. 1962. Selections from the History of the World, Commonly Called the Natural History of C. Plinius Secundus (translated by P. Holland from Pliny's pre-79 AD work). Centaur Press Ltd., London.

Tyler, J.E. 1959. Natural water as a monochromator. Limnology and Oceanography 4(1): 102-105.

Uher, G. and Andreae, M.O. 1997. Photochemical production of cabonyl sufide in North Sea water: A process study. Limnology and Oceanography 42(3): 432-442.

Utterback, C.L. and Boyle, J.W. 1933. Light penetration in the waters of the San Juan Archpelago. Journal of the Optical Society of America 23(10): 333-338.

Valentine, R.L. and Zepp, R.G. 1993. Formation of carbon monoxide from the photodefradation of terrestrial dissolved organic carbon in natural waters. Environmental Science and Technology 27: 409-412.

Van Baalen, C. and Marler, J. E. 1966. Occurrence of hydrogen peroxide in sea water. Nature 211: 951.

Vernet, M. and Whitehead, K. 1996. Release of ultraviolet-absorbing compounds by the red-tide dinoflagellate *Lingulodinium polyhedra*. Marine Biology 127: 35-44.

Visser, S.A. 1983. Comparative study on the elementary composition of fulvic and humic acids of aquatic origin and from soils and microbial substrates. Water Research 17(10): 1393-1396.

Vodacek, A., Blough, N.V., DeGrandpre, M.D., Peltzer, E.T. and Nelson, R.K. 1997. Seasonal variation of CDOM and DOC in the Middle Atlantic Bight: terrestrial inputs and photooxidation. Limnology and Oceanography 42: 674-686.

Vodacek, A., Hoge, F., Swift, R. N., Yungel, J. K., Peltzer, E. T., and Blough, N.V. 1995. The use of in situ and airborne fluorescence measurements to determine UV absorption coefficients and DOC concentrations in surface waters. Limnology and Oceanography 40(2): 411-415.

Warren, S. G., Hahn, C. J., London, J., Chervin, R. M. and Jenne, R. L. 1988. Global Distribution of Total Cloud Cover and Cloud Type Amounts over the Ocean, publ. U.S. Dept. of Energy, NCAR Technical Notes, DOE/ER-406, Washingon, DC and Boulder Colorado.

Wedgwood, P. 1952. Notes on humus. Institute of Sewage Purification, Journal and Proceedings Part 1: 20-31.

Weiss, P.S., Andrews, S.R., Johnson, J.E. and Zafiriou, O.C. 1995. Photoproduction of carbonyl sulfide in south Pacific Ocean waters as a function of irradiation wavelength. Geophysical Research Letters 22(3): 215-218.

Wells, M.L., Zorkin, N.G. and Lewis, A.G. 1983. The role of colloid chemistry in providing a source of iron to phytoplankton. Journal of Marine Research 41: 731-746.

Wetzel, R.G., Hatcher, P.G. and Bianchi, T.S. 1995. Natural photolysis by ultraviolet irradiance of recalcitrant dissolved organic matter to simple substrates for rapid bacterial metabolism. Limnology and Oceanography 40(8): 1369-1380.

Williams, P.M., Oeschger, H. and Kinney, P. 1969. Natural radiogenic activity of dissolved organic carbon in the north-east Pacific Ocean. Nature 224: 256-258.

Xie, H., Moore, R.M. and Miller, W.l. 1998. Photochemical production of carbon disulfide in seawater. Journal of Geophysical Research 103(C3): 5331-5644.

Yentsch, C.S. 1962. Measurement of visible light absorption by particulate matter in the ocean. Limnology and Oceanography 7: 207-217.

Yentsch, C. S. and Phinney, D. A. 1996. Yellow substances in the coastal waters of the Gulf of Maine: implications for ocean color algorithms. *Abstract in* SPIE Volume 2963,. Ocean Optics XIII Proceedings, Halifax, Nova Scotia, p. 120.

Yentsch, C.S. and Yentsch, C.M. 1982. The attenuation of light by marine phytoplankton with specfic reference to the absorption of near-UV radiation. In: J. Calkins (Editor), The Role of Solar Ultraviolet Radiation in Marine Ecosystems. Plenum Publishing Corporation.

Zafiriou, O.C. 1974. Sources and reactions of OH and daughter radicals in seawater. Journal of Geophysical Research 79(30): 4491-4497.

Zafiriou, O.C. 1977. Marine organic photochemistry previewed. Marine Chemistry 5: 497-522.

Zafiriou, O.C. and Dister, B. 1991. Photochemical free radical production rates: Gulf of Maine and Woods Hole-Miami transect. Journal of Geophysical Research 96(C3): 4939-4945.

Zafiriou, O.C. and True, M.B. 1979. Nitrate photolysis in seawater by sunlight. Marine Chemistry 8: 33-42.

Zepp, R.G. 1978. Quantum yields for reaction of pollutants in dilute aqueous solution. Environmental Science and Technology 12(3): 327-329.

Zepp, R.G. 1982. Experimental approaches to environmental photochemistry. In: O. Hutzinger (Editor), The Handbook of Environmental Chemistry, vol2. Springer-Verlag, Berlin, pp. 19-41.

Zepp, R.G. and Andreae, M.O. 1994. Factors affecting the photochemical production of carbonyl sulfide in seawater. Geophysical Research Letters 21(25): 2813-2816.

Zepp, R.G., Baughman, G.L. and Schlotzhauer, P.F. 1981. Comparison of photochemical behaviour of various humic substances in water: II. Photosensitized oxygenations. Chemosphere 10: 119-126.

Zepp, R.G. and Cline, D.M. 1977. Rates of direct photolysis in aquatic environment. Environmental Science and Technology 11(4): 359-366.

Zepp, R.G., Faust, B.C. and Hoigné, J. 1992. Hydroxyl radical formation in aqueous reactions (pH 3-8) of iron(II) with hydrogen peroxide: The photo-Fenton reaction. Environmental Science and Technology 26(313-319).

Zepp, R.G., Gumz, M.M., Miller, W.L. and Gao, H. 1998. Photoreaction of valerphenone in aqueous solution. Journal of Physical Chemistry A 102(28): 5716-5723.

Zepp, R.G. and Schlotzhauer, P.F. 1981. Comparison of photochemical behavior of various humic substances in water: III. Spectroscopic properties of humic substances. Chemosphere 10(5): 479-486.

Zhou, X. and Mopper, K. 1990. Determination of photochemically produced hydroxyl radicals in seawater and freshwater. Marine Chemistry 30:71-88.

Zika, R. G., Moffett, J. W., Petasne, R. G., Cooper, W. J., and Saltzman, E. S. 1985. Spatial and temporal variations of hydrogen peroxide in Gulf of Mexico waters. Geochimica et Cosmochimica Acta 49:1175-1184.